CFD modeling of a modified Ahmed Car Body for Reduced Drag

Abul Kalam Azad

DEPARTMENT OF MATHEMATICS

KHULNA UNIVERSITY OF ENGINEERING & TECHNOLOGY

Khulna-9203, BANGLADESH

CFD modeling of a modified Ahmed Car Body for Reduced Drag

A THESIS SUBMITTED FOR PARTIAL FULFILMENT
OF THE REQUIREMENT OF DOCTOR OF
PHILOSOPHY IN MATHEMATICS

BY

Abul Kalam Azad

Roll No.-0651751
Session: July 2006

To

DEPARTMENT OF MATHEMATICS

KHULNA UNIVERSITY OF ENGINEERING & TECHNOLOGY

Khulna-9203, BANGLADESH

JUNE, 2014

Approval

This is to certify that the thesis work submitted by ***Abul Kalam Azad*** entitled " *CFD Modeling of a Modified Ahmed Car Body for Reduced Drag* " has been approved by the board of examiners for the partial fulfillment of the requirements for the degree of *Doctor of Philosophy* in the Department of *Mathematics*, Khulna University of Engineering & Technology, Khulna, Bangladesh in December 2014.

BOARD OF EXAMINERS

1. 4/12/14 — Chairman (Supervisor)
Prof. Dr. Mohammad Arif Hossain
Department of Mathematics
KUET, Khulna-9203

2. Member (Co-Supervisor)
Prof. Dr. A.K.M. Sadrul Islam
Department of MCE
IUT, Gazipur.

3. 04.12.14 — Member
Head
Department of Mathematics
KUET, Khulna-9203

4. 04.12-14 — Member
Prof. Dr. M.M. Touhid Hossain
Department of Mathematics
KUET, Khulna-9203

5. 04.12.14 — Member
Prof. Dr. Khandkar Aftab Hossain
Department of Mechanical Engineering
KUET, Khulna-9203.

6. Member
Prof. Dr. Mohammad Mashud
Department of Mechanical Engineering
KUET, Khulna-9203

7. 12.14 — Member
Prof. Dr. Md. Shamsul Alam Sarkar
Department of Applied Mathematics
University of Rajshahi, Rajshahi.

8. 4.12.14 — Member (External)
Prof. Dr. M K Chowdhury
Department of Mathematics
Bangladesh University of Engineering and Technology, Dhaka-1000.

9. Member (External)
Dr. Firoz Alam
Associate Professor & Deputy Head of School, Teaching & Learning School of Aerospace, Mechanical and Manufacturing Engineering, RMIT University, Melbourne, Australia.

DECLARATION

This is to certify that the thesis work entitled **"CFD Modeling of a Modified Ahmed Car Body for Reduced Drag"** has been carried out by Abul Kalam Azad in the Department of Mathematics, Khulna University of Engineering & Technology, Khulna, Bangladesh. The above research work or any part of this work has not been submitted any where for the award of any degree or diploma.

10.06.14

Abul Kalam Azad

Roll No.-0651751

Arif 10/6/14

Supervisor

Mohammad Arif Hossain

Professor

Department of Mathematics,
Khulna University of Engineering & Technology
Khulna, Bangladesh

10/6/14

Co-Supervisor

A. K. M. Sadrul Islam

Professor

Department of Mechanical and Chemical Engineering,
Islamic University of Technology,
Dhaka, Bangladesh

List of Publications from the present thesis

Comparison of Turbulence Models for Ahmed Car Body Simulation

Abul Kalam Azad[1], Mohammad Arif Hossain[1], A. K. M. Sadrul Islam[2]

[1]Department of Mathematics, Khulna University of Engineering & Technology, Khulna, Bangladesh

[2] Department of Mechanical and Chemical Engineering, Islamic University of Technology, Dhaka, Bangladesh
5th BSME International Conference on Thermal Engineering, IUT, Dhaka, Bangladesh, 2012.

Effect of Roughness Height on the Turbulence Models for Ahmed Car Body Simulation

Abul Kalam Azad[1], Mohammad Arif Hossain[1], A. K. M. Sadrul Islam[2]

[1]Department of Mathematics, Khulna University of Engineering & Technology, Khulna, Bangladesh

[2] Department of Mechanical and Chemical Engineering, Islamic University of Technology, Dhaka, Bangladesh
International Conference on Mechanica , Industrial and Materials Engineering, RUET, Rajshahi, Bangladesh, 2013.

Passive Strategies to Control the Flow Around the Ahmed Body

Abul Kalam Azad[1], Mohammad Arif Hossain[1], A. K. M. Sadrul Islam[2]

[1]Department of Mathematics, Khulna University of Engineering & Technology, Khulna, Bangladesh

[2] Department of Mechanical and Chemical Engineering, Islamic University of Technology, Dhaka, Bangladesh
18th International mathematics Conference, IUB, Dhaka 2014.

Effect of channeling at the slant surface of the Ahmed car body

Abul Kalam Azad[1], Mohammad Arif Hossain[1], A. K. M. Sadrul Islam[2]

[1]Department of Mathematics, Khulna University of Engineering & Technology, Khulna, Bangladesh

[2] Department of Mechanical and Chemical Engineering, Islamic University of Technology, Dhaka, Bangladesh

National Conference on Physics for Sustainable Development,, KUET, Khulna, Bangladesh, 2014.

Abstract

The wake flow behind the car presents the major contribution to a car drag. The flow over a car body is very complex. Hence MOVA consortium partners agreed to study the vehicle shape employed by Ahmed and Ramm (1984), known as Ahmed body. The aerodynamic drag of the body has great impact on the fuel consumption by a car. So for economic and for environmental reasons also drag reduction is very important. The CFD model is used to investigate and for the better understanding of the aerodynamic behavior of the flow in the surrounding area of the vehicle.

The development of a good CFD model depends firstly on investigating and selecting the best grid configurations. In this simulation experiment the total element count after final refinement was within an acceptable limit 1.7 to 2 million grids. The performance of a CFD model is not only depends on the number of grids but also on the turbulence model chosen for the simulation. Sometimes on the basis of the turbulence model chosen it is also required to select the roughness height.

For the above mention purpose in this simulation study it has been found that a total of 1.7 million grids are suitable and acceptable. To select this number grid dependence test is performed. To choose the turbulence model a comparison among different turbulence models is done. On the basis of Azad et al. (2012) the k-ε model, which is better suited, is chosen for the simulations. As k-ε model has dependence on the roughness height it was required to choose also. A further study is done to find it and the findings are published. Azad et al. (2013) has shown the results and according to them the selection of the roughness height as 0.0002m is the best choice.

Out of the two strategies active and passive, a passive strategy is chosen to reduce the drag over the Ahmed car body. To manipulate the flow insertion of grooves has been considered. The grooves are placed at the top, at the slant, at the top and slant, and at the rear surface of the body.

The drag, after modeling the Ahmed body, is then calculated using ANSYS-11. The results thus obtained are compared with the results obtained by Lienhart et al. (2000). It has been found that overall drag has reduced.

Acknowledgement

The author would like to express his deepest gratitude and appreciation to his honourable supervisor Dr. Mohammad Arif Hossain, Professor, Department of Mathematics, Khulna University of Engineering & Technology (KUET), Khulna, under whose guidance the work was accomplished. The another would also like to thank Prof. Arif Hossain for his earnest feelings and help in matters concerning author's research affairs as well as personal affairs.

I express my deepest sense of gratitude to my reverend co-supervisor Prof. Dr. A.K.M. Sadrul Islam, Department of Mechanical and Chemical Engineering, Islamic University of Technology, Dhaka, Bangladesh, for his willingness to accept me as a research student. He helped me immensely with his supervision, invaluable instructions, encouragement and constructive discussion throughout this research work.

I thank all other teachers of the Department of Mathematics, KUET for their necessary advice and cordial cooperation during the period of study. I thank all the research students of this department for their help in many respects.

I express my earnest gratitude to Md. Hamidur Rahman, Asst. Prof. of the Department of Mechanical and Chemical Engineering, Islamic University of Technology, Dhaka, Bangladesh, for his personal tribute to my thesis.

I would also like to thank the authority of Rayermohal (Honours) College, Khulna for providing me with an opportunity to undertake this work in the Department of Mathematics, Khulna University of Engineering & Technology (KUET), Khulna.

Finally, I would express a special thank to my beloved wife Perveen Sultana for her constant encouragement and generous help. My profound debts to my father and mother are also unlimited.

Table of Contents

List of Figures

List of Tables

Abbreviations and Acronyms

Cp-	Coefficient of Static Pressure
CFD –	Computational Fluid Dynamics
DDES-	Delayed Detached- Eddy Simulation
DES-	Detached- Eddy Simulation
DNS-	Direct Numerical simulation
ENSB.-	Extension of Near-wake Separation Bubble
HTM-	Hybrid Turbulence Model
LES-	Large Eddy Simulation
LSTM-	Lehrstuhl fur Stromungsmechanik
MOVA-	Models for Vehicle Aerodynamics
Pr-	Prandtl number
RANS-	Reynolds Averaged Navier-Stokes equation
RMS-	Root Mean Square
RNG-	Re-Normalization Group
RSM-	Reynolds Stress turbulence Model
SST-	Shear Stress Transport
TRANS-	Transient Reynolds Averaged Navier-Stokes
VGs-	Vortex Generators

Nomenclature

U-	Characteristic velocity
u, v, w-	Instantaneous Velocity component in the x, y and z directions
l, L, d-	Length Scale
ρ-	Density
$\hat{\upsilon}$	Kinematic viscosity
I_u, T_i –	Turbulent Intensity
k-	Turbulence kinetic energy
κ-	Karman constant
U, V, W –	Mean Velocity in the x, y and z directions
x, y, z –	Spatial Dimension in the Streamwise, Crosswise and Vertical directions
p-	Instantaneous Pressure
P-	Mean Pressure
f–	Frequency
T_{ij}-	Lighthill Stress Tensor
S-	Mean Strain Rate, Source Term
ε-	Dissipation Rate
ω	Specific Dissipation Rate
u_*-	Friction Velocity
u^+-	Dimensionless Velocity from the Wall
$y+$-	Dimensionless Distance from the Wall
Ω-	Vorticity Term
δ-	Kronecker Delta
τ-	Turbulent Shear Stress
μ-	Coefficient of Viscosity of the Fluid/Dynamic Viscosity
t, T –	Time

Chapter 1

1.0 INTRODUCTION

1.1 Research Background and Motivation

1.1.1 History of Vehicle Aerodynamics: A General Background

There are many interesting phenomena appearing in the laminar flow with the growth of Reynolds number. For some value Re_{crit}, the disturbance introduced into flow, instead of being damped, becomes amplified. The flow became unstable and this value of Reynolds number is called critical. Flow stability analysis is usually performed for simple geometries. The nonparallel flow formulation extends the validity of the analysis to general flow. Study of vehicle aerodynamics first began during the earlier part of the 20th century and has continued up until the present day. During the earlier part of the 20th century, vehicle aerodynamics study was associated with vehicle performance, Hucho (1998). Drag reduction, more efficient engine technology and weight reduction, becomes the primary design goals for vehicle engineers and designers around the world in the 1960's to 1980's. Average drag coefficient for typical cars dropped substantially from around 0.5 in the 1960's to typically 0.3 in the late 1980's and mid 1990's Hucho (1998), Wathkins and Alam (2012). At low speeds the main source of drag is the rolling resistance. To achieve high vehicle performance, much of the attention focuses on lowering the vehicle drag coefficient (C_D), which accounted to about 75% to 80% of total motion resistance at 100km/h, Hucho (1998). However, in the latest part of the 20th century, during the oil crisis of 1973-1974, the focus on vehicle aerodynamics study shifted towards lowering the drag coefficient in order to produce vehicles with better fuel economy, Hucho (1998). The trend shifted again in the early 1990's especially in North America where a low fuel price coupled with the increased popularity of light trucks and sport utility vehicles have, reduced the importance the need on research to reduce drag coefficient, George et al. (1997).

According to the conclusions of International Energy Agency in World Energy Outlook 2007, the gas emissions with greenhouse effect will increase close to 57% in 2030 with strong effects on the environment and the climate.

The human activities became main cause of the increase of the greenhouse gases effect and average global temperature. The activities included the transportation sector where the growth number of automobile is rapidly increasing and make the fuel consumption increases as well. It tends to create harmful effect on the environment because it increases air pollution in the world. Based on these problems it has become a must for automobile industry in the word to immediately create an environmentally friendly automobiles and efficient in fuel consumption.

Fuel consumption of automobile is related to its aerodynamics drag, and the magnitude of aerodynamic drag is highly influenced by separation flows around its shape. Meanwhile, the flow around a traveling automobile is complex and presents nonlinear interactions between different parts of the automobile so that many research institutions and industrial laboratories have been focusing their investigations automotive aerodynamics with numerical studies, Gad-El-Hak (1996). It is necessary to modify locally the flow, to remove or delay the recirculation zone at the back end of the separated swirling structures. This can be mainly obtained by controlling the flow near the wall with or without additional energy using active or passive devices, Fieldler and Femholz (1990). Harinaldi et al. (2011) worked on the reversed Ahmed body; they used an active flow control solution by suction and blowing to reduce the aerodynamic drag. The maximum drag reductions associated with these modifications are close to 15.83%.

The optimization of vehicle, shapes and the incorporation of commonly used passive control devices have already brought about a significant aerodynamic drag reduction (from C_x= 0.45 in 1975 to C_x = 0.35 in 1985, C_x being the average drag coefficient), Hucho (1998) and Gad-El-Hak (1996). The need to further reduce fuel consumption and provide automobile designers with more creative liberty is prompting the automobile industry to develop innovative active flow control solutions. Such solutions Glezer and Amitay (2002) use an external energy source to modify the topology without necessarily modifying the shape of the vehicle. Different control techniques have been analyzed in university and industrial laboratories and significant results have been obtained on academic geometries, Glezer and Amitay (2002). Continuous suction and or blowing solutions offer a promising alternative, Kourta and Vitale (2008) and seen well- adapted to the automobile context, Gillieron et al. (2002). For example, the efficiency of a suction system in controlling the separation of the boundary layer has been highlighted experimentally on a cylinder by Bourgois and Tensis (2003) and Fournier et al.(2004).

The results indicate that significant drag reductions, close to 30%, are obtained by moving the flow separation downstream. Similar results are obtained by Roumeas et al. (2005) on a simplified 2D fastback car geometry. In this case, the drag reduction is associated with the elimination of the separated layer on the rear window when suction is applied.

Many active control techniques which have been developed by focusing on local intervention in wall turbulence deal with steady blowing or suction, Kogstad (2000), Park and Choi (1999), and Sano and Hirayama (1985). A blowing devices installed in an ONERA D profile can shift or even prevent the flow separation to occur, Evanic and Gillieron (2004). A local suction system located on the upper part of the rear window is capable of eliminating the rear window separation on simplified fastback car geometry. Bruneau et al. (2007) has used passive strategies for flow manipulation around the Ahmed body. Aerodynamic drag reductions close to 17% have been obtained, Roumeas et al. (2009).

However, to be practically implemented in controlling the flow separation in the automotive application the passive control methods still need further comprehensive investigations to obtain some fundamental insights of the governing mechanism of separation control. Hence, the current investigation was a part of a long-term fundamental investigation to develop a passive control to the turbulent flow separation which is a fundamental phenomenon governing the aerodynamics performance of vehicle body. In this study, the Ahmed Car Body is modeled.

The wake flow behind the car is the major contribution around a car body and is responsible for creating severe problems to numerical prediction and experimental study of the flow. The location at which the flow separates determines the size of the separation zone, and consequently the drag force. Clearly, a more exact simulation of the wake flow and of the separation process is essential for the correctness of drag predictions.

1.1.2 Ahmed Body

A real- life automobile is a very complex shape to model or to study experimentally. Therefore the "Models for Vehicle Aerodynamics" (MOVA) consortium partners (TU Delft, University of Manchester, LSTM, Electricite de France, AVL List, and PSA

Peugeot Citroen) agreed to study the vehicle shape employed by Ahmed (1984), known as the Ahmed body, Lienhart et al. (2000).

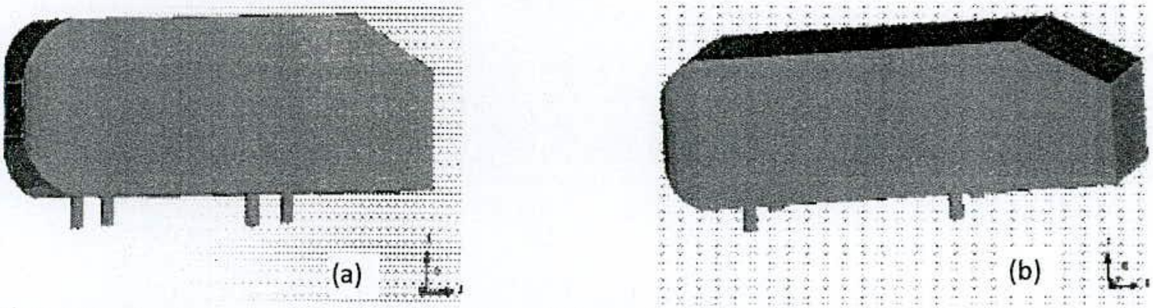

Figure 1.1 (a, b): Geometric presentation of the body with 25° slant angle.

The geometry of body is shown in Fig.1.1 (a, b). All the geometric quantities are normalized with the body height H=0.288m. The values of the geometric quantities are $l_r/H=2.928$, $G/H=0.697$ and $W/H=1.35$, where l_r is the length from the beginning of the slant to the front, G is the length of the slant region and W is the width of the body. The front part is rounded with a radius of $R/H=0.347$in the plane, $y=0$ and $z=0$. The body is lifted from the floor, producing a ground clearance of $C/H=0.174$ on the four pillar. The center of the both front pillars are located at a distance of 0.753H from the front face of the body The center of the both back pillars are located at a distance of 1.632H from the front pillar center. The distance of front two pillars' center is 1.135H. Radius of the all pillars is 0.052H. The ground plane is $z = 0$ and $x = 0$ and $y = 0$ are at the position of the rear vertical surface and the symmetry plane of the body. The slant angle is taken as 25°.

1.1.3 Airflow Around a Ground Vehicle

Analysis of flows around a ground vehicle however, presents a different problem. In contrast to a streamline body of an aircraft, ground vehicle can be tired as a bluff body. The streamline feature of an aircraft causes airflow around it to be nearly two-dimensional. This results in airflow around the aircraft to be fully attached over most of its surface, Barnard (1996). On ground vehicle, the flows are strongly turbulent and three dimensional with steep pressure gradients, Ahmed (1998). According to Alam (2000), ground vehicles operate in the surrounding ambient turbulent wind that almost constantly present. This is different for aircraft since they travel above the turbulent atmospheric boundary layer. Furthermore, road vehicles can also travel at various high yaw angles depending on the nature of cross wind. Traveling at various yaw angles causes increased separated flow on the leeward side of the vehicle, adding more complexity to the flow field. Airflow movement around the vehicle starts from the front. According to Barnard (1996) the airflow movement will cause the development of boundary layer close to the vehicle wall surface. The boundary layer thickness will increase as the airflow movement progressed around the vehicle. Barnard (1996) classified the boundary layer generation on the vehicle wall surface into two stages, laminar and turbulent. During the initial stage, boundary layer flow exists in a laminar form. Near the front edge of the vehicle, with in boundary layer due to viscous effect layer closed to the vehicle wall surface will have more fractions and that will cause the outer air layer moving faster than the inner one. This will slow down the flow. The slowing effect spreads outwards and the boundary layer gradually becomes thicker. According to Barnard (1996), on most ground vehicles, the laminar boundary layer does not extend for much more than about 30 cm from the front. Further downstream to the flow, instability develops and a transition to a turbulent flow takes place. In the turbulent boundary layer, the flow is still streamlined in the sense that it follows the contours of the body. The turbulent motions are still of very small scale. In the turbulent boundary layer, eddies are found (groups of air molecules) resulting in rapid mixing of fast and slow moving masses of air (turbulent diffusion) . The turbulent mixing will then move further outwards from the surface. However, very close to the surface within a turbulent boundary layer flow, a thin sub layer of laminar flow still exists. An important differences between the flow mechanisms in the laminar and turbulent flow is that in laminar flow, the influence of the surface is transmitted outwards mainly by a process of molecular impacts, whereas in the turbulent flow the influence is spread by turbulent mixing.

In the turbulent boundary layer, some of the energy is dissipated in friction, slowing airflow velocity, resulting in a pressure increase. If the increase in pressure is gradual, the process of turbulent mixing will cause a transfer of energy from the fast moving eddies in the turbulent boundary layer. If the rate of change in pressure is too great, for example in sharp corners, the mixing process will be too slow to push the slower air molecules moving. When this happens, the boundary layer flow stops following the contours of the surface, resulting in separation. Air particles downstream of the separation region will then moves towards the lower pressure region in the reverse direction to the main flow. This is known as an adverse pressure gradient. At downstream of the flow, the separation region will reattach. The point between the region of separation and reattachment, where air is circulating is called the 'separation bubble'. Separation will normally occur if the resultant flow encounters a sharp edge. It is always important for ground vehicles to have smoothly rounded edges everywhere. Each type of separation can form a separation bubble zone either by reattaching itself downstream to the flow or it can be transformed into a wake, which recirculate frequently. Hucho named this frequent circulation as 'dead water' zone, a term used in navel architecture. Farabee (1986) pointed that the length of the separation bubble can be up to 100 timed its height. Separation bubble zone happens normally on area in front of the windshield and on the side of the fenders while "dead water" zone normally happens on the rear surface of the ground vehicle.

The effect of separation and reattachment dominates most of the ground vehicle surface region. According to Ahmed (1998), vehicle aerodynamics operates mainly in the Reynolds number region in excess of 10^6. Typical areas around the vehicle that exhibit small region of separation are the body appendages such as the mirror, headlights, windshield wipers, door handles and windshield junction. Larger flow separation regions around the vehicle include the A-pillar, body underside, rear body of the vehicle and in the wheel wells, Hucho (1998). In a similar perspective, Ahmed (1998) defined the airflow as three dimensional with steep pressure gradients and having regions of separated flow.

Although airflow around a ground vehicle exists predominantly in three-dimensional form, Hucho (1998) indicated that a quasi two-dimensional flow types also exist. The quasi two-dimensional type flow separates on the edge running perpendicular to the local direction of flow. The separation causes vortices to roll up with their axes almost parallel to the separation line. Turbulent mixing dissipates most of their kinetic energy making their development as continuing free trailing vortices, often weak and even untraceable. The quasi two-dimensional flow often occurs around areas such as the hood front edge and the front part of the vehicle windshield. Furthermore, according to Hucho (1998), the second type of separation normally occurs at edges around which are flows at some angle. According to Hucho, the air stream then forms a cone-shaped helical vortex. The regions where these vortices tend to be generated most are behind the A and C pillars on a car. The axes of these vortices run essentially in the stream wise direction, The three dimensional vortices are very rich in kinetic energy and this containment in kinetic energy are determined by the ground vehicle geometrical conditions.

1.1.4 Vehicle Aerodynamics: Numerical and Computational Evaluation Methods

Numerical evaluation methods involving vehicle aerodynamics can be done either analytically or by using Computational Fluid Dynamics (CFD). Analytical methods in solving airflow behavior realistically can be done on simple generic type flow problems in either two-dimensional or three-dimensional form. As airflow behavior gets more complex when subjected to flow around complex geometrical domain or bluff bodies, (with the presence of turbulence or compressibility effect), solving airflow properties cannot be done analytically. This is because in order to obtain its complete turbulent and aerodynamic properties, full unsteady Navier-Stokes (taking into account inertia, viscous and pressure forces) together with the continuity equation (mass conservation) need to be solved. However, obtaining a direct numerical solution of Navier-stokes equations are still not yet possible even for modern day computers. The main reason being that grid positions needed for a typical CFD model to be solved are $Re^{9/4}$. For a typical flow with Reynolds number of 10^6, it will take the computer to generate and solve equations for 3.16×10^{13} gird points. This is far beyond the reach of even the most state of the art supercomputers available in the world today. In order to come up with a comparable solution, steady or time averaged Navier-stokes equation is used (called Reynolds Average Navier-stokes equation – RANS) together with turbulence model, developed to take into closure problems involving Reynolds stresses resulting from the time averaging process

CFD approach for turbulence modeling was first intended for the aerospace community in the 1960s and 1970s (Anderson, 1995). In the early development stage of CFD for automotive applications, codes were expected to provide actual quantitative data that is similar to measured wind tunnel data. Knowing that this is not yet possible, present use of CFD in automotive are used to provide information about flow characteristics and phenomena, which dictates aerodynamic performance. However, the ultimate goal in CFD is to obtain model of flow as actual as possible and current and future research on CFD is ongoing in order to achieve that goal. Furthermore, current applications of CFD in the automotive industry are determined by economic viability. To be economically viable, the codes should be able to simulate the correct physics of the flow and at the same time achieve computational turnaround time that is the same or less than that of a wind tunnel test cycle time. Ahmed (1998) has showed that for a typical vehicle, current testing time taken in a wind tunnel in order to achieve desired level of C_D reduction has increased. This will be an expensive exercise for automobile manufacturers. With the reduction on computational cost, aerodynamic simulation by using CFD, being run at a faster turnaround time will only be at a fraction of the cost.

However, this will only put more demand on the current performance of computers speed and memory. These are due to several factors:

- An increase in sophistication of flow physics modeled.
- An increase in modeled geometries complexities.
- An increasing number of multidisciplinary approaches of flow simulation.

These increases in computational demands are intended in achieving the ultimate goal 'fluid flow realism', in CFD simulation as mentioned earlier. A much more complex three-dimensional vehicle geometries are now being used in automotive CFD simulation coupled with high grid density to achieve better flow resolution. Usually this also leads to a more accurate and realistic flow simulation. In an unsteady three-dimensional flow, a doubling of grid density (to double the accuracy) results in a (with three space coordinates and a time dimension) sixteen-fold increase in computation effort. In addition, better CFD post processing flow visualization effect such as colour-coded pressure distributions over the entire body surface and observation of particle traces in real time animation also puts extra demand on computer speed and memory.

1.1.5 Turbulence

Turbulence in a fluid refers to three dimensional, unsteady motions of particles that are practically in chaotic manner. It appears in the flow field as a random process that is completely unpredictable. This is quite in contrast with the laminar state, where flow is apparently uniform and well-behaved. In a large variety of applications, it is possible to identify a base flow that is reasonably well-behaved and superimposed on which are random fluctuations in flow properties.

Turbulences have their great importance in computational fluid dynamics (CFD). The understanding of the physics of turbulence is critical and many different models have evolved to explain them. Sometimes the turbulence models are validated through vehicle aerodynamics. For many years computers have been used to solve fluid flow problems.

Numerous programs have been written to solve either specific problems, or specific classes of problems. In the mid-1970's general purpose CFD solvers were started to develop. Recent advances in computing power, together with powerful graphics and interactive 3D manipulation of models have made the process of creating a CFD model and analyzing results much less labor intensive and reducing time. Robust solutions of the flow field can be achieved through advanced solvers that contain algorithms which enable to solve the problem in a reasonable time.

1.1.6 Some Important Types of Flows

(a) Laminar and turbulent flows: A flow, in which each fluid particle traces out a definite curve and the curves traced out by any two different fluid particles do not intersect, is said to be laminar. On the other hand, a flow, in which each fluid particles does not trace out a definite curve and curve traced out by fluid particles intersect, is said to be turbulent. Practically in turbulent flow the fluid velocity varies very rapidly in an irregular manner. In other words, turbulence in a fluid refers to three dimensional, unsteady motions of particles that are practically in chaotic manner. Turbulent fluid motion is an irregular condition of flow in which the various quantities show a random variation with space and time coordinates, so that statistically, only distinct average values can be discerned (Hinze, 1959). The origin of turbulence lies in a region in the physical or parameter space adjacent to the laminar regime and is called as the transition region.

(b) Steady and unsteady flows: A flow in which properties condition (P, say) associated with the motion of the fluid are independent of the time so that the flow patterns remain unchanged with respect to time, is said to be steady. On the other hand, a flow, in which properties and conditions associated with the motion of the fluid depend on the time so that the flow pattern varies with time, is said to be unsteady.

(c) Homogeneous isotropic turbulence: The peculiarity of turbulence is that its behavior in different scales- both of time and of space is different, and it has been amply demonstrated that the smaller scales demonstrate a considerable degree of isotropy, for they are less affected by the boundaries of the flow. Homogeneity, again though rare in the large scale, is often present in the smaller scales. So the study of homogeneous isotropic flows is not altogether wasted even if we consider real flows. Homogeneity is really a contraction of 'spatial homogeneity' and indicates that mean properties do not vary with absolute position in a particular direction.

1.1.7 Consequences of Turbulence

A majority of engineering flows are turbulent; natural flows are invariably so. The presence of velocity fluctuations greatly enhance transfer rates of mass, momentum and energy and create effects that cannot be explained in intuitive terms. Heat transfer from a surface greatly increases if the flow is turbulent. Free stream turbulence or a turbulent boundary layer can delay flow separation on bluff objects and substantially lower drag. One of the harmonics of velocity fluctuation can induce resonance in structures exposed to flow by locking on to its natural frequency. Even otherwise, turbulence can induce vibrations, a phenomenon of great concern to aerospace engineers. The state of flow in rivers, oceans and atmosphere of our planet is turbulent, as a rule. Hence, all associated problems such as soil erosion, migration of marine life, dispersion of pollutants and to some extent, atmospheric convection are dependent on the structure of turbulence.

1.1.8 Physics of Turbulence Motion

Turbulence in fluids must satisfy the laws of classical physics, namely conservation of mass, Newton's second law of motion and conservation of energy. The fact that turbulence is chaotic shows that these constraints are not sufficiently strong to generate a unique flow field. Recently it has been originated to analyze turbulence as the result of a sequence of bifurcations of a low order dynamical system that is governed by a system of first order non-linear ordinary differential equations. These research initiatives throw light on details of physical processes observed in turbulent flow fields. An understanding in terms of turbulence physics is quite useful in evaluating models or developing new ones.

1.1.9 Numerical Computation of Turbulent Flows

The problem of calculating turbulence can be seen as part of the more general field of computational fluid dynamics (CFD). CFD is extensively concerned with the numerical representation and computation of the partial differential equations which govern the motion of real fluids. The subject tends to divide into two areas: the development of numerical methods, and the creation of algorithms to implement these methods. At the same time, progress in CFD must necessarily depend on developments in computing process. In particular, we should perhaps mention the growing use of concurrent computer architectures, which offer large increases in memory and speed. In the present day various type of turbulence models develop for simulating turbulent flows.

1.1.10 Vortex or Rotational Motion

Rotational motions differ from potential flows in that, as the name applies, all particles of the fluid or at least part of them rotate about an axis which moves with the fluid. Potential flow, on the other hand, is irrotational by definition.

1.1.11 Vortex Stretching

High levels of fluctuating vorticity are characteristic of all turbulent flows. This fact taken in conjunction with the historical development of fluid dynamics as a subject very much concerned with vortex motions, made it natural to interpret turbulence in terms of vortex stretching. Conservation of angular momentum (per unit fluid mass) can then be expressed in form

$$\omega_1^2 r = constant$$

where r is the radius of the vortex tube. Therefore, as r decreases under the influence of the extensional gradient, the angular velocity (proportional to ω_1) will increase, and accordingly the energy $(\omega_1^2 r)^2$ associated with scale r will also increase. Hence energy is transferred to the small scales.

1.1.12 Body and Surface Force

In the study of fluid dynamics we distinguish between two types of forces acting on a fluid element, namely, body forces and surface force. The body forces are distributed throughout the volume of the body, and these are usually expressed as 'force per unit mass of the element'. Examples are gravity and inertia forces. A force acting over the surface area is called the surface force. Surface force arises due to the action of surrounding fluid on the element under consideration through direct contract.

1.1.13 No slip Condition

This is the most common type of wall boundary condition. A real fluid, the existence of intermolecular attractions causes the fluid to adhere to a solid wall and this gives rise to shearing stress. The inner layers of a real fluid transmit tangential and normal stresses. On the boundary between a perfect fluid and a solid wall there exists a difference in relative tangential velocities i. e. there is slip. The existence of tangential (shearing) stresses and the condition of no slip near solid walls constitute the essential differences between a perfect and a real fluid. The real fluids have a zero velocity at the walls and hence they cannot slip at the boundary wall. This is known as no slip condition.

1.1.14 Boundary Layer Theory

(a) Prandtl's boundary layer theory: For convenience, consider laminar two-dimensional flow of fluid of small viscosity (large Reynold's number) over a fixed semi-infinite plate. It is observed that, unlike an ideal (non-viscous) fluid flow, the fluid does not slide over the plate, but "sticks" to it. Since the plate is at rest, the fluid in contact with it will also be at rest. As we move outwards along the normal, the velocity of the fluid will gradually increase and at a distance far from the plate the full stream velocity U is attained. However, it will be assumed that the transition from zero velocity at the plate to the full magnitude U takes place within a thin layer of fluid in contract with the plate. This is known as the boundary layer.

(b) Importance of Prandtl's boundary layer theory in the fluid dynamics: Although the boundary layer is thin, it plays a vital role in fluid dynamics. It has become a very powerful method of analyzing the complex behavior of real fluids. The concept of a boundary layer can be utilized to simplify the Navier-Stokes equations to such an extent that it becomes possible to take many practical problems of great importance. The drag on ships and vehicle the efficiency of compressors and turbines in jet engines, the effectiveness of air intakes for ram-and turbojets and so on depend on the concept of the boundary layer and its effects on the main flow. The boundary layer theory is able to predict flow separation. It can explain the existence of a wake. There exist a viscous stress on the boundary region and it acts in the direction of flow.

(c) Boundary layer thickness: The boundary layer thickness is defined as the elevation above the boundary which covers a region of flow where there is a large velocity gradient and consequently non-negligible viscous effect.

The boundary-layer thickness $\delta_{ij} = \sqrt{(\frac{\mu x}{\rho U_{\infty}})}$, where U_∞ is the velocity of the outer flow. ρ is the density, μ is coefficient of viscosity and x is the length of the plate.

(d) Displacement thickness: Because of viscosity the velocity on the vicinity 0f the plate is smaller than in the free-flow region. The displacement thickness is that distance by which the potential field of flow is displaced outwards as a consequence of the decrease in velocity in the boundary.

The displacement thickness $\delta_1 = \int_0^\infty \left(1 - \frac{u}{U_\infty}\right) dy$

(e) Momentum thickness: It is defined by comparing the loss of momentum due to wall-friction in the boundary to the momentum in the free flow region. The loss of momentum in the boundary layer as compared with potential flow is given by $\rho \int_0^\infty u(U_\infty - u)dy$.

The momentum thickness $\delta_2 = \int_0^\infty \frac{u}{U_\infty}\left(1 - \frac{u}{U_\infty}\right) dy$.

(f) The energy thickness: There is always a loss in energy because of the viscosity of the fluid. The loss of kinetic energy in the boundary layer at a distance y from the plate is $\frac{1}{2}\rho\left({U_\infty}^2 - u^2\right)$. The energy thickness δ_3 is defined as

$$\delta_3 = \int_0^\infty \frac{u}{U_\infty}\left(1 - \frac{u^2}{{U_\infty}^2}\right) dy.$$

1.1.15 Kolmogorov Hypothesis

Kolmogorov realized that the geometry and anisotropy of a flow-field will influence only the large scales (low wave number) of turbulent flow. The small scales of the flow will be less affected by the gross features of the flow and more influenced by the interaction between small eddies in the turbulent field. The statistics of this interaction will be approximately in equilibrium because even if the large scales are evolving in time the small eddies having much smaller time-scales will quickly settle into a quasi-equilibrium.

Taking the argument one step further we see that the statistics of the small scales being independent of the large scales of the flow and also being independent, by virtue of the equilibrium state, of the inertial conditions of the flow can therefore depend only on the energy dissipation rate ε and the viscosity ν, for viscous dissipation is inherently small-scale phenomenon. Using these broad physical arguments Kolmogorov postulated his first hypothesis: At sufficiently high Reynolds numbers there will exist a range of high wave numbers in which the turbulence is in a state of statistical equilibrium influenced only by the parameters ε and ν (energy dissipation rate ε and viscosity ν).

1.1.16 Some Important Non dimensional Quantities

(a) Reynolds number, Re: It is the most important parameter of the fluid dynamics of a viscous fluid. It represents the ratio of the inertia force to viscous force a and is defined as

Re = inertia force /viscous force = $\rho U^2L^2/\mu UL = UL/\vartheta$

where U, L, ρ, μ and ϑ are the characteristic value of velocity, length, density, coefficient

of viscosity or coefficient of dynamic viscosity and coefficient of kinematic viscosity of the fluid respectively. When the Reynolds number of the system is small the viscous force is predominant and the effect of viscosity is important in the whole velocity fluid. When the Reynolds number is large the inertia force is predominant, and the effect of viscosity is important only in a narrow region near the solid wall or other restricted region which is known as boundary layer. If the Reynolds number is enormously large ($Re \geq 2000$), the flow becomes turbulent. A critical Reynolds number $Re_{crit} = 5\times10^5$ is visible in the drag coefficient C_D (Re) of a flat plate at zero incidence. For Reynolds numbers which are smaller than Re_{crit}, the flow past the plate is laminar: and above Re_{crit} the flow past the plate is turbulent.

(b) Prandtl number, Pr: The Prandtl number is defined by

$Pr = \mu g c_p/k$,

which is the ratio of kinematic viscosity to the thermal diffusivity,

where c_p is the specific heat at constant pressure and k is the conductivity. Evidently Pr depends only on the properties of the fluid. For air Pr = 0.7 approx. and for water (at 60°F) Pr = 7 approximately.

(c) Mach number M: The mach number M is defined by $M = q/a$,

where q is the velocity of flow and a is the velocity of sound. Mach number is also expressed in terms of the ratio of inertia force and the elastic force. When the Mach number is small (i. e., $M \ll 1$), the fluid can be taken as incompressible. On the other hand, if Mach number is nearly one or greater than one, the fluid will be taken as compressible.

(d) Euler number Eu: Eu = pressure force / Inertia force = $P/V^2\rho$

where P, V and ρ are the characteristic pressure, characteristic velocity and density respectively. When the pressure force is the predominating force, Euler's number must be the same for dynamic similarity of two flows.

1.1.17 Grid Points

To compute a turbulent flow by directly using the Navier- stokes equations would require us to use approximately $Re^{3/4}$ grid points in each direction and about $Re^{1/2}$ time-steps. So for a typical Reynolds number of 10^6 we would need more than 10000 grid points in each direction (or a total of 10^{12} grid points for a three dimensional calculation) and more than 1000 time-steps to get a reasonable simulation of the flow.

1.1.18 Turbulence Modeling

Generating turbulence information by solving the full Navier–Stokes or Reynolds-Stress equations remains incomplete at the time. Instead, analysts resort to approximate approaches, called as modeling. Turbulence modeling is based on the assumption that the real flow field may be substituted by an imaginary field of mathematically defined continuous functions. These functions usually represent physical quantities measurable in the flow field. Many turbulence modeling techniques deal with approximation to the Navier-Stokes or Reynolds-Stress equations. Any model, up to some extent can be analytically derived from Reynolds- stress equations. The main goals of turbulence modeling are: develop a set of constitutive relations valid for any general turbulent flow problem; yield sufficiently reliable answers and offer a degree of universality sufficient to justify their usage in comparison to cheaper, less general methods or to more expensive but potentially more reliable methods.

Early work on modeling turbulence was attracted by Newton's law of viscosity. An eddy viscosity a new property of turbulence was introduced and specified for different turbulent flows. Many simple models based on the eddy viscosity concept, particularly Prandtl mixing length models were developed to predict the mean velocity profiles in turbulent flows. These models continue to be in use because of their simplicity and sufficient accuracy in determining global quantities such as boundary-layer thickness, wall shear stress and point of separation. Use of these models produced analytical solutions for many simple engineering problems. Advanced engineering applications require identification of structures and calculation of statistical parameters, spectral functions, Reynolds stress distribution and turbulence heat and mass flux distributions. The model that must then be selected depends on the level of detail to be captured by the solution.

1.1.19 Drag Coefficient

The drag experienced by a plate is purely friction drag. This can easily be determined from the equation given below.

$$D = b\int_0^l \tau_w(x)dx \tag{1.1}$$

From the equation (1) we get the drag of one side of the plate, where b is the width of the plate and l its length. Now the local wall shear stress is

$$\tau_w(x) = \mu(\frac{\partial u}{\partial y})_w = \mu U_\propto \sqrt{\frac{U_\propto}{2\nu x} f_w''} = 0.332\mu U_\propto \sqrt{\frac{U_\propto}{\nu x}} \tag{1.2}$$

where f_w'' is the characteristic value for the boundary layer on a flat plate at zero incidence. The skin-friction coefficient in the equation

$$C_f(x^*) = \frac{2\tau_w(x^*)}{\rho V^2} \tag{1.3}$$

With the reference velocity $U_\propto$ it becomes

$$C_f(x) = \frac{2\tau_w(x)}{\rho U^2} = \frac{0.664}{\sqrt{\text{Re}_x}} \tag{1.4}$$

where the Reynolds number formed with the length x has been used:

$$\mathrm{Re}_x = \frac{U_\alpha x}{\nu} \tag{1.5}$$

If we want to estimate the value of drag coefficient in the usual manner, then we use the following equation:

$$C_D = \frac{2D}{\rho U_\alpha^2 bl} \tag{1.6}$$

where the wetted area *bl* serves as a reference area.

1.1.20 Roughness Height

The roughness height is the height of the surface irregularities for uniform sand grain roughness, or a mean height value for non-uniform sand- grain roughness. All surfaces in technical applications like the surface of a car are rough with a deviation in roughness height. We have it even for very smooth surface. In most CFD program a standard roughness is set. But if we have a much rough surface like sand corn size we have to modify the wall functions for the turbulence model with the right roughness height.

1.1.21 Computational Fluid Dynamics CFD

Computational Fluid Dynamics CFD is a computer- based tool for simulating the behavior of systems involving fluid flow, heat transfer, and other related physical processes. It works by solving the equations of fluid flow (in a special form) over a region of inter the history of CFD.

1.2 Research Objectives

In this study the flow behavior will be studied around the Ahmed car body. Ahmed car body has been considered to investigate the flow patterns around it to understand the drag behavior and its possible reduction. To achieve this goal the objectives of this study are as follows:

(i) To test various turbulence models namely, k-ε, k-ω, Shear Stress Transport (SST) and Baseline k-omega (BSL) in order to find out which model gives the more accurate results.

(ii) To test the effect of roughness height of the Ahmed car body.

(iii) To use passive strategies for drag reduction.

1.3 Thesis Outline

The thesis titled 'CFD Modeling of a Modified Ahmed Car Body for Reduced Drag' will be presented in five chapters. The Chapter 1 is naturally introduction, in which research background and motivation along with research objectives are presented. Research background and motivation contains history of vehicle aerodynamics; air flow around a ground vehicle, including Ahmed body; vehicle aerodynamics, different types of flow, turbulence and many other fundamental topics related to the research.

The literature review is presented as Chapter 2. In literature review a total of 23 articles are discussed. That has been presented in the chronological order.

The title of Chapter 3 is methodology. In this chapter discussion about the CFD software; model geometry; transport equation, boundary conditions and solution procedure are presented. Special attentions are given on the different turbulence models and some turbulence models are discussed in this chapter.

Chapter 4 contains results and discussion. Here the parameter chosen for the studies is discussed in 'code validation'. The dependence of the results on the number of grid is presented in this chapter as 'grid dependence test'. To reduce the drag we have proposed to introduce grooves at different positions over the body which is of course basically a passive strategy. A total of 30 cases are studied with different number, shape and position of grooves that provides different drags.

Finally the conclusion of the studies is presented in Chapter 5.

References, list of tables, list of figures, abbreviations and acronyms and nomenclatures are presented separately.

Chapter 2

2.0 LITERATURE REVIEW

Over the years, research studies concerning vehicles aerodynamics have focused mainly in understanding the mechanics of airflow behavior when exposed to various vehicles. Research studies conducted are predominantly using experimental and numerical method or a combination of both.

Fricke and Stevenson (1968) and Fricke (1971) conducted studies on pressure fluctuations on separated flow and concluded that the wall pressure fluctuations of subsonic separated flow are an order of magnitude higher than those beneath a boundary layer and that the source of wall pressure fluctuations is in the shear layer above the re-circulating flow, close to the reattachment point. This was different to the findings of Mohsen (1967) in which he discovered that maximum pressure fluctuations occur near the reattachment region of the flow.

Watanabe et al. (1978) experimented with a slanted angle A-pillar model that showed a conical vortex structure generated behind the A-pillar region. High-pressure region centered at the vortex core with intense pressure distribution being strongest at the A-pillar base and area close to the A-pillar (Cp values is around -2.0). The vortex flow grew weaker as it rotates further from the A-pillar base, particularly around the roof region, next to the A-pillar (Cp values is around -0.7).

Simpson (1987, 1989) explained that the effective pressure fluctuations of vortex flow might be near the locus of maximum shear stress position of the separating turbulent boundary layer. The large-scale motions produced in the vortex flow separation do not contribute much to the turbulent shear stresses. It only changes the mean flow-field to produce low frequency pressure fluctuations at the low Mach number.

Bearman et al. (1989) conducted several experimental tests with numerical type validation of a passenger car and simplified scale models. The tests were carried out to examine the effect of vortices generation in vehicle under wind yaw condition while exposed to wind of 20m/s. A maximum yaw angle of 20° was investigated with increment of 5°. It was observed that the effect of vortex increases at higher yaw angle in the leeward region of the car with sudden escalation after 10°. It was not mentioned in the paper about the windshield angle and radius used in the experiment. When surface pressure measurements were taken on the surface of the A-pillar region (did not mention where exactly) at 0° yaw, it was found that minimum Cp was between -1.4 and -1.5. In addition it was stated that the A-pillar region of flow were highly unsteady and the vortex strength kept changing with time.

Popat (1991) experimented on effect of windshield angle on A-pillar vortex. Popat noted some Reynolds number sensitivities at different A-pillar slant angle except for when the inclination angle is at 60°. Popat noted in his thesis three stage of vortex formation at different A-pillar slant angle with only bubble separation occurring below 20°, vortex-bubble separation occurring between 30° to 40° and fully developed conical vortex occurring between 50°to 60° slant A-pillar angle, which is what normally experienced on a normal production car. Popat concluded that the critical angle at which peak mean and fluctuating pressure values occurred at 40° inclination.

Nienaltowska (1993) studied the flow behind the A-pillar at various velocities and measured pressure and velocity fluctuations at points away and perpendicularly from the side window. Nienaltowska found that turbulence generation is independent of velocity and that it decreases with wall distance. Turbulence generation is highest in the direction perpendicular to the flow (w-component).

Uchida et al. (1997) conducted simulation by using SCRYU, a commercial CFD software, to demonstrate the capabilities of using solution adaptive grids in modeling A-pillar flow with side mirrors. Although they managed to show an improved vortex generation from their simulation, they did not justify their findings with any validations against experimental data. The study was more of a parametric study for qualitative observation and focused on showing the effectiveness of the solution adaptive grid techniques for mesh refinements and further evaluation and behaviour of airflow behind the A-pillar region was not discussed.

Alam et al. (1998) experimented with scale vehicle models exposed at various wind tunnel velocities at different yaw angle and found some Reynolds number dependency at low velocity (40 and 60km/h). Furthermore, they observed that there is a larger separation on the leeward side with associated velocity drop and increased turbulence intensity.

Alam (2000) extended his experimental testing on various windshield radii to see its effects on A-pillar flow behaviour. It was found that the pressure fluctuations have strong dependence on A- pillar region. This dependence is highest at negative yaw angle (leeward side) followed by 0° yaw angles and least at positive yaw angle (wind ward side) respectively. Alam also found that the surface mean and fluctuating pressure coefficients are independent of Reynolds number at higher velocities. In line with previous investigations, Alam found that the maximum hydrodynamic pressure fluctuations occur between the areas of separation and reattachment of the A-pillar vortex. In addition, Alam conducted results on modified A-pillar radius (making it smother). The highlight of the study was based on results plotted on a graph of maximum Cp RMS values at various yaw angles versus windshield radius. The results showed that as the windshield radius increase, the maximum value of Cp RMS for different yaw angle would decrease.

Lienhart at el. (2000) worked on the flow and turbulent structures in the wake of a simplified car model (Ahmed Model). A two-component laser-Doppler anemometer (LDA) was installed on an existing three dimensional computer controlled traversing system. LDA measurements were made for all three components of velocity in the symmetry plane from upstream of the Ahmed model to some distance downstream behind the closure of the wake. LDA measurements were also made in several transverse planes in the wake. They found two counter-rotating trailing vortices about 25° slant body. In the velocity distribution around the 25 degree slant Ahmed body they found two counter-rotating trailing vortices which they have shown in the transverse plane of turbulent kinetic energy (TKE) contour plots. Peaks in TKE occur in the centers of the vortices. These vortices are responsible for maintaining attached flow at the slant up to a slant angle of approximately 30°. Vortical structures extend more than 500mm beyond the end of the Ahmed body. Further they found that at 80mm downstream from the trailing edge of the Ahmed body, there is a large and strong region of recirculation back towards the Ahmed surface. At LSTM the drag coefficients they obtained at the nose, back, rear slop and the total are 0.0135, 0.1290, 0.1210 and 0.2635 respectively.

Liu and Moser (2003) discussed the wake flow behind the near wall region of Ahmed body for the effectiveness of three different turbulence models, including the $k-\varepsilon-v^2$ model, the k-ε model and the full stress model (in which SST and RMS models both have been considered). They used non-uniform structured grid with the near wall region where the total element number is 460000. They found that the unsteady wake comprises two vortices behind the rear with the larger one in the higher part and the smaller one in the lower part. It is found that the peak value of turbulent kinetic energy k is located in the centre of the small vortex downstream of the body, as observed in the experiment of Lienhart et al. (2000).They again found that the vertical structures extend more than 0.5m beyond the end the body rear. The reverse flow climbs up to the rear slant, as observed in the experiment of Lienhart et al. (2000). It confirms that two counter rotating trailing vortices are generated downstream of the Ahmed body, and the effect of the vortices, through very small, still remains at more than 1.5m away from the rear, and the velocity deficit still visible at more than 4m behind the Ahmed body. On the basis of the comparison of drag coefficients of LSTM experimental data, they have concluded that Durbin's $k - \varepsilon - v^2$ model gives the best result, followed by k-ε, SST and RMS model.

Zimmer (2003) extended Alam's (2000) testing; in that he conducted testing of A-pillar aerodynamic and aero-acoustics effect on full size vehicle. Zimmer conducted both wind tunnel and on road testing. Results obtained by Zimmer for wind tunnel testing showed different static and fluctuating pressure coefficient values with Alam when vehicle was yawed. Static pressure coefficient results obtained during on road testing were different, the difference may occur due to the presence of transient and crosswind. However, similar values were obtained when comparing fluctuating pressure coefficient results.

Krajnovic and Davidson (2005 a) worked with large eddy simulation (LES) that were made of flows around a Ahmed car body with 25° slant angle. Their target was to demonstrate the capacity of the LES to represent to flow around the Ahmed car body. For the purpose they concentrated on presenting the comparison of the LES and the experimental data. The three LES on different grids compared among themselves. They discussed about how flow changes with geometry where they used different computational grids those are 3.5 million nodes for coarse grid, 9.6 million for medium grid and 16.5 million for fine grid. They found that the length from the separation on the upper edge of the rear slant surface to the reattachment and near wake separation bubble are not equal in the coarse, medium and fine grid. Again they found that the time-averaged pressure drag and lift coefficients are different for different grid. Farther they found that the coarse grid simulation predict very unrealistic flow far above the boundary layer with oscillations.

Krajnovic and Davidson (2005 b) also worked to the flow structures and their interactions on the Ahmed body and study with various visualization tools. They found that, two structures distinguish themselves, cone-like vortices along the rear slanted edges and hairpin-like vortices in the regions of separated flows on the front and the rear slanted surface of the body. Both the time and the length scales of these two structures differ. While the cone-like vortices are of the size of the body and are relatively steady, the hairpin-like vortices are very small structures that change in shape over a short period of time. In the wake region they found also the existence of two vortices, one above the other. The core of the lower vortex keeps approximately, the same height with respect to the floor.

Stankiewicz et al. (2005) worked on the global stability analysis of Ahmed body. They performed experiments at two stages. First, the distance from Ahmed body to ground D was reduced at constant value of Reynolds number Re = 100. The object was placed in the middle of the domain (distance D = 4.5h). In second step, it was placed in proper distance (D = 0.17361h) from ground. The distance from ground to body was constant, and the Reynolds number was being changed. They investigated the influence of position of the body and Reynolds number on the stability properties. They found that when placed in middle of the domain (distance D = 4.5h), the Ahmed body behaves similar to circular cylinder. This behavior persists until D = 1.5h. During further reduction of the distance between the body and the ground the influence of boundary becomes more and more important, and for D < 0.66h the results begin to be similar to backward-facing step solution, with longer separation in steady solution. Again they worked to the influence of Reynolds number and found that at Re> 300 the flow is unstable. At Re = 325 there are three pair of unstable modes. The separation area for Re > 400 crosses the boundary of domain.

Bruneau et al. (2007) discussed passive strategies to manipulate flow around the Ahmed body. They have pointed that several separations of the flow appear along the body from the front to the back. They mentioned quoting (Gillieron and Spohn (2002) and Onorato et al.(1984)) that the resulting recirculation zones contribute to a significant part of the drag coefficient. They used passive control to porous interfaces to modify the boundary layer behavior and consequently to move downstream the separation line, to reduce the pressure gradients in the near wake and therefore the aerodynamic drag. A porous medium layer is inserted between the flow and the body to change the stress force (Caltagirone (1994) and Achdone et al.(1998)). They have used penalization method. This method was introduced in Arquis (1984)) a studied and validated in Angot et al.(1999), applied to turbulent flows in Kevlahan and Ghidaglia (2001) and to flow control in Bruneau and Mortazavi (2004). The best drag reduction they obtained by insertion of straight and continuous porous sheaths placed both on bottom and roof regions. Their numerical experimentations showed that front layers have no significant effect on the drag reduction. They also pointed that when back vorticity is reduced, the eddy is detached from the wall. This coincides with an increase of the back static pressure and therefore with a decrease of the drag forces.

Martinat et al. (2008) worked on the Ahmed body for numerical simulation of the flow in the wake at 25° and 35° slant angle. The 35° case studied with URANS turbulence model is able to predict the reattachment of the flow after the edge of the slant. They found that in case of strong non-equilibrium turbulence, which is the case of detached unsteady flows, traditional URANS are often insufficient to predict properly the detachment of the flow because of the assumption of equilibrium turbulence which leads to an over estimation of the eddy viscosity.

They again found that on the 35° test case, URANS models provided good result. On the 25° test case, none of the URANS models is able to predict the reattachment of the flow after lee edge of the slant. Detached Eddy Simulation (DES) approach was also unable to predict the reattachment of the flow. Using Delayed DES (DDES) solves the problem and in the case, the results provided, considering the reasonable small size of the mesh are very accurate.

Roumeas et al. (2009) worked for drag reductions on the Ahmed car body through flow separation control. For the purpose they have used suction and analyzed the sole suction to present flow separation which enhance the drag. They have studied the influence of suction on the rear window separated zone, on the longitudinal vortices and on the near-wake flow. They found that suction velocity has its influences on the drag reduction and obtained a reduction about 17% when suction velocity was 0.6 times of the external flow velocity.

Uruba and Hladik ((2009) discussed stationary and dynamical behavior of structures in wake. Two configurations of Ahmed body with slant angles of 25° and 35° are considered as the test-case. In 25° case they found very strong down-flow in the vicinity of the plane of symmetry and relatively weak contra-rotation vortex pair, while in 35° case much stronger vortices. The size of the back-flow region differs considerably for two cases in question, for the 35° case that is much bigger. They recognized the most intense turbulent activity near the bottom edge of the Ahmed body. In the case of 35° slant angle the secondary maximum of turbulent energy is located close just below roof level. They pointed that in 25° case the flow is more or less attached, while angle 35° generates fully detached flow from the ramp.

Harinaldi et al. (2011) have tested active flow control solution by suction and blowing to reduce the aerodynamic drag on reversed Ahmed body. In this van model they obtained a reduction of drag about 15.8% when suction velocity was 0.3 times of outer velocity. On the other hand in case of blowing about 14.3% drag reduction was obtained when blowing velocity was 0.06 times of the outer velocity.

Azad et al. (2012) compared the turbulence models for Ahmed car body simulation. The comparison was done among the velocity profiles at different locations over the Ahmed car body for k- ε, k- ω, Shear stress transport (SST) and Baseline k- ω (BSL) turbulence models. Velocities 40, 20, and 15m/s were taken in the simulations and the respective velocity profiles were compared for the different turbulence models. They found that all the four turbulence models are capable to capture most of the features of the velocity profile of the experimental data. Furthermore, they observed that near the body the performance of the k- ε model was best among the models considered but the deviation from the experimental was also larger at the height considered.

Azad et al. (2013) worked on the effect of roughness height on the turbulence models for Ahmed car body simulation. They compared the drag coefficients at different roughness heights over the Ahmed body for k-ε and Renormalization group (RNG) k-ε turbulence models. Velocity 40 m/s was taken in those simulations. They found that k-ε turbulence model has dependency on the roughness height, so in simulations care must be taken to choose this parameter when k-ε turbulence model be used.

Mashud et al. (2013) worked on reduction of fuel consumption of a car by aerodynamic drag reduction. The car they have chosen was a sedan and they introduced vortex generators for the purpose. They proposed that, "purpose of adding vortex generators (VGs) is to supply the momentum from higher region where has large momentum to lower region where has small momentum by stream wise vortices generated from VGs located just before the separation point. This allows the separation point to shift further downstream. Shifting the separation point downstream, therefore, provides dual advantages in drag reduction:-one is to narrow the separation region in which low pressure constitutes the cause of drag; another is to raise the pressure of the flow separation region. A combination of these two effects reduces the drag acting on the vehicle".

Chapter 3

3.0 METHOLODOGY

3.1 CFD Software

Computational Fluid Dynamics (CFD) is a computer-based tool for simulating the behavior of systems involving fluid flow, heat transfer, and other related physical processes. It works by solving the equations of fluid flow (in a special form) over a region of interest with specified conditions on the boundary of region.

The history of CFD

Computers have been used to solve fluid flow problems for many years. Numerous programs have been written to solve either specific problems, or specific classes of problems. From the mid-1970's, the complex mathematics required to generalize the algorithms began to be understood, and general purpose CFD solvers were developed. These began to appear in the early 1980's and required what were then very powerful computers as well as in-depth knowledge of fluid dynamics, and large amounts of time to set up simulations. Consequently CFD was a tool used almost exclusively in research.

Recent advances in computing power, together with powerful graphics and interactive 3D manipulation of models have made the process of creating a CFD model and analyzing results much less labor intensive, reducing time and hence, cost. Advanced solvers contain algorithms which enable robust solutions of the flow field in a reasonable time.

As a result of these factors Computational Fluid Dynamics is now an established industrial design tool, helping to reduce design time scales and improve processes throughout the engineering world. CFD provides a cost effective and accurate alternative to scale model testing, with variations on the simulation being performed quickly, offering obvious advantages.

The set of equations which describe the processes of momentum, heat and mass transfer are known as the Navier-Stokes equations. These partial differential equations were derived in the early nineteenth century and have no known general analytical solution but can be discretized and solved numerically.

Equations describing other processes can also be solved in conjunction with the Navier-Stokes equations. Often, an approximating model is used to derived these additional equations, turbulence models being a particularly important complex.

There are a number of different solution methods which are used in CFD code. The most common and the one on which ANSYS CFX is based, is known as the finite volume technique. In this technique, the region of interest is divided into small control volume. As a result an approximation of the value of each variable at specific points throughout the domain can be obtained. In this way one derives a full picture of the behavior of the flow.

In this simulations Ansys 11$^{©}$ with high resolution advection scheme along with Physical timescale (physical time = length of the tunnel/velocity of the fluid) is used.

3.2 Model Geometry

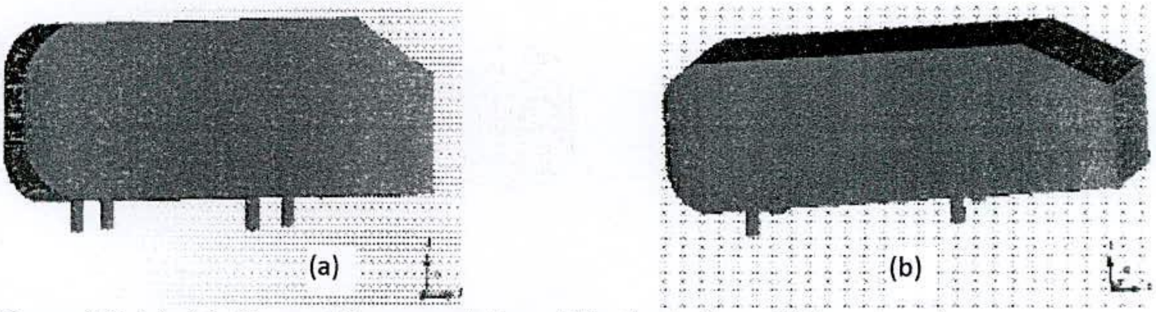

Figure 3.2.1 (a,b): Geometric presentation of the body from different angle.

The geometry of body is shown in Figure 3.2.1(a,b). All the geometric quantities are normalized with the body height H=0.288m. The values of the geometric quantities are $l_r/H=2.928$, $G/H=0.697$ and $W/H=1.35$, where l_r is the length from the beginning of the slant to the front, G is the length of the slant region and W is the width of the body. The front part is rounded with a radius of $R/H=0.347$in the plane, $y=0$ and $z=0$. The body is lifted from the floor, producing a ground clearance of $C/H=0.174$ on the four pillar. The center of the both front pillars is located at a distance of 0.753H from the front face of the body. The center of the both back pillars is located at a distance of 1.632H from the front pillar center. The distance of front two pillars' center is 1.135H. Radius of the all pillars is 0.052H. The ground plane is $z = 0$ and $x = 0$ and $y = 0$ are at the position of the rear vertical surface and the symmetry plane of the body. The slant angle is taken as 25°. It generates all essential features of flow around car (flow displacement around the nose, uniform flow at the middle and separation and wake at the end of body). Ahmed body wake may be considered as a combination of bluff-body wake and sudden-expansion channel or backward-facing step.

The body is placed in the channel with a cross section of $B \times F$=6.493H × 4.861H (width × height). The front face of the body is located at a distance of 7.3H from the channel inlet and the downstream length between the rear face of the body and the channel outlet is 21H. As a result the channel length is about 8.8069 times of the body length and the blockage is about 4.27%.

3.3 Transport Equations

3.3.1 Turbulence Models

For a three-dimensional flow, the system of equations consists of three RANS equations and continuity equation, which totals up to four equations. However, with four equations, the system needs to close up ten unknowns. This consists of one mean pressure, three mean velocity and six Reynolds stresses. Therefore, additional equations are needed to close the system. Closure of the system can be obtained through modeling of the Reynolds stress term in the RANS equation. This is also known as turbulence modeling. The realism of flow simulated by the RANS equations will be dependent on the turbulence model used.

Turbulence models based on RANS equations can be categorized into two groups. The first group use the 'eddy-viscosity' concept by modeling the Reynolds stresses based on the Boussinesq eddy-viscosity approximation. The second group is the non-eddy viscosity group, which attempts to solve for the Reynolds stresses directly. The eddy-viscosity turbulence models can be further classified into several groups.

(i)Algebraic (zero-equation) models

(ii)One-equation models

and (iii)Two-equation models

3.3.2 Algebraic (zero-equation) Turbulence Models

The most simplistic turbulence model is the algebraic Turbulence Model. It is also known as the zero-equation turbulence model. Prandtl (1925) was responsible for the origin of the algebraic turbulence model. Prandtl's work was inspired by the earlier work of Boussinesq (1877). Turbulence mixing length scale will be prescribed form values obtained empirically, limiting the application of the algebraic turbulence model. Therefore, different values of the turbulence mixing length are needed for different type of flow application. The accuracy of the predicted flow will depend on the prescribed turbulence empirical mixing length scale. Because of this, the algebraic turbulence models perform at its best when the local turbulence flow is behaving in an isotropic manner.

The first algebraic model that was developed by Prandtl (1925) was the mixing length model. The mixing length model is a simple model and was first developed for boundary layer type flow. It is put in the following mathematical form

$$\tau_{ij} = \mu_t \left(\frac{\partial U_i}{\partial x_j} + \frac{\partial U_j}{\partial x_i} \right) - \frac{2}{3} \rho k \delta_{ij} \tag{3.1}$$

where $\mu_t = \rho l_{mix}^2 \left| \frac{\partial U_i}{\partial x_j} + \frac{\partial U_j}{\partial x_i} \right| \left(\frac{\partial U_i}{\partial x_j} + \frac{\partial U_j}{\partial x_i} \right)$

and δ_{ij} = boundary layer thickness.

To close the equation, the value for l_{mix} must be prescribed experimentally and it varies with different type of flow application.

Important modifications on the mixing length model were also made by Theodore Von Karman (1938), Van Driest (1956), Clauser (1956) and Corrsin et al. (1954) and Klefanoff (1954) to improve on Prandtl's mixing length equation. Smith-Cebeci (1967) and Baldwin-Lomax (1978) then developed their own algebraic turbulence model by using and combining ideas proposed on improving the algebraic model made by researchers prior to them. The end product was a two layer algebraic model developed for boundary layer type flow. According to Wilcox (2002), although both models are equally superior, the Baldwin-Lomax model is more popular among researchers due to its robustness.

3.3.3 One Equation Turbulence Models

It is important to take into account the turbulent scales in order to develop a more complete turbulence model. Proper turbulence historical profile upstream of the flow will be needed to properly calculate the flow characteristics of the turbulence profile downstream to the flow. This resulted in the development of the one equation turbulence model. In this model, the turbulent velocity scales are modeled via a transport equation for mean turbulence kinetic energy in order to close the system.

Prandtl realized the deficiencies of the mixing length model. To further improve on his previous work on mixing length model, in 1945 he proposed the inclusion of the time-averaged turbulent kinetic energy as a turbulent property in order to determine a better turbulent eddy viscosity. By taking the trace of the Reynolds stress tensor, the turbulent kinetic energy (per unit mass) is defined as:

$$\tau_{ij} = -\overline{u_i' u_i'} = -2k \qquad (3.2)$$

Which will lead to the definition of the isotropic turbulent kinetic energy as:

$$k = \frac{1}{2}\overline{u_i' u_i'} = \frac{1}{2}\left(\overline{u'^2} + \overline{v'^2} + \overline{w'^2}\right) \qquad (3.3)$$

From this Prandtl came to a conclusion that the turbulent eddy kinematic viscosity is defined as:

$$\nu_T = k^{1/2} l \qquad (3.4)$$

The turbulent kinetic energy in equation (3.4) will be solved through a transport

equation. The transport equation for the turbulent kinetic energy is:

$$\frac{\partial k}{\partial t} + U_j \frac{\partial k}{\partial x_j} = \tau_{ij}\frac{\partial U_i}{\partial x_j} - \nu\overline{\frac{\partial u_i'}{\partial x_k}\frac{\partial u_i'}{\partial x_k}} + \frac{\partial}{\partial x_j}\left[\nu\frac{\partial k}{\partial x_j} - \frac{1}{2}\overline{u_i' u_i' u_j'} - \frac{1}{\rho}\overline{p' u_j'}\right] \qquad (3.5)$$

In order to close for the transport equation for the turbulent kinetic energy, the Reynolds stress in the production term, the dissipation term and the turbulence and pressure diffusion term needs to be prescribed. For the Reynolds stress, the one equation still utilizes Bousssinesq eddy viscosity approximation.

Since Boussinesq eddy viscosity approximation is still being used to determine the Reynolds stress, the one model equation still holds the same deficiency of the algebraic turbulent model in associating mean velocity gradient in shaping the turbulent property of the flow.

The Prandtl (1945) one-equation model was also attributed to Kolmogrov, Emmons (1954) and Glushko (1965). Kolmogrov was attributed due to his involvement in their effect to develop the model. Emmons on the other hand coincidently proposed the same one equation model in 1954. Apart from the Prandtl one equation model, a few notable one equation turbulence model was developed in the 1960s by Bradshaw, Ferriss and Atwell (1967), Nee and Kovasznay (1968) and Wolfstein (1967 and 1969).

Recent efforts to improve the one equation model have been made by Baldwin et al. (1990) and Spalart et al. (1992). These one-equation turbulence models are dubbed complete since the need to prescribed empirical values for the length scale is no longer needed.

The Spalart-Allmaras turbulence model only showed a slight advantage against the algebraic turbulence model. Prediction of boundary layer flow near the wall is within close similarity with the algebraic turbulence model. Separated flow showed a slight better prediction by the Spalart-Allmaras turbulence model over the algebraic turbulence model. However, the Spalart-Allmaras turbulence model still suffers from setbacks. It has problems in predicting jet flows, separated and decaying turbulence flow (Wilcox, 2002).

In summary, it can be said that although it is a good move to include turbulent kinetic energy as a representation of the turbulent velocity scale, the one equation model is only slightly better than the algebraic turbulence model and suffer from the lack of proper modeling of the turbulence length scale. Both zero and one-equation models are good in modeling isotropic equilibrium flows in region of low Reynolds number in which the production of turbulence and dissipation are in balance. However, in non-equilibrium flow, properly modeling needs to be done to accommodate the rapid changes in turbulence length scale.

3.3.4 Two Equation Turbulence Models

Two equation models are among the most popular turbulence models for scientific and engineering calculations. In these models, two separate transport equations are solved to determine the length and the velocity scales for the eddy-viscosity. The two-equation models were probably the first complete turbulence models. In the two-equation turbulence model, in addition to the turbulence velocity scale (mean turbulence kinetic energy), the turbulence length scale is also modeled via a transport equation. The modeling turbulence length scale will then be added together with the mean turbulence kinetic energy in the turbulence eddy viscosity for a better prediction of the Reynolds stresses using the Boussinesq approximation. Several verson of the modeled turbulence length scale exists and it will be later explained in this section. Launder and Spalding (1972) described the generalized form of the modeled length scale as:

$$z \equiv k^m l^n \tag{3.6}$$

where m and n are constants.

Kolmogorov proposed the first two-equation model in 1942. Kolmogorov proposed the z equation to be defined as the specific dissipation rate, ω. Ever since Kolmogorov postulated his two-equation model, several researchers have come up with their version of the two-equation model. A summary of the two-equation models is provided in the following table.

Out of all the versions listed in Table 3.1.1 the k-ω model and the k-ε model have been popular and widely used. The focus in this section will be on these two equations models. Details on the other version of the two-equation models are available from Launder and Spalding (1972) and Wilcox (2002).

According to Wilcox (2002), Kolmogorov came up with his proposed transport equation for ω through dimensional analysis and reasoning. Kolmogorov transport equation for ω was defined as:

$$\frac{\partial \omega}{\partial t} + U_j \frac{\partial \omega}{\partial x_j} = -\beta \omega^2 + \frac{\partial}{\partial x_j}\left[\sigma \nu_T \frac{\partial \omega}{\partial x_j}\right] \tag{3.7}$$

Table 3.1.1: Versions of the two-equation models.

Researcher	Length scale	Symbol
Kolmogorov (1942), Saffman (1970), Wilcox-Alber (1972), Saffman-Wilcox (1974), Wilcox-Traci (1976), Wilcox-Rubesin (1980), Coakley (1983), Wilcox (1988, 1998),Menter (1992), Peng-Davidson-Holmberg (1997)	$k^{\frac{1}{2}}/l$	ω
Chou (1942), Davidov (1961),Harlow-Nakayama (1968), Jones–Launder (1972), Launder-Sharma (1974), Yakhot-Orszag (1986), Shih-Liou-Shabbir-Zhu (1995)	$k^{\frac{3}{2}}/l$	ε
Rotta (1951), Spalding (1967)	l	l
Rotta (1968, 1971), Rodi-Spalding (1970), Ng-Spalding (1972)	kl	kl
Zeierman-Wolfshtein (1986), Speziale-Abid-Anderson (1990)	$k^{\frac{-1}{2}}/l$	τ
Spalding (1969), Robinson-Harris-Hassan (1995)	k/l^2	ω^2

This represents the convective term, the dissipation term and also the diffusion term. Wilcox (2002) described Kolmogorov equation should have included the term for production. Although Kolmogorov first postulated that ω represented dissipation of the smallest eddies and therefore should not contain a production term, it was later found out large eddies are actually responsible in determining the time scale of turbulence, hence the rate of dissipation. Furthermore, Kolmogorov equation did not include a molecular diffusion term making it only valid for high Reynolds number flow and cannot be integrated through the viscous sub-layer flow.

The Wilcox k-ω turbulence model

The Kolmogorov k-ω equation was then modified and further developed by researchers (Refer Table 3.1.1) over the years and the most popular version was the one by Wilcox (2002), which was defined as:

$$v_t = \alpha * \frac{k}{\omega}$$

$$\frac{\partial k}{\partial t}+U_j\frac{\partial k}{\partial x_j}=\tau_{ij}\frac{\partial U_i}{\partial x_j}-\beta^* k\omega+\frac{\partial}{\partial x_j}\left[\left(\nu+\sigma^*\nu_T\right)\frac{\partial k}{\partial x_j}\right] \tag{3.8}$$

$$\frac{\partial \omega}{\partial t}+U_j\frac{\partial \omega}{\partial x_j}=\alpha\frac{\omega}{k}\tau_{ij}\frac{\partial U_i}{\partial x_j}-\beta\omega^2+\frac{\partial}{\partial x_j}\left[\left(\nu+\sigma^*\nu_T\right)\frac{\partial \omega}{\partial x_j}\right]$$

where the closure coefficients are obtained empirically. Both the closure coefficients and auxiliary relations are further defined as:

$$\alpha=\frac{13}{25},\ \beta=\beta_0 f_\beta,\ \beta^*=\beta_0^* f_{\beta^*},\ \sigma=\sigma^*=\frac{1}{2}$$

$$\beta_0=\frac{9}{125},f_\beta=\frac{1+70x_\omega}{1+80x_\omega},x_\omega\equiv\left|\frac{\Omega_{ij}\Omega_{jk}\Omega_{ki}}{\left(\beta_0^*\right)^3}\right|$$

$$\beta_0^*=\frac{9}{100}\left(\frac{4/15+(\mathrm{Re}_t/R_\beta)^4}{1+(\mathrm{Re}_t/R_\beta)^4}\right),R_\beta=8 \tag{3.9}$$

$$f_{\beta^*}=\begin{cases}1, x_k \\ \dfrac{1+680x_k^2}{1+400x_k^2}, x_k>0\end{cases}$$

$$x_k=\frac{1}{\omega^3}\frac{\partial k}{\partial x_j}\frac{\partial \omega}{\partial x_j}$$

$$\varepsilon=\beta^*\omega k, l=k^{1/2}/\omega$$

$$\alpha^*=\alpha_\infty^*\left(\frac{\alpha_0^*+\mathrm{Re}_t/R_k}{1+\mathrm{Re}_t/R_k}\right)$$

$$\mathrm{Re}_t=\frac{\rho k}{\mu\omega},R_k=6,\alpha_0^*=\frac{\beta_i}{3},\beta_i=0.072$$

$$\alpha^*=\alpha_\infty^*=1 \tag{3.10}$$

$$\alpha=\alpha_\infty=0.52$$

$$\alpha = \frac{\alpha_{\infty}}{\alpha^{*}}\left(\frac{\alpha_0 + \mathrm{Re}_t / R_{\omega}}{1 + \mathrm{Re}_t / R_{\omega}}\right)$$

$$R_{\infty} = 2.95$$

The Wilcox k-ω turbulence model is an empirical turbulence model and was first developed as a high Reynolds number turbulence model. It was then later that a low Reynolds number version of the Wilcox k-ω was developed, Wilcox (2002), Fluent (2003).

The k-ε turbulence model

As with the k-ω turbulence model, the k-ε turbulence model exists in many versions, Jones and Launder developed the current standard version of the k-ε turbulence model in 1972, Launder and Spalding (1972). The model of Jones and Launder was developed for high Reynolds number application but accounted for low Reynolds number effects as well. Launder Sharma (1974) later improved the k-ε turbulence model of Jones Launder (1972) by modifying its closure coefficients and damping functions for low Reynolds number application. However, despite being very popular and widely used, the standard k-ε turbulence model has its deficiencies, which will be discussed later in this section. This led to the development of several improved version of the k-ε turbulence models designed to overcome the deficiencies of the standard k-ε turbulence model. Such models that will be discussed in this section are the RNG k-ε turbulence model by Yakhot and Orszag (1986) and the Realizable k-ε turbulence model by Shih et al. (1995).

Turbulence model has two tasks:

(a) to relate the Reynolds Stresses $\overline{u_i' u_j'}$ to the turbulent parameters and to the mean flow field

(b) to determine the distribution of the parameters over the field .

Many models employ the eddy-viscosity concept, which is given by

$$-\overline{u_i' u_j'} = v_t\left(\frac{\partial \overline{u_i}}{\partial x_j} + \frac{\partial \overline{u_j}}{\partial x_i}\right) - \frac{2}{3} k \delta_{ij} \tag{3.11}$$

where δ_{ij} = boundary layer thickness.

The turbulent viscosity in equation (3.11), ν_t is computed from a velocity scale ($k^{1/2}$) and a length scale ($k^{3/2}/\varepsilon$) which are predicted at each point in the flow via solution of the following transport equations for turbulent kinetic energy (k) and its dissipation rate (ε):

$$\frac{\partial k}{\partial t}+\overline{u_i}\frac{\partial k}{\partial x_i}=\frac{\partial}{\partial x_i}\left(\frac{\nu_t}{\sigma_k}\frac{\partial k}{\partial x_i}\right)+\nu_t\left(\frac{\partial \overline{u_i}}{\partial x_j}+\frac{\partial \overline{u_j}}{\partial x_i}\right)\frac{\partial \overline{u_i}}{\partial x_j}-\varepsilon \tag{3.12}$$

$$\frac{\partial \varepsilon}{\partial t}+\overline{u_i}\frac{\partial \varepsilon}{\partial x_i}=\frac{\partial}{\partial x_i}\left(\frac{\nu_t}{\sigma_\varepsilon}\frac{\partial \varepsilon}{\partial x_i}\right)+C_{1\varepsilon}\frac{\varepsilon}{k}G-C_{2\varepsilon}\frac{\varepsilon^2}{k} \tag{3.13}$$

where G is the generation of k and is given by

$$G=\nu_t\left(\frac{\partial \overline{u_i}}{\partial x_j}+\frac{\partial \overline{u_j}}{\partial x_i}\right)\frac{\partial \overline{u_i}}{\partial x_j} \tag{3.14}$$

The turbulent viscosity is then related to k and ε by the expression

$$\nu_t=C_\mu\frac{k^2}{\varepsilon} \tag{3.15}$$

The coefficients $C_\mu, C_{1\varepsilon}, C_{2\varepsilon}, \sigma_k$ and σ_ε are constants which have the following empirically derived values

$$C_\mu=0.09,\ C_{1\varepsilon}=1.44,\ C_{2\varepsilon}=1.92,\ \sigma_k=1.0,\ \sigma_\varepsilon=1.3$$

The standard k-ε turbulence model is defined as:

$$\nu_T=C_\mu k^2/\varepsilon \tag{3.16}$$

$$\frac{\partial k}{\partial t}+U_j\frac{\partial k}{\partial x_j}=\tau_{ij}\frac{\partial U_i}{\partial x_j}-\varepsilon+\frac{\partial}{\partial x_j}\left[\left(\nu+\nu_T/\sigma_k\right)\frac{\partial k}{\partial x_j}\right]$$

$$\frac{\partial \varepsilon}{\partial t}+U_j\frac{\partial \varepsilon}{\partial x_j}=C_{\varepsilon 1}\frac{\varepsilon}{k}\tau_{ij}\frac{\partial U_i}{\partial x_j}-C_{\varepsilon 2}\frac{\varepsilon^2}{k}+\frac{\partial}{\partial x_j}\left[\left(\nu+\nu_T/\sigma_\varepsilon\right)\frac{\partial \varepsilon}{\partial x_j}\right] \tag{3.17}$$

$$C_{\varepsilon 1}=1.44, C_{\varepsilon 2}=1.92, C_\mu=0.09, \sigma_k=1.0, \sigma_\varepsilon=1.3$$

$$\omega = \varepsilon / (C_\mu k), l = C_\mu k^{3/2} / \varepsilon$$

The k-ε turbulence model predicts the kinematic eddy viscosity value through the modeling of the turbulence velocity and length scale. This is achieved by solving additional transport equation of mean turbulent kinetic energy (velocity scale) and dissipation rate (length scale). Over the years the standard k-ε turbulence model has proved to be both economical and robust. However, it has its deficiencies, such as the inability to predict highly strained flow, swirling flow, rotating and separating flow, Naser (2003). However, due to the deficiencies of the standard k-ε turbulence model, improvements have been made to overcome such setbacks, which lead to the development of the RNG k-ε model and the Realizable k-ε model. Yakhot and Orszag (1986) developed the RNG k-ε turbulence model in 1986 based on a statistical formulation called the Renormalization Group Theory. The main objective of the development of this turbulence model was to modify the kinematic eddy viscosity and the dissipation transport equation so that they are able to adapt to high strained flows, the effect of swirl flows and to account for low Reynolds number effects, Fluent (2003).

The RNG k-ε turbulence model is defined as:

$$\mu_t = \rho C_\mu \frac{k^2}{\varepsilon}$$

$$\frac{\partial k}{\partial t} + U_j \frac{\partial k}{\partial x_i} = \tau_{ij} \frac{\partial U_i}{\partial x_j} - \varepsilon + \frac{\partial}{\partial x_j}\left(\alpha_k \mu_{eff} \frac{\partial k}{\partial x_j} \right) \tag{3.18}$$

$$\frac{\partial \varepsilon}{\partial t} + U_j \frac{\partial \varepsilon}{\partial x_i} = C_{1\varepsilon} \frac{\varepsilon}{k} \tau_{ij} \frac{\partial U_i}{\partial x_j} - C_{2\varepsilon}^* \frac{\varepsilon^2}{k} + \frac{\partial}{\partial x_j}\left(\alpha_k \mu_{eff} \frac{\partial \varepsilon}{\partial x_j} \right)$$

where the closure coefficients and auxiliary functions are given as:

$$C_{2\varepsilon}^* = C_{2\varepsilon} + \frac{C_\mu \lambda^3 (1 - \lambda/\lambda_0)}{1 + \beta\lambda^3}, \lambda \equiv \frac{k}{\varepsilon}\sqrt{2S_{ij}S_{ji}}$$

$$C_{1\varepsilon} = 1.42, C_{2\varepsilon} = 1.68, C_\mu = 0.085, \sigma_k = \sigma_\varepsilon = 0.72 \tag{3.19}$$

$$\beta = 0.012, \lambda_0 = 4.38$$

For highly strained mean flow, the RNG k-ε turbulence model modified the closure coefficient in the dissipation term of the dissipation transport equation. Instead of taking C2ε as a constant, it has been modified to include mean strain effect, which can be seen from equation (3.19). In highly strained mean flow, C*2ε will be smaller than C2ε, thus reducing the effect of dissipation in the dissipation term. This will result in a reduction in the mean turbulent kinetic energy effect and therefore reducing the turbulent eddy viscosity value, μ_T. This will reduce the over diffusive behavior, experienced in the standard k-ε turbulence model.

As with the standard k-ε turbulence model, the RNG k-ε turbulence model take into account for low Reynolds number effects. The diffusion term on both transport equation was modified for this matter. For low Reynolds number flow, the integration of equation (3.20) and the inverse effective Prandtl number, α_k and α_ε is used to account for the varying Reynolds number. The calculation from equation (3.20) will then be incorporated into the diffusion term for both transport equation, and will also be used to determine the value for the turbulence eddy viscosity, μ_T. For high Reynolds number flow, the default μ_T from equation (3.18) will be used.

$$d\left(\frac{\rho^2 k}{\sqrt{\varepsilon\mu}}\right) = 1.72\frac{\hat{v}}{\sqrt{\hat{v}_v^3 - 1 + C_v}}\, d\hat{v}, \hat{v} = \frac{\mu_{eff}}{\mu}, C_v \approx 100$$

$$\left|\frac{\alpha - 1.3929}{\alpha_0 - 1.3929}\right|^{0.6321}\left|\frac{\alpha + 2.3929}{\alpha_0 + 2.3929}\right|^{0.3679} = \frac{\mu}{\mu_{eff}} \tag{3.20}$$

$$\alpha_0 = 1.0$$

$$\frac{\mu}{\mu_{eff}} << 1, \alpha_k = \alpha_\varepsilon \approx 1.393$$

For swirling effects the RNG k-ε turbulence model incorporates the function from equation (3.21) into the turbulence eddy viscosity, μ_T.

$$\mu_t = \mu_0 f\left(\alpha_\varepsilon, \Omega, \frac{k}{\varepsilon}\right) \tag{3.21}$$

where μ_0 can be taken from either high or low Reynolds number flow formulation for turbulence eddy viscosity, μ_T.

However, although the RNG k-ε turbulence model is an improvement from the standard k-ε turbulence model, it still has its limitations. This is due to the transport equation for the dissipation term, ε. Because of the fact that the transport equation for the dissipation term is derived based on physical reasoning and dimensional analysis alone, certain mathematical limitation will exist and needs to be satisfied in order to be consistent with the prediction of Reynolds stresses, hence the turbulence flow, Fluent(2003). The RNG and standard k-ε turbulence model does not satisfy these mathematical limitations, making them not 'Realizable'. Due to this fact, Shih et al. developed the Realizable k-ε turbulence model in 1995 to address these mathematical limitations and improve on it. From their research, they have developed a new transport equation for the dissipation term from the exact equation based on the mean-square vorticity fluctuation transport equation, Shih et al. (1995). In addition, they also modified the formulation for the turbulence eddy viscosity term, μ_T, by improvising on the closure constant C_μ , varying it in order to adjust to different flow applications.

The Realizable k-ε turbulence model is defined as:

$$\nu_T = C_\mu k^2 / \varepsilon$$

$$\frac{\partial k}{\partial t} + U_j \frac{\partial k}{\partial x_j} = \tau_{ij} \frac{\partial U_i}{\partial x_j} - \varepsilon + \frac{\partial}{\partial x_j}\left[\left(\nu + \nu_T / \sigma_k \right) \frac{\partial k}{\partial x_j} \right]$$

$$\frac{\partial \varepsilon}{\partial t} + U_j \frac{\partial \varepsilon}{\partial x_j} = C_1 S \varepsilon - C_2 \frac{\varepsilon^2}{k + \sqrt{\nu \varepsilon}} + \frac{\partial}{\partial x_j}\left[\left(\nu + \nu_T / \sigma_\varepsilon \right) \frac{\partial \varepsilon}{\partial x_j} \right] \qquad (3.22)$$

where the closure coefficients and the formulation for C_μ are defined as;

$$C_1 = \max\left[0.43, \frac{\eta}{\eta + 5} \right], \eta = S\frac{k}{\varepsilon}, C_2 = 1.9, \sigma_k = 1.0,\ \sigma_\varepsilon = 1.2$$

$$C_{\mu}=\frac{1}{A_0+A_{\varepsilon}\dfrac{kU}{\varepsilon}},A_0=4.04,A_{\varepsilon}=\sqrt{6}\cos\phi \tag{3.23}$$

$$\phi=\frac{1}{3}\cos^{-1}(\sqrt{6}w),w=\frac{S_{ij}S_{jk}S_{ki}}{\tilde{S}}$$

$$\tilde{S}=\sqrt{S_{ij}S_{ij}},S_{ij}=\frac{1}{2}\left(\frac{\partial U_i}{\partial x_j}+\frac{\partial U_j}{\partial x_i}\right)$$

$$U^{*}\equiv\sqrt{S_{ij}S_{ij}+\Omega_{ij}\Omega_{ij}}$$

$$\Omega_{ij}=\overline{\Omega_{ij}}-\varepsilon_{ijk}\omega_k$$

From equation (3.22) it can be seen that the transport equation of the dissipation term is different from the standard and RNG k-ε turbulence model. The main difference lies in the production and dissipation term. According to Fluent (2003), the dissipation term in the dissipation transport equation was modified so that the denominator will not be singular, eliminating the change of the dissipation term of becoming too big. This will provide a reasonable value for dissipation in the k transport equation and therefore overcoming the problem of non- decaying eddy viscosity, Wilcox (2002). Furthermore, according to Shih et al. (1995), the modification of the production term will encourage a better transfer of spectral energy. Both modification of the dissipation transport equation term promotes a better description of the turbulent vortex stretching, which is required to better predict free shear flows, especially the spreading rates of jets, Wilcox (2002). In addition, the closure coefficient C_{μ} was not made constant. It will correspond to different flow application. As was described in Shih et al. (1995), boundary layer flow will yield a C_{μ} value of 0.09, as per measured value. For homogeneous shear flow, the C_{μ} will yield a value of 0.06, which is close to the measure value of 0.05. However, it can be seen from Shih et al. that since the Realizable k-ε turbulence model is primarily designed for high Reynolds number flow, providing good prediction of free shear flows. However, its performance close to the boundary layer especially under the influence of pressure gradients is not very good. Only free shear flows yields better prediction than the standard k-ε turbulence model.

Deficiencies of the two equation turbulence model:

Deficiency of the two–equation model can be traced to three main reasons, which is the inability to predict flow in the presence of pressure gradient close to the wall and due to the inability to take into account the effect of rapid change in mean strain rate due to the sharp streamline curvature of the geometry.

3.3.5 Pressure Gradient Effects

The two-equation model, especially the k-ε still fails to accurately predict flow in the boundary layer region, close to the wall even after treating it. Perturbation of the defect layer then showed that the reason for this was due to large turbulence scale developed close to the boundary layer especially in the presence of adverse pressure gradient effect. Analysis by Wilcox (2002) showed that by adding a cross diffusion term to the k-ε turbulence model, the increase of the turbulence scale close to the wall could be suppressed. Furthermore, Coles and Hirst.(1969) analyzing wake strength parameter in the defect layer against a function of pressure gradient showed that as adverse pressure gradient effect increases close to the wall, the wake strength parameter was being under predicted as a result of an increase in skin friction coefficient close the wall.

According to Rodi and Sheuerer (1986), two-equation turbulence model perform badly in region close to the wall due to the fact that the dissipation length scale rises sharply near the wall. However, Bradshaw (1969) have shown through experimental data that the dissipation length scale is independent in the region close to the wall. Coles and Hirst (1969) also supported this and described that the turbulent boundary layer close to the wall exists in different scales and physical processes. Rodi and Sheuerer (1986) also suggest that under adverse pressure gradient, the rate of kinetic energy production is more than the rate of dissipation itself, resulting in an increase in turbulence dissipation length scale. This will lead to an increase and over prediction of turbulent eddy viscosity and wall shear stress. However, although the k-ε versions of the two-equation model have proved inaccurate in predicted a wide range of flow due to its deficiencies, the k-ω turbulence model has proved to be rather successful. Part of the reason is the presence of the cross diffusion term in the k-ω as a way to suppress the increase of the turbulence dissipation length scale close to the wall. However, the addition of cross diffusion term can cause instability to the calculation of the flow, since it augments the influence of convection in the flow. Therefore, treatment is needed to curb this instability, prediction of boundary layer flow by the k-ω turbulence model only differ by 3.5% from measurement and have shown to predict separation rather successfully as well. However, a minor setback of the k-ω turbulence model is that the sub-layer region has to be integrated which means grid generation near the wall must be sufficiently fine.

3.3.6 Effect of Rapid Change of Mean Strain Rate and Streamline Curvature

According to Wilcox (2002), the main flaw of the eddy viscosity model, which assumes Boussinesq approximation, is the fact that it assumes the Reynolds stress which is proportional to the mean strain rate at all part of the flow, a postulation from Stokes based on laminar flows. The constant of proportionality was defined as the eddy turbulent viscosity. However, turbulent flow is affected by the change of geometry, anisotropy and flow history. With the presence of curvature in the flow, the individual Reynolds stress values will be different and hence, again the Boussinesq assumptions will become flawed. Bradshaw (1973) described that eddy- viscosity models offers inaccurate prediction of flows that undergo rapid changes in rates of strain. The main reason for this is because the adjustment of Reynolds stresses to such change is unrelated to turbulence mean flow and time scale effect. Therefore, the effect of curvature can be treated either by making correction to the two-equation models on the Reynolds stress transport model can be used. Naser (1990) described from Bradshaw (1973) that since the effect of curvature causes large changes in the Reynolds stresses and triple velocity correlations, the Boussinesq approximations must be corrected. Bradshaw (1973) proposed that the extra effect of strain rate would modify the Boussinesq assumption to include a factor of an order of higher magnitude. Therefore, the Reynolds stresses from the Boussinesq assumption will be modeled as:

$$\overline{u'v'} = \nu_T\left(\frac{\partial u}{\partial y} + \alpha\frac{\partial v}{\partial x}\right) \tag{3.24}$$

where α is of the order of 10.

Modifying certain aspect in the two-equation turbulence model can also treat the effect of flow curvature. Leschnizer and Rodi (1981) made modifications in the C_μ to take into account the effect of curvature and obtained good prediction in parallel jet flow. Furthermore, Bradshaw (1969) proposed a dimensionless number that takes into account the curvature effect. Sharma (1975) and Launder et al. (1977) modified the dissipation equation in the k-ε to take into account the curvature effect. With that respect, they modified the $C_{\varepsilon 2}$. Rodi(1979) made corrections in the $C_{\varepsilon 1}$ constant. Finally, Wilcox and Chambers (1977) proposed a correction to the k-ω turbulence model within the k equation term and the logarithmic law equation.

3.3.7 Reynolds Stress Turbulence Models

Deficiencies of the eddy viscosity turbulence model inspired early turbulence models developer such as Chou (1945) and Rotta (1951) to propose a turbulence model where the Reynolds stresses, $-\overline{u_i u_j}$ are not modeled through the Boussinesq assumption and the Reynolds stresses, are solved directly through a set of transport equations. This turbulence model is known as the Reynolds stress turbulence model (RSM) or second order/ moment closure. According to Wilcox (2002), such early contributors to the development of the RSM include Donaldson et al. (1968), Daly et al. (1970) Launder et al. (1975), Gibson and Launder. (1978), Lumley (1978), Speziale (1985, 1987, 1991) and Reynolds (1987). Through the years, Launder et al. (1975) RSM has become the one of the most popular and has been set as a baseline for RSM.

The direct use of Reynolds stresses to for turbulence modeling, especially in a three-dimensional flow, generates six extra transport equations, which represents the individual components of the Reynolds stresses. In addition, a transport equation is also used to solve for the turbulence length scale and this is normally employed through the use of dissipation transport equation, ε.

The transport equation for Reynolds stress is given as:

$$\frac{\partial \tau_{ij}}{\partial t} + U_k \frac{\partial \tau_{ij}}{\partial x_k} = -\tau_{ik} \frac{\partial U_j}{\partial x_k} - \tau_{jk} \frac{\partial U_i}{\partial x_k} + 2\nu \overline{\frac{\partial u'_i}{\partial x_k} \frac{\partial u'_j}{\partial x_k}} + \overline{\frac{u'_i}{\rho} \frac{\partial p'}{\partial x_j}} + \overline{\frac{u'_j}{\rho} \frac{\partial p'}{\partial x_i}} + \frac{\partial}{\partial x_k}\left[\nu \frac{\partial \tau_{ij}}{\partial x_k} + \overline{u'_i u'_j u'_k} \right] \quad (3.25)$$

Equation (3.25) consists of convective term on the left hand side of the equation. The first two terms on the right hand side of the equation is the production term, followed by the dissipation term, two pressure strain redistribution term and the diffusion term. For a three-dimensional flow, the six extra Reynolds stress transport equations generate extra 22 unknowns. Ten unknowns generated are in the form of triple velocity correlation that forms the turbulent diffusion term. A further six unknowns are generated from the dissipation term and six more unknowns from the pressure strain distribution term. The extra unknowns generated are of higher order correlations and the main challenge in Reynolds stress modeling is to model these unknowns. The terms that need to be modeled consists of the dissipation term, the turbulent diffusion term and the pressure strain redistribution term. The resulting Reynolds stress equation will be:

$$\frac{\partial \tau_{ij}}{\partial t} + U_k \frac{\partial \tau_{ij}}{\partial x_k} = P_{ij} + \varepsilon_{ij} - \Pi_{ij} + \frac{\partial}{\partial x_k}\left[\nu \frac{\partial \tau_{ij}}{\partial x_k} + C_{ijk} \right] \tag{3.26}$$

where the production term, the dissipation term, the pressure strain redistribution term and the turbulent diffusion term. $P_{ij,} \varepsilon_{ij,} \Pi_{ij}$ and C_{ijk} respectively are given as:

$$P_{ij} = -\tau_{ik} \frac{\partial U_j}{\partial x_k} - \tau_{jk} \frac{\partial U_i}{\partial x_k}$$

$$\varepsilon_{ij} = 2\nu \overline{\frac{\partial u'_i}{\partial x_k} \frac{\partial u'_j}{\partial x_k}}$$

$$\Pi_{ij} = \overline{\frac{P'}{\rho}\left(\frac{\partial u'_i}{\partial x_j} + \frac{\partial u'_j}{\partial xi} \right)} \tag{3.27}$$

$$\rho C_{ijk} = \rho \overline{u'_i u'_j u'_k} + \overline{P' u'_i} \delta_{jk} + \overline{P' u'_j} \delta_{ik}$$

The Reynolds stress component in the production term P_{ij} is solved through the Reynolds stress transport equation. The dissipation term, ε_{ij}, is modelled based on high Reynolds number flow conditions where the effect of ε_{ij} can be assumed to be isotropic (Hanjalic et al. 1976) and is defined as:

$$\varepsilon_{ij} = \frac{2}{3} \varepsilon \delta_{ij} \tag{3.28}$$

Where, δ_{ij} is the boundary layer thickness, which accounts for the effect of near wall anisotropy. The transport equation used to solve for ε is similar to the dissipation transport equation from the standard k-ε turbulence model. Hanjalic and Launder (1972) and Launder et al. (1975) defined their transport equation for ε as:

$$\frac{D\varepsilon}{Dt} = C_{\varepsilon}\frac{\partial}{\partial x_k}\left[\frac{k}{\varepsilon}\tau_{km}\frac{\partial \varepsilon}{\partial x_m}\right] - C_{\varepsilon 1}\frac{\varepsilon \tau_{ik}}{k}\frac{\partial U_i}{\partial x_k} - C_{\varepsilon 2}\frac{\varepsilon^2}{k} \tag{3.29}$$

The turbulence diffusion term, ρC_{ijk}, which consists of higher order velocity fluctuation correlation components was firstly modeled by Daly and Harlow. (1970) using a simple gradient–diffusion hypothesis, which defines C_{ijk} to be:

$$C_{ijk} = C'_s \frac{k}{\varepsilon}\tau_{km}\frac{\partial \tau_{ij}}{\partial x_m} \tag{3.30}$$

Hanjalic and Launder (1972) and Launder et al. (1975) proposed another version of the modelled C_{ijk} term, which was defined as:

$$C_{ijk} = C_s \frac{k}{\varepsilon}\left(\tau_{im}\frac{\partial \tau_{jk}}{\partial x_m} + \tau_{jm}\frac{\partial \tau_{ki}}{\partial x_m} + \tau_{km}\frac{\partial \tau_{ij}}{\partial x_m}\right) \tag{3.31}$$

The constant C'_s and C_s are given approximately as 0.25 and 0.11 respectively. However, according to Lien and Leschziner (1994), the equation derived in (3.30) and (3.31) might have destabilising effect especially in three- dimensional flow. Therefore an isotropic version of C_{ijk} is provided and defined as:

$$C_{ijk} \equiv C_s \frac{k\overline{v'^2}}{\varepsilon} \tag{2.32}$$

where C_s was defined as 0.22 and $\overline{v'^2} \cong 0.361\,k$

Shir (1973) have also come up with a simple gradient diffusion concept, in which C_{ijk} is defined as:

$$C_{ijk} = C_s \frac{k^2}{\varepsilon}\left(\frac{\partial \tau_{ij}}{\partial x_k}\right) \tag{3.33}$$

The last term that requires modeling for the Reynolds stress turbulence model is the pressure strain term. According to Wilcox (2002), the pressure strain term is the term that received the most attention. The reason for this is because since the pressure strain term has the same order as the production term, it plays an important role in the majority of engineering flows of interest. In addition, the pressure strain term requires some degree of creativity to model in order to achieve approximate closure.

For homogeneous turbulence, the pressure strain term is divided into two parts, a slow fluctuating pressure and a rapid fluctuating pressure.

$$\Pi_{ij} = \phi_{ij,1} + \phi_{ij,2} \tag{3.34}$$

Where the first term on the right hand side of Equation (3.34) represents the slow pressure strain rate term and the second term represents the rapid pressure strain term.

Rotta (1951) postulated that the slow pressure term could be modeled linearly as:

$$\phi_{ij,1} = C_1 \frac{\varepsilon}{k}\left(-\tau_{ij} + \frac{2}{3} k \delta_{ij} \right) \tag{3.35}$$

Where C_1 is a closure coefficient obtained from the empirical measurement of Uberoi (1956) to lie between $1.4<C_1<1.8$.

Launder et al. (1975) proposed a model to solve for the rapid pressure strain redistribution term based on the analysis of Rotta (1951), which is strictly valid only for homogeneous turbulence. Gibson and Launder (1978) then proposed a simplified version of the Launder et al. (1975) model, which defines the rapid pressure strain redistribution term as:

$$\phi_{ij,2} = -C_2\left(P_{ij} - \frac{2}{3}\delta_{ij} P \right)$$

$$P_{ij} \equiv -\tau_{ik}\frac{\partial U_j}{\partial x_k} - \tau_{jk}\frac{\partial U_i}{\partial x_k} \tag{3.36}$$

$$P \equiv -\tau_{ik}\frac{\partial U_i}{\partial x_k}$$

SSG Model

Speziale (1991) have developed a simple, non-linear pressure strain redistribution model for incompressible flow, which is often called as the SSG model. This has become a popular choice among pressure strain redistribution model since it does not require a correction for the near wall reflection effect. The SSG model is defined as:

$$\Pi_{ij} = -\left(C_1\varepsilon + C_1^{*}\tau_{mn}\frac{\partial U_m}{\partial x_n}\right)b_{ij} + C_2\varepsilon\left(b_{ik}b_{kj} - \frac{1}{3}b_{nm}b_{nm}\delta_{ij}\right) + \left(C_3 - C_3^{*}\sqrt{b_{ij}b_{ij}}\right) +$$

$$C_4 k\left(b_{ik}S_{jk} + b_{jk}S_{ik} - \frac{2}{3}b_{mn}S_{mn}\delta_{ij}\right) + C_5 k\left(b_{ik}\Omega_{jk} + b_{jk}\Omega_{ik}\right) \tag{3.37}$$

Where, b_{ij}, is defined as:

$$b_{ij} \equiv \frac{\tau_{ij} - \frac{1}{3}\tau_{kk}\delta_{ij}}{\tau_{mm}} \tag{3.38}$$

And the constants are given as:

$$C_1 = 3.4, C_1^{*} = 1.8, C_2 = 4.2, C_3 = 0.8, C_3^{*} = 1.3, C_4 = 1.25, C_5 = 0.4$$

The main advantage of the RSM is that it takes into account the anisotropic nature of turbulence in predicting flows by incorporation nonlocal and history effect of turbulence. Due to this, RSM provide better prediction of flow over streamline curvature, swirling flows, rotation, and flow with rapid change in the mean strain rate. According to Wilcox (2002), unlike eddy viscosity turbulence models, which uses treatment and compensation through the manipulation of mathematical formulation to predict complex flows, the RSM provides better prediction of complex flow in a more natural way by direct modeling of the Reynolds stresses.

Furthermore, RSM modeling of each individual stress component enables accurate prediction of anisotropic turbulence, which often plays a crucial role as a major source of energy in complex flows, such as in stagnation region, secondary motion and in vortex flows. RSM also provide accurate prediction of the unequal wall-normal stress component, which is important in reproducing wall shear stress and mass transfer close to the wall.

However, despite the advantage that have been showed by the RSM in predicting complex flows, it does not offer any superiority over eddy viscosity models in predicting free stream flows and boundary layer flow and it also share the shortcomings experienced by the eddy viscosity model especially in poor prediction of three dimensional and separated flows. This deficiency can be traced back on the modeling of higher correlation terms such the pressure strain redistribution term and also on the modeling turbulence length scale through the dissipation (ε) term. According to Wilcox (2002) the usage of the dissipation term in predicting the turbulence length scale will inadvertently transfer the deficiency of the two equation eddy viscosity models to the Reynolds stress turbulence model. Wilcox (2002) has also shown from the direct numerical simulation (DNS) of Parneix et al. (1998) that deficiency of the RSM can also be traced back through the modeling of the pressure strain rate correlation. The DNS showed inaccurate results was obtained despite accurate modelling of dissipation, ε. The inability for Reynolds stress turbulence model to provide better prediction for three-dimensional flows can be traced back on the application of two-dimensionality in boundary layer flows. Current turbulence models have been developed based on the knowledge of two-dimensional flows. In three-dimensional boundary layer, the eddy viscosity is not isotropic. Latest work of Schwarz and Bradshaw (1994) has studied the performance of some Reynolds stress turbulence model in three-dimensional boundary layer flow. Based on their findings, they have concluded that the main cause of error in the performance of RSM models in a three dimensional boundary layer is due to the inadequacy of the modelling of dissipation.

HTM turbulence model

A new and attractive alternative to the RSM is the use of hybrid turbulence model that incorporates attributes from the eddy viscosity two-equation models and the RSM. The hybrid turbulence model offer the advantages of the RSM turbulence model in terms of its accuracy and its applicability over curved flows and at the same time offer the robustness and convergence speed of the eddy viscosity two equation model. For this instance, Basara et al. (2003) proposed a hybrid turbulence model (HTM) that combines both the advantages and applicability of the RSM and k-ε turbulence models. In the HTM model proposed by Basara et al. (2003), the solution of the Reynolds stress is obtained from the Boussinesq assumption of equating stress to the mean strain of the flow. The solution for the turbulence eddy viscosity is obtained similarly from the k-epsilon model. The calculation of k and ε to solve for the turbulent eddy viscosity is obtained similarly from the RSM turbulence model. The k equation obtained from the summation of normal Reynolds stresses. The dissipation term is solved from the transport equation for dissipation. The main difference in the HTM turbulence model is the C_μ constant used in defining the turbulent eddy viscosity. C_μ is defined by:

$$C_\mu = \left(-\overline{u_i u_j}\frac{\partial U_i}{\partial x_j}\right) / \left(\frac{k^2}{\varepsilon}S^2\right), S = \sqrt{2S_{ij}S_{ij}} \qquad (3.39)$$

Which is the ratio between the RSM production term and the k-ε production term. The rationale from the variable value of C_μ is due to the fact that according to Basars and Jakirlic (2003) that C_μ varies not only from flow to flow but also varies at different points in the same flow. C_μ is defined as:

$$C_\mu = \left(-\overline{u_i u_j}/k\right)^2 \qquad (3.40)$$

Was originally determined to be around 0.09, but was later discovered to vary somewhere in between 0.06 to 0.12 depending on the type of flow. Validation of HTM against various flow applications has showed results that lie in between RSM and k-ε turbulence model

3.3.8 Direct Numerical Simulation and Large Eddy Simulation

The ideal method to obtain accurate results for turbulence flow is to directly solve for the Reynolds stresses and in turn the non-linear Navier-Stokes and continuity equations. This can be achieved by using either the method of Direct Numerical Simulation (DNS) or by using Large Eddy Simulation (LES). DNS and LES are also known as the unsteady viscous methods.

In DNS, unsteady Navier-Stokes equations are solved directly without any modeling of the turbulence. The fluctuation velocity and viscous force components within the body surface and in the computational domain is obtained together with components of Reynolds stresses. On the other hand, the LES approach directly solves the large eddies motions using the unsteady Navier-stokes equations and models the small eddies through the use of a sub-grid scale filters. The motivation behind this lie on the fact that small eddies has a more universal character. They are more isotropic and dissipative in nature, which makes its behaviour independent to the flow. Large eddies are highly anisotropic and unsteady in nature, which makes it dependent to the flow.

However, according to Ahmed (1998), the LES approach is a more preferred option for technical flows, because it requires significantly less computer capacity then DNS, and yet at the same time promises to be more accurate and robust than the conventional RANS approach.

At the moment, DNS is used purely for research purposes. According to Wilcox (2002), current DNS application is mostly limited to low Reynolds number in two dimensional and simple three-dimensional flows (incompressible and compressible) with homogeneous turbulence. The extremely high demand that DNS put on computational capacity leads back to the extremely high grid generation needed to resolve all turbulent scale in both spatial and temporal dimension.

According to Ahmed (1998), DNS requires grid points that increase with 9/4 power of Reynolds number. It has been estimated that to capture the effect of the smallest turbulence motion and solves the flow around a structure the size of a vehicle, grid points around 10^{18} would be needed. By the mid 1990s, the largest number of grid points that could be handled computationally was only around 10^{6}, which makes it so impractical in using DNS vehicle aerodynamics in the immediate future.

Due to this, the approach of using LES is better suited than using DNS. According to Wilcox (2002) LES grid size can be at least one order of magnitude smaller than DNS. Furthermore, a large time step can be used with flow achievable at a high Reynolds number. Available LES models are from the Smagorinasky (1963) simple gradient-diffusion model, the Lilly (1966) one equation model and the second order closure of Deardorff (1973).

3.3.9 Near Wall Treatment

Turbulence models discussed in the preceding section was mainly developed for flows of high Reynolds numbers. For laminar boundary layer flow near to the wall, molecular viscous effects that dominate the turbulent eddy viscosity must be accounted for, Ahmed (1998). According to Wilcox (2002), one of the main reason for high Reynolds number turbulence model (most two-equation, HTM and RSM models) inability to predict accurate values for flow near the wall especially in the presence of adverse pressure gradients was traced down to the inaccurate reproduction of the law of the wall constant, C. Analysis showed that in the example of a standard k-ε turbulence model, predicted C value of -2.2 as oppose to the measured value of 5.0. In another analysis conducted by Rodi and Sheuerer (1986), the deficiency of high Reynolds number turbulence model can be traced back to the deficiency in the model of the dissipation rate, ε to predict an accurate length scale value near to the wall. According to Rodi and Sheuerer (1986), for most high Reynolds number turbulence model, the production of turbulence kinetic energy, k and length scale near to the wall is too steep, resulting from a lower production in the rate of dissipation. This will result in a high value of Reynolds stress near the wall region. In order to overcome this problem, proper treatment is needed to compensate for this deficiency, for a more reliable near wall prediction.

Two different approaches are often used for near wall treatment. They are:

- Wall function approach
- Low Reynolds number model approach

Wall function approach

The first algebraic model that was developed by Prandtl (1925) was the mixing length mode. The mixing length model is a simple model and was first developed for boundary layer type flow. It was described as:

$$\tau_{ij} = \mu_t \left(\frac{\partial U_i}{\partial x_j} + \frac{\partial U_j}{\partial x_i} \right) - \frac{2}{3} \rho k \delta_{ij}, \mu_t = \rho l_{mix}^2 \left| \frac{\partial U_i}{\partial x_j} + \frac{\partial U_j}{\partial x_i} \right| \left(\frac{\partial U_i}{\partial x_j} + \frac{\partial U_j}{\partial x_i} \right) \qquad (3.41)$$

To close the equation, the value for l_{mix} must be prescribed experimentally and it varies with different type of flow application. Theodore Von karman in 1930 produced a similarity hypothesis based on Prandtl mixing length model. Through similarity rule, Von Kerman expresses l_{mix} as:

$$l_{mix} = \kappa \left| \frac{dU}{dy} / \frac{d^2U}{dy^2} \right| \qquad (3.42)$$

where l_{mix} is prescribed in terms of space coordinates and κ is the universal turbulence constant or Karman constant, which can be determined experimentally. However, according to Launder and Shima (1989), Von Kerman similarity hypothesis is only valid at area very close to the wall. With this, Prandtl proposed an assumption that the mixing length is proportional to the distance from the wall(y) when at ${}^{y}/_{\delta_{ij}} < 0.20, \delta_{ij}$ is defined as the boundary layer thickness. Therefore l_{mix} is then defined as:

$$l_{mix} = \kappa y \tag{3.43}$$

Where κ in equation (3.43) was later determined through experimental as approximately as 0.41.

Von Kerman similarity hypothesis can then be simplified to:

$$U = \frac{u_*}{\kappa} \ln y + C \tag{3.44}$$

The constant C can be further evaluated to be:

$$\frac{U}{u_*} = \frac{1}{\kappa} \ln \frac{u_* y}{\nu} - \frac{1}{\kappa} \ln \beta \tag{3.45}$$

Where, $\frac{U}{u_*}$ is the ratio of the mean flow to the friction velocity and is defined as $u^+ . \frac{u_* y}{\nu}$, is the dimensionless distance from the wall and is defined as y^+. Equation (3.45) is famously known as the law of the wall or the universal velocity-distribution law. Therefore, equation (3.45) can be simplified further to be:

$$u^+ = \frac{1}{\kappa} \ln y^+ + 5.0 \tag{3. 46}$$

The first and the most common approach in treating near wall effect are by using the wall function approach of Launder and Sharma. (1974). The wall function approach uses a semi-empirical model, which assumes the behaviour of fluid flow near the wall to follow the law of the wall profile, which will enforce the proper value for C in the wall of the wall region. Another advantage for using the wall function approach is a shortened computational time since the steep flow gradients occurring in the sub-layer region does not need to be resolved. This allow for coarse grid to be generated close to the wall. For the first cell next to the wall, the wall function approach automatically assumes a law of the wall profile, which is valid in the region of $y^+ < 30$ to 500, Roberson and Crowe. (1997).

3.3.10 Low Reynolds Number Model

The second method in treating near wall effect is using a low Reynolds number model approach. The main difference between the wall function approach and the low Reynolds number model approach lies in the grid generation near to the wall. In the low Reynolds number model approach, the grid generation in the normal component to the wall must be small enough to resolve flow down until the sub-layer region of the flow. High Reynolds number turbulence model that employs this approach undergoes modification to include damping functions particularly in the dissipation equation (ε) and in the turbulent eddy viscosity term, Ahmrd (1998). Popular low Reynolds number model that has been developed includes the low Reynolds number model of Jones and Launder (1972), Launder and Sharma (1974), Lam and Bremhorst (1981) and Chien (1982). According to Wilcox (2002), for a two-equation turbulence model, the modification of the transport equation of dissipation near the wall and turbulent eddy viscosity term are defined as:

$$\nu_T = C_\mu f_\mu \frac{k^2}{\tilde{\varepsilon}}$$

$$U\frac{\partial k}{\partial x} + V\frac{\partial k}{\partial y} = \nu_T\left(\frac{\partial U}{\partial y}\right)^2 - \varepsilon + \frac{\partial}{\partial y}\left[\left(\nu + \frac{\nu_T}{\sigma_k}\right)\frac{\partial k}{\partial y}\right] \qquad (3.47)$$

$$U\frac{\partial \tilde{\varepsilon}}{\partial x} + V\frac{\partial \tilde{\varepsilon}}{\partial y} = C_{\varepsilon 1} f_1 \frac{\tilde{\varepsilon}}{k}\nu_T\left(\frac{\partial U}{\partial y}\right)^2 - C_{\varepsilon 2} f_2 \frac{\tilde{\varepsilon}}{k} + E + \frac{\partial}{\partial y}\left[\left(\nu + \frac{\nu_T}{\sigma_k}\right)\frac{\partial \tilde{\varepsilon}}{\partial y}\right]$$

Equation (3.47) was developed by Lam and Bremhorst (1981), where, the ε term is defined as $\varepsilon = \varepsilon_0 + \tilde{\varepsilon}$, in which the $\tilde{\varepsilon}$ term is solved through the modified dissipation transport equation. The damping functions generated for the low Reynolds number to take place are given as $f_1, f_2, f_\mu, \varepsilon_0$ and E . In addition, as described previously, the application of the damping function and low Reynolds number models are dependent on the turbulence Reynolds number and y^+ values near the wall.

In certain cases, a one-equation model is preferred in the near wall region to couple with either the high Reynolds number two-equation or RSM turbulence model. This ease due to the fact that the empirical nature of the one-equation model often provides good prediction for near wall flow. Popular one-equation model used for near wall model approach include Wolffsrein (1969) and Norris and Reynolds (1975). This kind of approach is also known as the two-layer model approach. When the low Reynolds number model is used, the switch from the high Reynolds number turbulence model to the low Reynolds number wall model is normally done when the turbulent Reynolds number is less then 200.

$$\mathrm{Re}_T \equiv \frac{\rho\sqrt{k}\,y}{\mu} = \frac{k^2}{\nu\varepsilon} \equiv \frac{k^{1/2} l}{\nu} \tag{3.48}$$

To resolve the flow all the way until the viscous sub-layer, the adjacent grid requirement next to the wall must be $y^+<5$ and at least 10 grids generated in the sub-layer region of Reynolds turbulence number lesser then 200.

For the one-equation of Wolfastein (1967, 1969), the turbulent kinetic energy, k, equation is and the turbulence eddy viscosity are defined as:

$$\mu_T = C_\mu \rho k^{1/2} l_\mu$$

$$\mu\frac{\partial^2 k}{\partial y^2} + \frac{\mu_T}{\sigma_k}\frac{\partial^2 k}{\partial y^2} + \mu_T\frac{\partial^2 u}{\partial y^2} - \frac{C_D \rho k^{3/2}}{l_D} = 0 \tag{3.49}$$

Where the turbulent and dissipation length scale, l_μ and l_D are defined as:

$$l_\mu = y(1 - e^{-\mathrm{Re}_T A_\mu})\ldots \tag{3.50}$$

$$l_D = y(1 - e^{-\mathrm{Re}_T A_\varepsilon})$$

In most cases, the length scale in equation (3.49) has been modified to suit the ones given by Chen and Patel (1988), which is defined as:

$$l_\mu = \kappa y C_\mu^{-3/4}(1 - e^{-\mathrm{Re}_T / A_\mu}) \tag{3.51}$$

$$l_D = \kappa y C_\mu^{-3/4}(1 - e^{-\mathrm{Re}_T / A_\varepsilon})$$

For the RSM turbulence model, the low Reynolds number flow effect is incorporated in the modelled dissipation term and also in the pressure strain redistribution term. Manceau and Hanjalic (2002) have introduced an elliptical blending model to take account of the near wall low Reynolds number effect. The model was based on the elliptical relaxation model of Durbin (1993) and is difined as

$$\phi_{ij} = (1-k\alpha)\phi_{ij}^{W} + k\alpha\phi_{ij}^{h} \tag{3.52}$$

Where ϕ_{ij}^{h} was taken as the high Reynolds number pressure strain redistribution model of Speziale (1991) and $\emptyset_{ij}^{W}$ is the wall reflection effect defined as:

$$\phi_{ij}^{W} = -5\frac{\varepsilon}{k}\left(\tau_{ik}n_j n_k + \tau_{jk}n_i n_k - \frac{1}{2}\tau_{km}n_k n_m (n_i n_j - \delta_{ij})\right) \tag{3.53}$$

However, results have shown that although low Reynolds number model for near wall treatment have managed to reproduce an appropriate C value for the logarithmic law equation, it still does not manage to predict good results for flow close to the wall, Wilcox (2002). It was shown in Wilcox (2002) that in most cases under adverse and favorable pressure gradient application, the low Reynolds number model still over predicts the values for skin friction coefficients. According to Wilcox (2002), the main reason why the low Reynolds number models failed to predict proper flow behaviour close to the wall is due to the inability of the two-equation model to proper predict the flow in the defect layer, which translate to poor prediction of the flow in the sub-layer.

3.3.11 DES Modeling

As said in Travin et al. (2000), "A Detached Eddy Simulation (DES) is a three-dimensional numerical simulation using a single turbulence model, which function as a sub-grid scale model in regions where the grid density is fine enough for a Large Eddy Simulation, and as a Reynolds-Average model in regions where it is not"

The DES length scale is chosen according to the following equation:

$$l_{DES} = \min(l_{RANS}, C_{DES} \times \Delta) \tag{3.54}$$

where C_{DES} is the DES constant calibrated by means of homogeneous, isotropic turbulence spectrum, and Δ is the largest dimension of the elementary control volume cell, $\Delta = \max(\Delta x, \Delta y, \Delta z)$.

For the one equation Spalart-Allmaras model (Spalart and Allmaras, 1993), it gives:

$$l_{DES} = \min(d_{\omega}, C_{DES} \times \Delta) \tag{3.55}$$

Where d_{ω} is the distance from the wall. The consequence of the length scale modification is an increase of the dissipation term in the eddy–viscosity transport equation:

$$D^{v} = \left(C\omega 1 f\omega - \frac{C_{b1}}{\kappa^{2}} f_{t2} \right) \left(\frac{\tilde{v}}{l_{DES}} \right)^{2} \tag{3.56}$$

3.3.12 DDES Modeling

In order to avoid a transition from URANS to LES in the shear layer that could produce nonphysical artefacts, Spalart, (2006) introduces a modification of the r parameter of the Spalart-Allmaras model (Spalart and Allmaras, 1993) in:

$$r_{d} = \frac{v_{t} + v}{\sqrt{U_{i,j} U_{j,i}} \kappa^{2} d^{2}} \tag{3.57}$$

By adding v on the numerator they ensure that r_{d} remains away from 0 in the near wall regions. Then we can write $f_{d} = 1 - \tanh(8 r_{d})^{3}$ which is 1 away from the wall an 0 in the near wall regions where $r_{d} << 1$. Finally we have: $l_{DES} = d_{\omega} - f_{d} \max(0, d_{\omega} - C_{DES} \Delta)$. If $f_{d} = 0$, we obtain $l_{DES} = d_{\omega}$ which yields to RANS modelling and if $f_{d} = 1$, $l_{DES} = \min(d_{\omega}, C_{DES} \times \Delta)$ which yields to the classical DES modelling (Spalart et al. 1997).

3.3.13 RANS Model

It is not practical to resolve all the scales for engineering problems such as the flow over the Ahmed body. While TRANS, a transient Reynolds average Navier-Stokes approach (RANS), offers a very promising approach because the large scales can be resolved while the small scales, which carry less turbulence energy compared to the large scale, are modeled by RANS sub-scale models. The averaged Navier-Stokes take the following form:

$$\frac{\partial \rho U_i}{\partial x_i} = 0 \tag{3.58}$$

$$\frac{DU_i}{Dt} = g_i - \frac{1}{\rho}\frac{\partial P}{\partial x_i} + \frac{\partial}{\partial x_i}\left[v\left(\frac{\partial U_i}{\partial x_j} + \frac{\partial U_j}{\partial x_i}\right)\overline{u_i u_j}\right] \tag{3.59}$$

According to the Boussinesq assumption, the isotropic eddy viscosity diffusivity formulation for Reynolds stress reads:

$$\overline{u_i u_j} = \frac{2}{3}k\delta_{ij} - v_t\left(\frac{\partial U_i}{\partial x_j} + \frac{\partial U_j}{\partial x_i}\right) \tag{3.60}$$

The above–mentioned assumption is not always true because of the an-isotropic nature of the flow in specific cases, such as the case that involve the flows in near wall region.

3.3.14 Three Equation Model (k-ε-v^2)

Durbin (1991 and 1995) devised a three-equation model, known as the k-ε-v^2 model or v2f model. The idea is to resolve the normal stress v^2, along with solving the modified k and ε equations. The near wall region is resolved exactly and the wall-reflection is considered by means of elliptic relaxation in the model. It has been reported (Durbin (1991 and 1995), Behnis et al. (1998), Georgi et al. (2000), Lien and Durbin (1996)) that this model is a significant improvement over the two-equation model for several test cases, such as channel flow, backward facing step, etc. Governing equations read:

$$\frac{Dk}{Dt} = P_k - \varepsilon + \frac{\partial}{\partial x_j}\left[\left(v + \frac{v_t}{\sigma_k}\right)\frac{\partial k}{\partial x_j}\right] \tag{3.61}$$

$$\frac{D\varepsilon}{Dt} = \frac{C_{\varepsilon 1}P_k - C_{\varepsilon 2}\varepsilon}{T} + \frac{\partial}{\partial x_j}\left[\left(v + \frac{v_t}{\sigma_\varepsilon}\right)\frac{\partial \varepsilon}{\partial x_j}\right] \tag{3.62}$$

$$\frac{D\overline{v^2}}{Dt} = kf_{22} - \overline{v^2}\frac{\varepsilon}{k} + \frac{\partial}{\partial x_j}\left[\left(v + \frac{v_t}{\sigma_k}\right)\frac{\partial \overline{v^2}}{\partial x_j}\right] \tag{3.63}$$

$$\frac{\partial}{\partial x_j}\left(\frac{\partial f_{22}}{\partial x_j}\right)-f_{22}=(1-C_1)\frac{\left[2/3-\overline{v^2}/k\right]}{T}-C_2\frac{P_k}{k} \tag{3.64}$$

f_{22} is a quotient of the pressure strain Φ_{22} by the turbulent kinetic energy k.

$$v_t = C_\mu \overline{v^2}T$$

$$C_\mu = 0.19, C_{\varepsilon 1} = 1.44, C_{\varepsilon 2} = 1.9, \sigma_k = 1.0, \sigma_\varepsilon = 1.3$$

$$P_k = v_t\left(\frac{\partial U_j}{\partial x_i}+\frac{\partial U_i}{\partial x_j}\right)\frac{\partial U_j}{\partial x_i}$$

The time scale T and length scale L can be obtained from the following

$$T = \max\left\{\frac{k}{\varepsilon}, 6\left(\frac{v}{\varepsilon}\right)^{1/2}\right\}$$

$$L = 0.3\max\left\{\frac{k^{3/2}}{\varepsilon}, C_\eta\left(\frac{v^3}{\varepsilon}\right)^{1/4}\right\}$$

$$f_{22w} = -\frac{20v^2}{\varepsilon_w}\left(\frac{\overline{v^2}}{y^4}\right)_p,$$

where w and p denote the values at the wall and that in the first cell above the wall, respectively.

3.4 Predefined Parameters

3.4.1 Boundary Conditions

Boundary conditions are a set of properties or conditions on surfaces of domains and are required to fully define the flow simulation. The type of boundary condition that can be set depends upon the boundary surface. A fluid boundary is an external surface of the fluid domain excluding surfaces where it meets other domains.

A fluid boundary supports following boundary conditions:

(a) Inlet – Fluid predominantly flows into the domain.

When we define an area to be an inlet then we anticipate that flow will be in to a domain. We can set either velocity or pressure at the point, and solver will calculate the other value.

In the inlet we applied the

velocity = 40 m/s and temperature = 298K.

(b) Outlet- Fluid predominantly flows out of the domain.

When we define an area to be an outlet then we anticipate that flow will be out from a domain.

The outlet boundary condition applied is:

Relative Static Pressure = 0 Pa.

(c) Wall – Impenetrable boundary to fluid flow.

There are three options for the influence of a wall boundary on the flow, namely:

(i) No Slip Wall (ii) Free Slip Wall and (iii) Rotating Wall.

No Slip: This is the most common type of wall boundary condition. A real fluid, the existence of intermolecular attractions causes the fluid to adhere to a solid wall and this gives rise to shearing stress. The real fluids have a zero velocity at the walls and hence they cannot slip at the boundary wall. This is known as no slip condition.

Free Slip: In this case the velocity component parallel to the wall has a finite value (which is computed) but the velocity normal to the wall, and the wall shear stress, are both set to zero.

Rotating Wall: This option applies to both stationary and rotating domains and allows the wall to rotate with a specified angular velocity. The angular velocity is always in relation to the local (relative) frame of reference. An axis must be specified in a stationary domain and can optionally be specified in a rotating domain.

We applied the following wall boundary conditions:

Wall influence on flow =No slip

Wall function =Scalable

Wall roughness =Rough wall

Roughness height = 0.0002m

Fixed temperature = 298K

3.4.2 Simulation Parameters

The following conditions are used as simulation parameters.

Simulation type	Stationary
Domain type	Fluid domain
Flow region	Subsonic
Fluid	Air at 298K
Buoyancy	Buoyant
Reference pressure	1[atm]
Gravity	X=0 Y=0 $Z=-9.807 m/s^2$
Buoyancy reference temperature	298K
Domain motion	Stationary
Heat transfer option	Isothermal
Buoyancy turbulence	Production and dissipation,
Turbulence balance	k- Epsilon
Equation class setting	Continuity, Turbulence Eddy Dissipation, Turbulence Kinetic Energy and Momentum
Solver control	
Advection scheme	High resolution
Maximum number of iterations	100
Timescale control	Physical timescale
Physical time	Length of tunnel/velocity of fluid
Residual type	Maximum
Residual target	0.0000001
Conservation target	0.01

3.5 Solution Procedure

3.5.1 General CFD Approach

There are three steps involved in a typical CFD simulation. The three steps are:

* Pre-Processing Stage

* CFD Solver Stage

* Post-Processing Stage

In the pre-processing stage, CFD users are needed to provide sufficient input to the computer in order to obtain the desired output. The pre-processing stage is divided into several steps:

* Geometry Generation

* Mesh Generation

* Input for Boundary Conditions

* Flow Type arraignment

* Selection of Discretization Scheme

* Selection of Turbulence and Near Wall Model

The second stage is the solving stage where the physics of the flow is being solved by the computer. The flow solver was run to produce a file of results that contains the variation of velocity, pressure and any other variables throughout the region of interest. The third and final stage is called the post-processing stage where analysis on graphical representation of the numerical results takes place.

3.5.2 CFD Grid /Mesh Generation and Discretization Methods

In order to generate the highest quality of grids for the highest level of accuracy on a CFD simulation, grids generated depends on the complexity of the flow problem. For high complex flow problems, a more complex high quality grids need to be generated for the CFD simulation. This high level of flow complexity applies for automotive type problems. However, the applications of complex grid generation in automotive flow problems are dependent on the overall performance of the modern day computers. The generation of grids and employing of discretization schemes for a simplified flow were done using a linear or potential flow method.

After the development of supercomputers that are capable in handling complex turbulence flows, a non-linear method was developed for grid generation and discretization schemes.

The linear methods or potential flow methods are applied on problems where flow is usually incompressible, inviscid and irrotational. Governing Navier-Stokes equation is reduced to its linear Laplace form. Flow that uses the linear methods are not practical in solving turbulent flow around a ground vehicle. This is because grid generation for a linear method is usually generated only on the body surface of the ground vehicle geometry. Despite its limitations, the linear methods are still widely used in the industry. However, modeling additional flow phenomena such as vehicle wake and vortex formation requires separate modeling techniques. It does not have the ability to automatically simulate flow separations around the vehicle especially the formation of A-pillar vortices. Further information on the linear methods is available in Ahmed (1998).

In the non-linear methods, the physics of the flow takes into account of complex phenomenon such as turbulent properties. Therefore, it requires a much more complex Navier-stokes equation. Since three-dimensionality is now in play, grids generation will occupy the whole computational domain around the geometry of the ground vehicle body. For non-linear methods, the coupling of grid generations and discretization of numerical schemes approximations can be done using either one of three grids discretization methods:

- Finite Difference
- Finite Volume
- Finite Element

The choice of using the finite difference, finite volume or finite element methods depends on the complexity of the geometry.

According to Ahmed (1998), the finite difference technique was the first to be developed. The basic idea of finite difference technique is to express the governing partial differential equations approximately into algebraic difference equations form using finite difference schemes at the grid nodal point. Finite difference methods often employ curvilinear orthogonal grid system that are difficult and time consuming to generate especially in three-dimensional computational domain. The resulting governing transport equations have more terms. This difficulty makes the finite difference techniques seldom used in automotive CFD.

In the finite volume methods, the computational domain is split up into many small control volumes. The partial differential governing equations are integrated over each of the control volumes and the resulting integrated governing equations are then discretized using finite-difference schemes. A resulting set of algebraic equations is then formed, which are then solved. The main advantage of finite volume methods over the finite difference methods is that the finite volume methods can use both structured orthogonal and non-orthogonal grid system. In the non-orthogonal grid system, irregular unstructured grids can be used. As a result, various grid shapes and size can be used for the finite volume methods. This is however, at the expense of additional computational resource, Because of the flexibility in grid generation of the finite volume methods, it is the most preferable methods used in automobile aerodynamics applications.

In the finite element methods, the computational domain is split up into small volumes, called elements. Within each element, values are being approximated as a liner combination of weighting residuals and use the integral form of the governing differential equations for each element volume without direct reference to other cells. Information is shared among all the other grid points in the element. This method generally uses irregular unstructured grid, often in a triangular shaped element. By employing irregular unstructured grids, the treatment of complex surface geometry is possible and furthermore, it also allows local grid refinements at critical areas without the penalty of simultaneous grid refinements at other areas. However, this also serves as a disadvantage since sufficient refined grids in finite element methods are needed to give solution of high accuracy, Du Pont (2001).

For structured grids, the computational domain is often divided into several blocks. This technique is often defined as Block-Structured or Multi-Block technique. Each block can be constructed with different grid density depending on the flow requirement on that region (i. e. separation, vortex generation). Often in a three-dimensional flow, hexahedral type grid is used for the computational domain. Hexahedral grids have small no skewness resulting in numerical results of high accuracy. The problem with multi-block structured grid is that most often, the grids do not align up against its adjacent interface of blocks.

Grids can also be arranged in an unstructured manner. In three-dimensional flow, grids that are normally arranged in an unstructured manner consist of prisms and tetrahedral grids. Unstructured grids offer flexibility and in especially on area with complex surface geometry. The overall grid generation process is faster with unstructured grids.

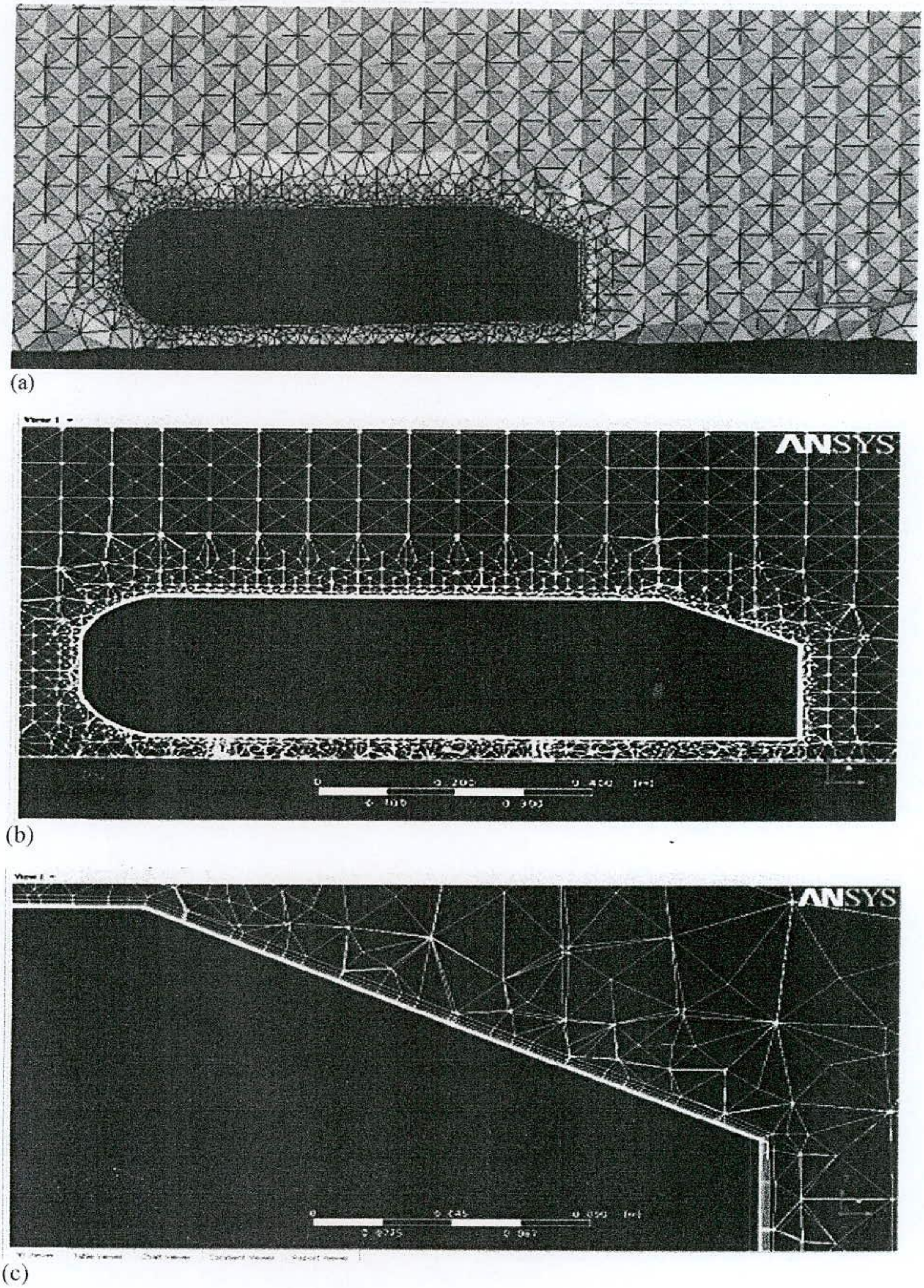

Figure 3.5.1 (a, b, c): Grids in different aspect ratio.

The present work was conducted by using a ANSYS- 11$^{©}$ Software to generated the grid. The unstructured grid used contained about maximum 2096000 elements and 467000 nodes. We considered 12 grid layers in the boundary layer of the body.

Chapter 4

4.0 RESULTS AND DISCUSSIONS

Our target is to reduce the Drag exerted by a Ahmed car body. For the purpose numerical simulation is chosen and ANSYS-11 is used as the simulation software. For the simulation a car body to be built. Some physical phenomena of the car body will be setup, along with property in the flow region. A primary check is required before the investigations for a procedure to reduce the drag. Through the cheek we need to assess the uncontrolled flow. While we are using ANSTS-11, it is required to choose the turbulence model and in some cases the roughness height of the body. While we are generating meshes over the car body and further away from the car body, special attention are required to choose the grids. Also number of iteration has its own importance for providing the output, thus demand attention to be selected.

As Ahmed car body is a standard one so whatever the results obtained through simulation cannot be accepted. If the results are only comparable to some benchmark then they are accepted. We have chosen Lienhart et al. (2000) as benchmark and so it is our primary duty to compare the simulated result with the benchmark. If the simulated result is comparable with the benchmark then only we can say that the parameters chosen for the simulations are valid. In the following we will discuss how the parameters are chosen in section 4.1 as code validation; dependence of the results on the number of grid is presented in section 4.2 as grid dependence test. To reduce the drag we have proposed to introduce grooves at different positions over the body which is of course basically a passive strategy and they will be presented in sections 4.3- 4.6.

4.1 Code Validation

As has been discussed, in this subsection the parameters specially the choice of turbulence model and selection of roughness height will be discussed. Of course the choices will be done on the basis of the comparison with the benchmark. For the comparison purpose the drags at the different parts of the body that is drags exerted by nose, rear slop and the back may be chosen differently but the total drag may also be chosen. We have compared the total drag as a whole but also we have chosen the drags exerted by different parts. Also we have cheeked the velocity profiles at different positions over the body to verify the obtained velocities at the positions (comparable or not).

4.1.1 Selection of Turbulence Models

Turbulance is of great importance in CFD. The understanding of the physics of turbulane is cretical and many different models have evolved. Sometimes the turbulance models are validated through vehacle aerodynamics. Computers have been used to solve fluid flow problems for many years. Numerous programs have been written to solve either specific problems, or specific classes of problems. From the mid-1970's, the complex mathematics required to generalize the algorithms began to be understood, and general purpose CFD solvers were developed. Recent advances in computing power, together with powerful graphics and interactive 3D manipulation of models have made the process of creating a CFD model and analyzing results much less labor intensive, reducing time and, hence, cost. Advanced solvers contain algorithms which enable robust solutions of the flow field in a reasonable time.

For the comparison purpose we have chosen $k-\varepsilon$, $k-\omega$, Shear Stress Transport (SST) and Baseline $k-\omega$ (BSL) turbulence models. The comparison is done on the basis of velocity profiles at different locations over Ahmed car body. A velocity of 40m/s, is taken in these simulations and the respective velocity profiles are compared for the different turbulence models. The experimental data of the Linhart et al. (2000) is also compared with the chosen turbulence models velocity profiles. A detail of these comparisons are discussed below:

The origin of the Cartesian coordinate system considered is placed at the floor beneath the rear end of the body, x-axis is placed in the longitudinal direction towards outlet, y-axis is placed along the width, and z axis is along the vertical. As a result the body is at the negative side of x (A brief description of the body is given in §- 3.2 earlier). Velocity profiles at different locations are taken but for the sake of brevity only six key locations are presented here with inlet flow velocity 40m/s. The locations are in front of the body, about the middle part of the body, close to the start of the slant, over the slant, close to the rear end and a bit away from the back. Velocity profiles of the simulations with k-ε, k-ω, SST and BSL turbulence models, are compared with the experimental data of Linhart et al. (2000). The velocity profiles at different locations along with the experimental data are presented in Fig 4.1.1(a-f).

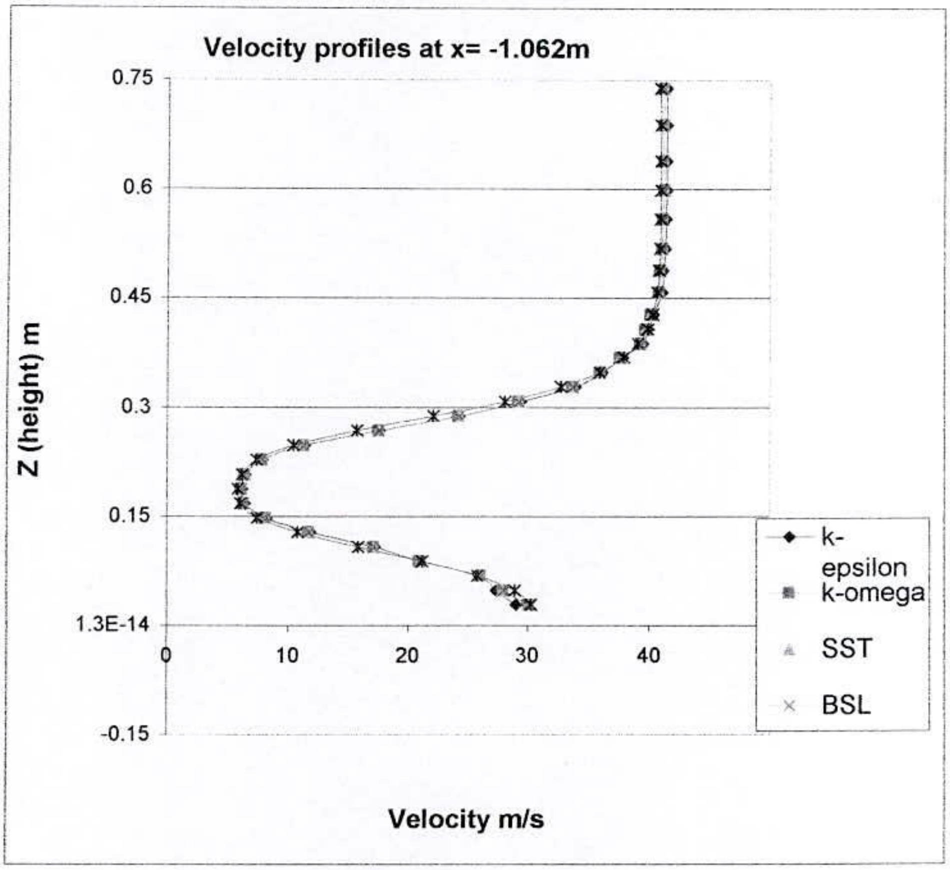

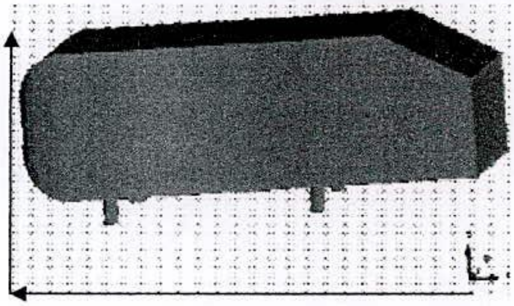

x = -1.062m

Figure 4.1.1(a):Velocity profiles at x= -1.062m.

In the front position (Fig 4.1.1a) the velocity profiles due to all the turbulence models matches well with the experimental value up to a certain height 0.45m. Above that height the velocity suggested by the models are more than the experimental, of them k-ε, models velocity deviates more with the increase of height.

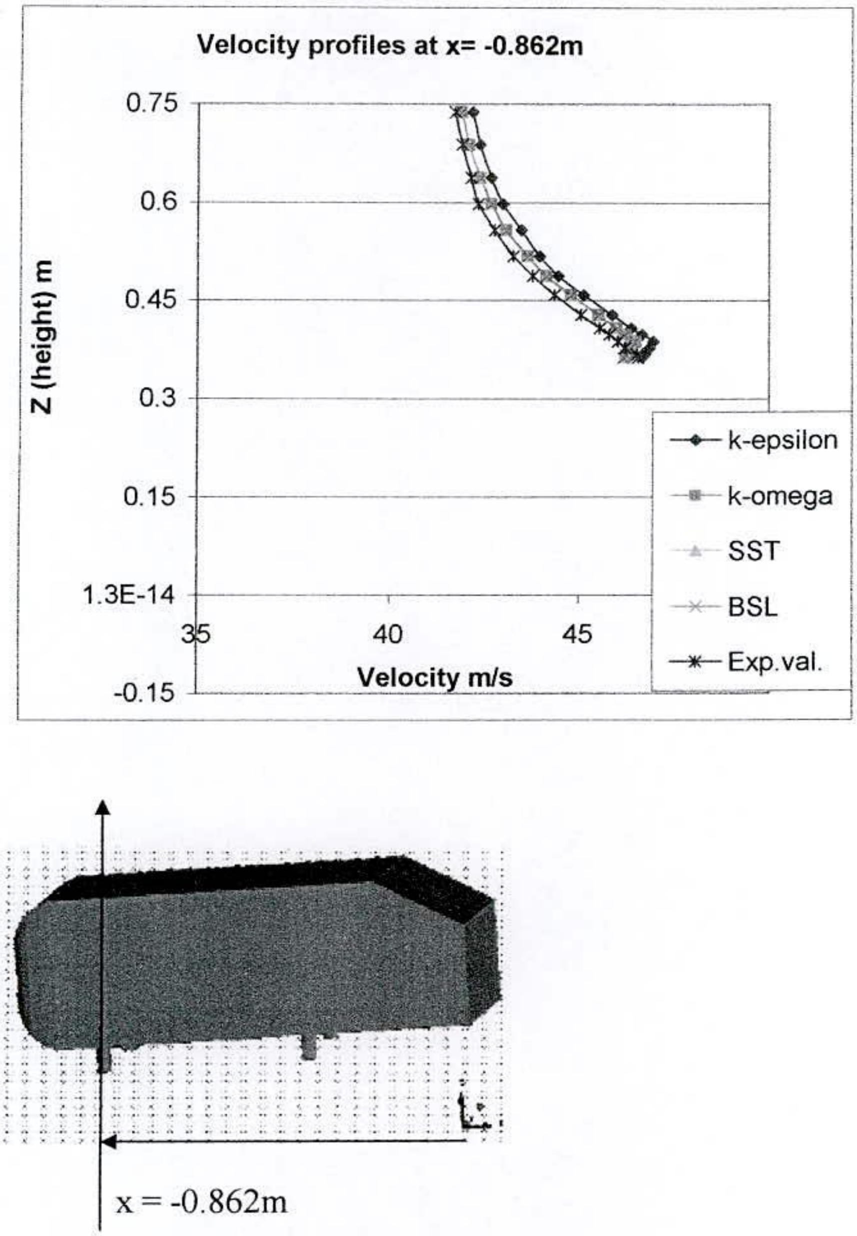

Figure 4.1.1(b): Velocity profiles at x= -0.862m.

Over the midpoint of the body (Fig 4.1.1b) all the patterns of the velocity profiles due to the different turbulence model matches well with the experimental one but differ in terms of velocities except nearer the body. Nearer the body, the shape of the experimental velocity profile mismatches with the model. Of the four, suggested velocity by k-ε model is closer to the experimental (little more) near the body. Its suggested velocity remains more than the experimental all through the height. Except close to the body velocity profiles of BSL remain close to the experimental.

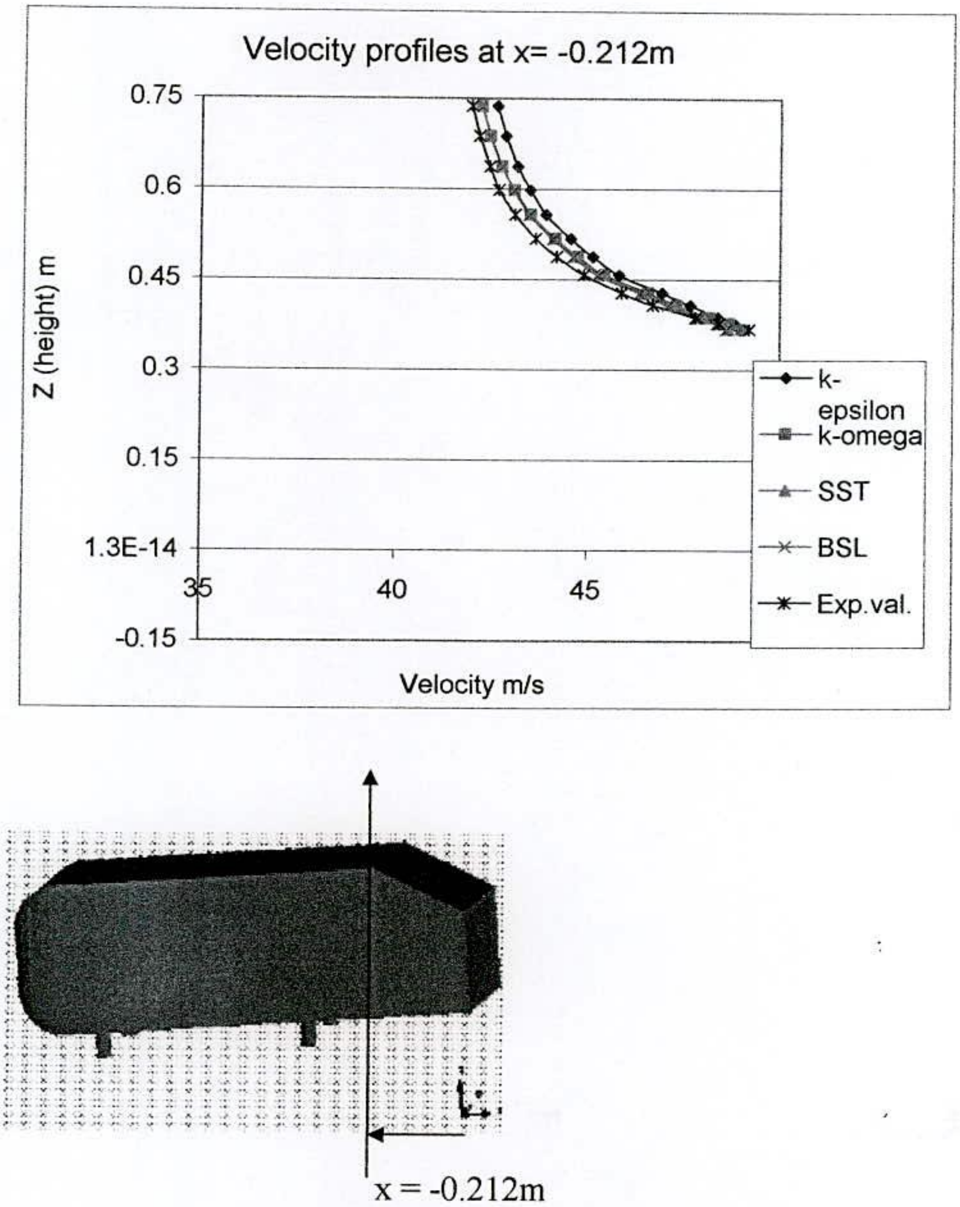

Figure 4.1.1(c): Velocity profiles at x= -0.212m

At the position near the start of the body (Fig 4.1.1c) velocity profiles suggested by k-ω model is close to the experimental (near the body). Velocity produced by the k-ε model is the next, but deviates more with the increase in height.

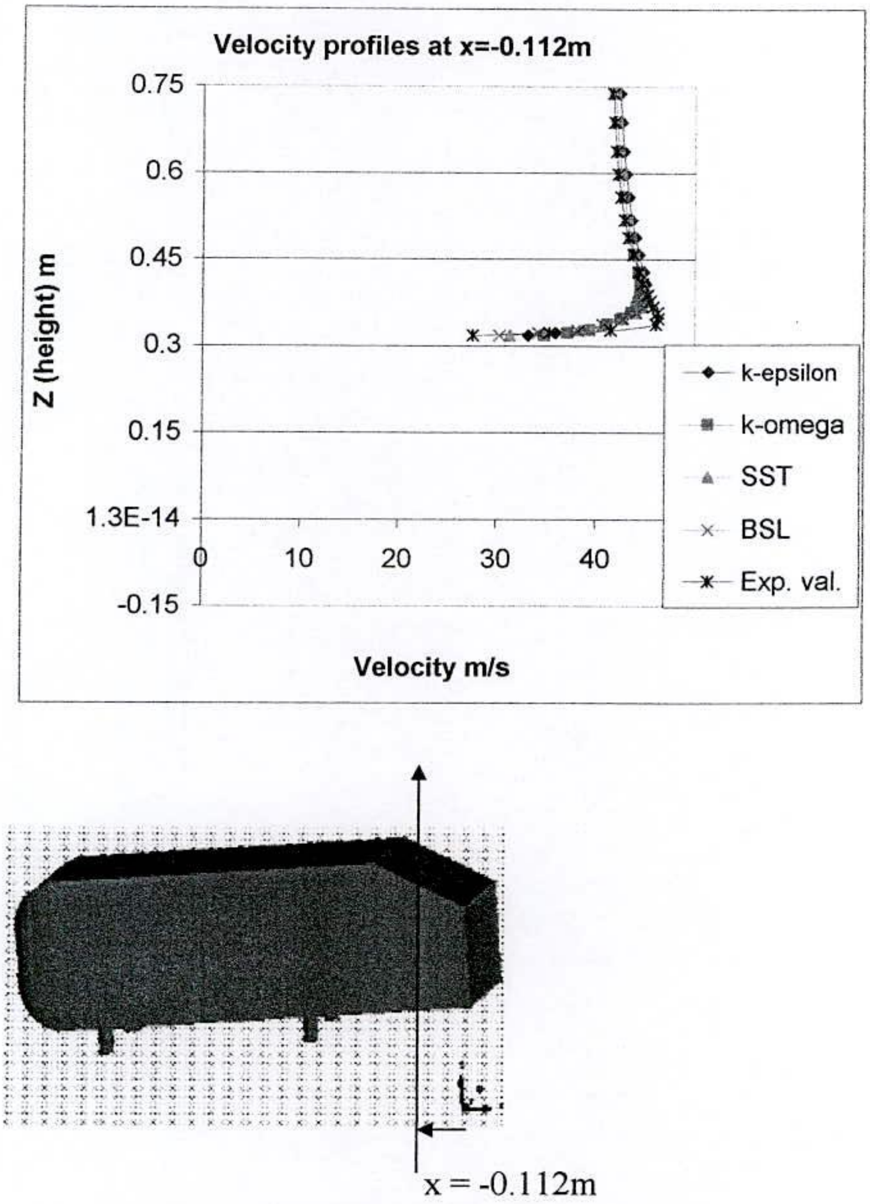

Figure 4.1.1(d): Velocity profiles at x=-0.112m.

Over the slant, near the body k-ε model's velocity is in the best match with the experimental data, BSL model suggested profile is next (Fig 4.1.1d). None of the model is showing the sharp turning as is found in the experiment.

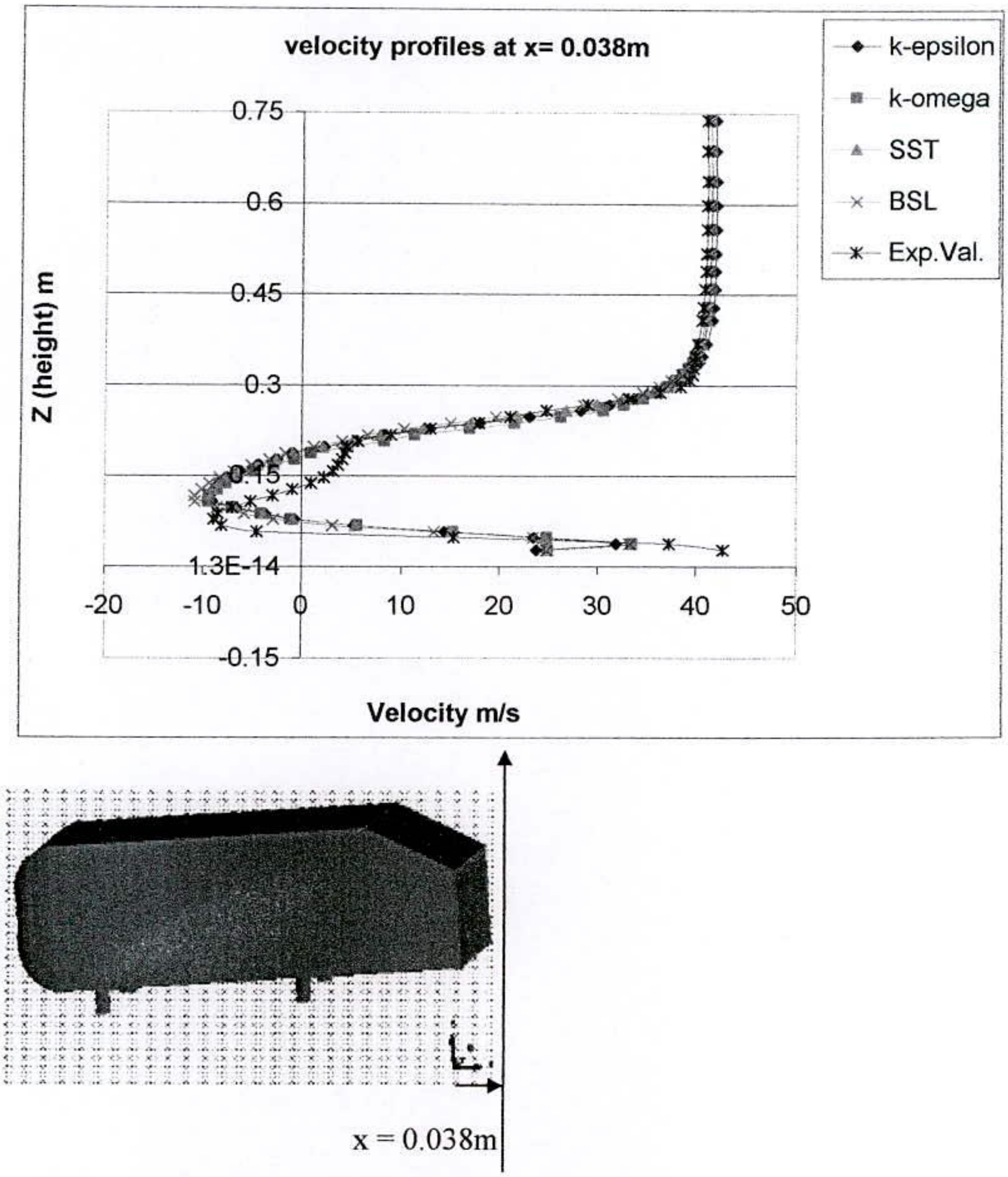

Figure 4.1.1(e): velocity profiles at x= 0.038m.

At the position after the rear end the shape prescribed by the experimental data is not found through models (Fig 4.1.1e). The models suggested shape is smooth but the experimental one is not that much. At the sharp turning performance of the k-ε is close to experimental. With the increase in height k-ε model's velocity differ more from the experiment.

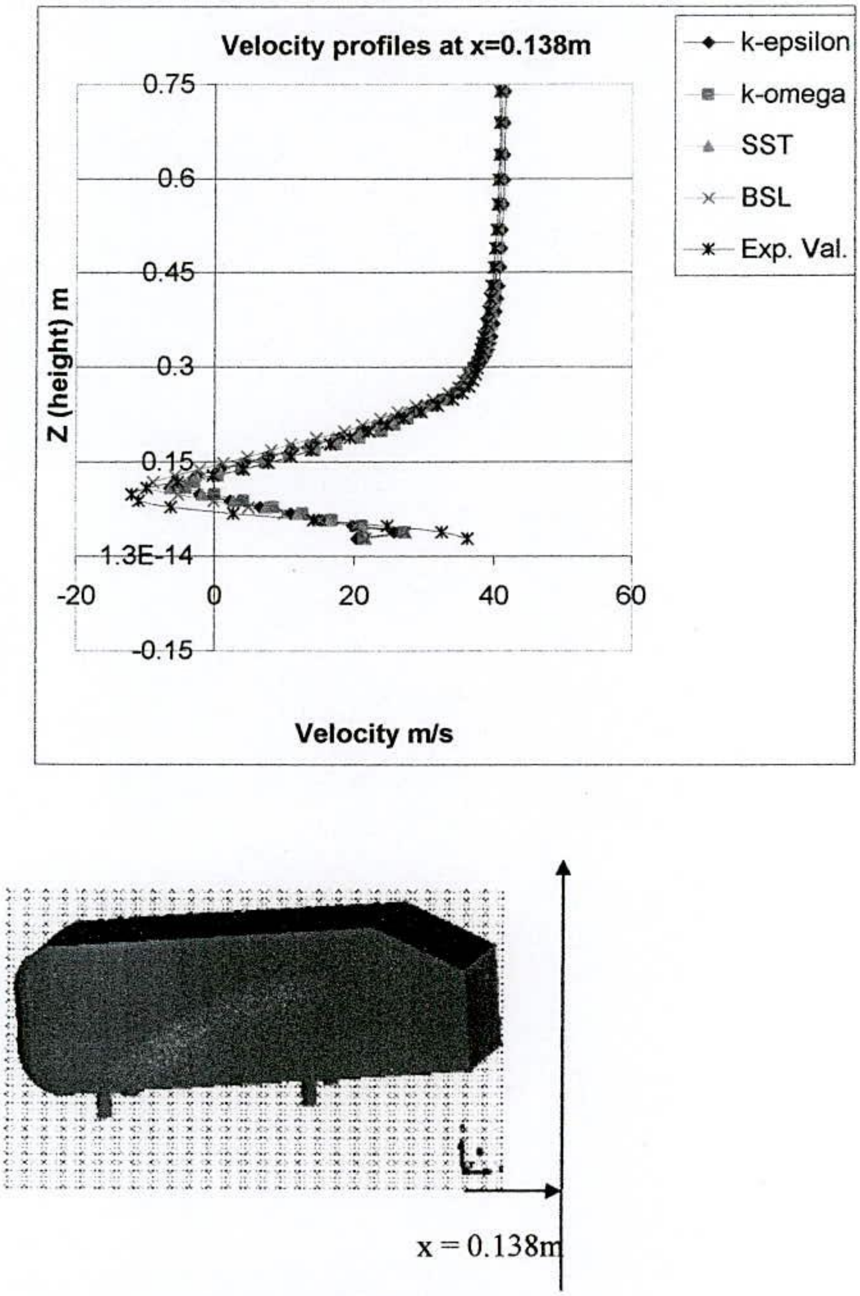

Figure 4.1.1(f): Velocity profiles at x=0.138m.

Away from the rear end the sharp turning is found in all model's velocity profile (Fig 4.1.1f) but the velocities and heights of turning are different for different models. The velocity and height at the turning produced by the BSL model is close to the experimental data, though the velocity-height relationship differ from the experimental data before the free stream.

From the above discussion it may be concluded that

(a) The geometry proposed by Ahmed (1984) has been well adapted in the simulation.

(b) The velocity profiles at different locations obtained through different turbulent models are comparable among them and also to the benchmark.

(c) Near the body the performance of the k-ε model is best among the models considered.

Hence for our further experiments purpose k-ε model will be considered.

4.1.2 Selection of Roughness Height

In most CFD program a standard roughness height is need to set. But if we take much rough surface like sand grain size, we need to modify the wall function for the turbulence model with the more active roughness height. Flow over rough surface has significant importance in industrial application but much less knowledge is available for flow over rough surface. Sometimes the roughness heights are validated through vehicle aerodynamics. To choose the roughness height comparison is done between the drag coefficients of k-ε and RNG k-ε turbulence models at different roughness heights over the Ahmed body. In these simulations 40 m/s velocity is taken.

As the all car body dimensions are normalized with the body height H so the roughness height is also normalized by the same. As a result though simulations are done with the roughness heights 0.0001m, 0.0002m etc but plots are not showing that values.

Figure 4.1.2 and Figure 4.1.3 are representing the overall effects of roughness height on the total drag coefficient for the k-ε turbulence model and RNG k-ε turbulence model respectively. From Figure 4.1.2 it is clear that with the increase in the roughness height the total drag primarily decreases and latter increases, which indicates that k-ε turbulence model has dependency on the roughness height. On the other hand, from Figure 4.1.3, the total drag increases rapidly with the increase in roughness height. After certain value though it remains increasing but the rate slows down.

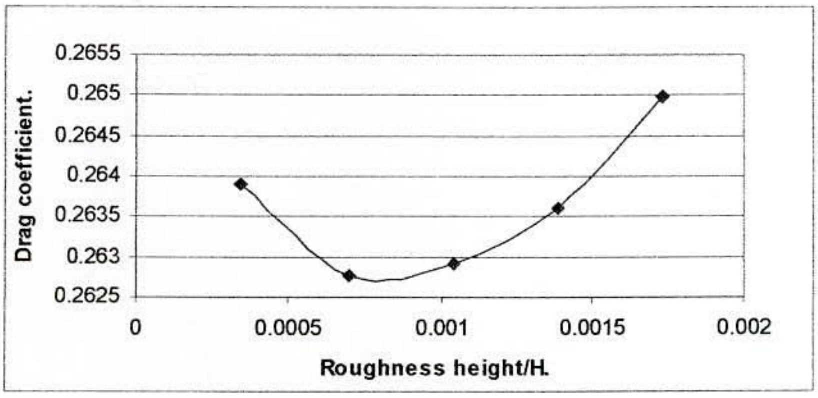

Figure.4.1.2. Drag coefficient profile for different value of λ for k-ε turbulence model

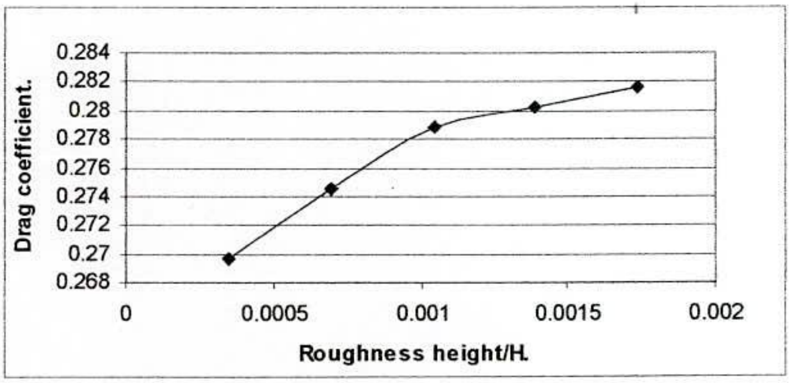

Figure.4.1.3. Drag coefficient profile for different value of λ for RNG k-ε turbulence model

Not only the total drag is the matter of interest but also the drags at the nose, rear slope and at the back are of interest. Thus the drag coefficients at the nose, at the back and at the rear slope along with their sum treated as the total drag coefficients are tabulated for different values of the normalized roughness height in Table 4.1.1 and 4.1.2 for k-ε and RNG k-ε turbulence model respectively.

Table 4.1.1: Drag coefficient values for k-ε model.

Roughness height/Body height	Drag coefficient at the nose	Drag coefficient at the rear slope	Drag coefficient at the back	Total drag coefficient
0.0003472	0.01400	0.13589	0.11400	0.26389
0.0006944	0.01795	0.12892	0.11590	0.26280
0.0010416	0.02058	0.12505	0.11728	0.26291
0.0013888	0.02270	0.12203	0.11888	0.26361
0.0017360	0.02466	0.12012	0.12021	0.26499

It is seen from Table 4.1.1 that with the increase in the normalized roughness height the drag coefficient at the nose is continuously increasing. The drag coefficient at the back is also monotonously increases but the drag at the rear slope decreases with the increase in the normalized roughness height. These up and down effects finally have produced primary decrease and then increase effect. From Table 4.1.2 it is observed that with the increase in the normalized roughness height the drag coefficient at the nose grows primarily faster but afterward slows down.

Table 4.1.2: Drag coefficient values for RNG k-ε model.

Roughness height/Body height	Drag coefficient at the nose	Drag coefficient at the rear slope	Drag coefficient at the back	Total drag coefficient
0.0003472	0.014552	0.115008	0.140176	0.269736
0.0006944	0.017966	0.115004	0.141573	0.274543
0.0010416	0.020612	0.114932	0.143282	0.278826
0.0013888	0.024207	0.113039	0.143021	0.280267
0.0017360	0.024788	0.114038	0.142814	0.281640

It is seen from Table 4.1.2 the drag coefficient at the back primarily increases but afterward decreases, whereas that at the rear slope primarily decreases and then increases, but at in sum, the total drag coefficient increases continuously with the increase in the normalized roughness height.

Finally the minimum coefficient of drags at the rear slant and at the back are in Table 4.1.3 to compare among k-ε and RNG k-ε turbulence models with LSTM benchmark values. It is observed that the simulations produced drags are comparable with the LSTM benchmarks.

Table 4.1.3: Comparison between drag coefficients of different models

Model	Drag coefficient at the rear slope	Drag coefficient at the back
LSTM(Lienhart et al. 2000)	0.121	0.129
k-ε	0.1289	0.1159
RNG k-ε	0.115008	0.140176

On the basis of the above discussion we may conclude that

(a) Drag exerted by nose, rear slop and back do not show coherent behavior, i.e. with the increase in one there may decrease in other.

(b) k-ε turbulence model has dependency on the roughness height.

As we have the intension to use the k-ε turbulence model in the simulations attention should be given to this parameter. It has been found that a roughness height 0.0002m (equivalent to normalized value 0.0006944) is to be chosen for better performance in terms of drag.

Thus for further experimentations k-ε model with roughness height as 0.0002m will be used.

4.2 Grid Dependency Test.

Krajnovic and Davidson (2005 a) divided mesh quality in three groups and proposed that the extension of near-wake separation bubble in the coarse, medium and fine grid simulations will be 0.6H, 0.65H and 0.65H, respectively (H, being the height of the body).

Many researchers used various numbers of elements for their simulation. Bruneau et al. (2007) presented 983040 cells (element) uniform mesh for numerical efficiency.

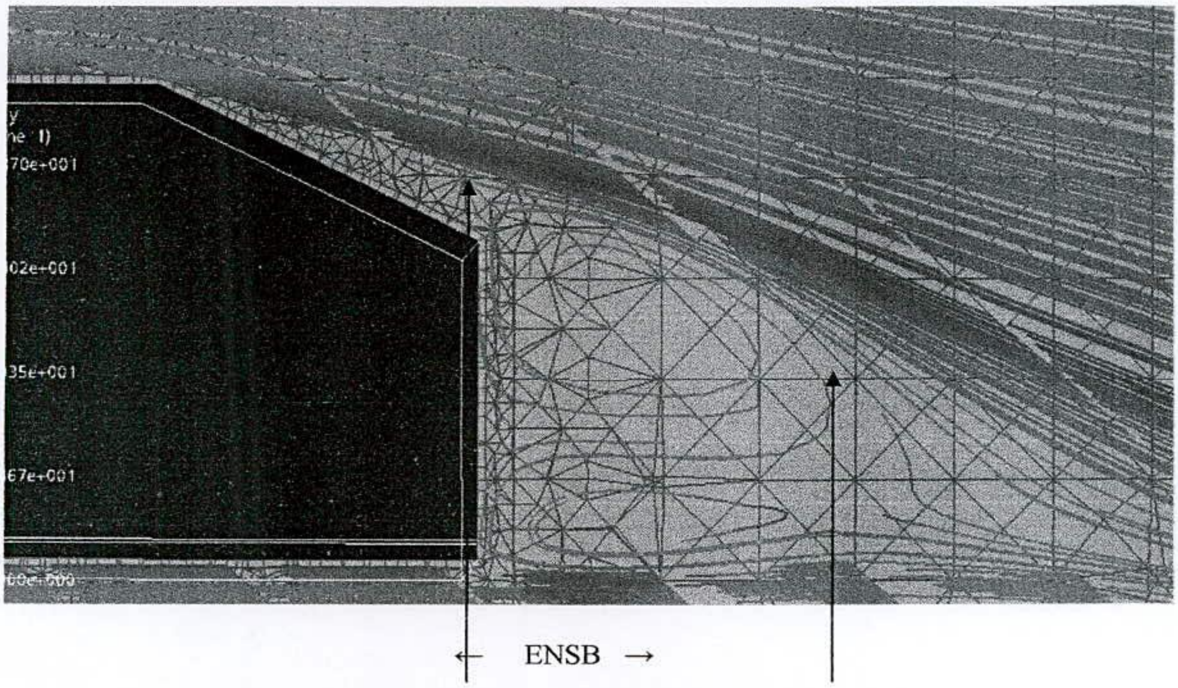

Figure 4.2.1: Extension of near-wake separation bubble (ENSB).

Harinaldi et al. (2011) used Gambit 2.4® software to generat the grid. Meshing was tetra/ hybrid element with hex core type and the grid number was more than 1.7 million (1700000) in order to ensure detail discretization and more accurate results.

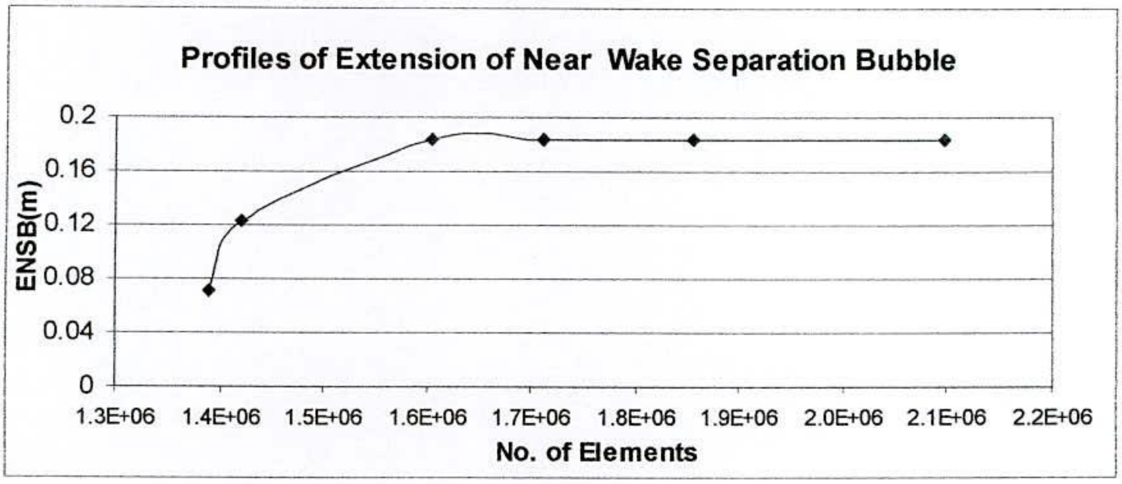

Figure 4.2.2: A profile of ENSB(m) against number of element.

Table 4.2.1: Data of Extension of the near-wake separation bubble (ENSB) for Krajnovic (2005a) and Experimental value.

S. No.	Grid Name	ENSB of Experimental value	ENSB of Krajnovic and Davidson(2005a)
1	Coarse grid	0.43H	0.6H
2	Medium grid	0.64H	0.65H
3	Fine grid	0.64H	0.65H

Table 4.2.2: Data element's number, ENSB and grid quality(name of grid).

S. No.	Grid Name	N. of Elements	ENSB
1	Coarse grid	1390049	0.071429m or 0.25H
2	Coarse grid	1420184	0.122449m or 0.43H
3	Medium grid	1603745	0.183673m or 0.64H
4	Fine grid	1711316	0.183673m or 0.64H
5	Fine grid	1854221	0.183673m or 0.64H
6	Fine grid	2096390	0.183673m or 0.64H

In our case trial and error process is used to find the number of elements suitable for the generation of Ahmed car body. For the purpose extension of near wake separation babble has been cheeked and it has been found that about 2096000 numbers of elements can be handled by the computing facility used and is suitable and the drag is comparable to the benchmark (LSTM).

The turbulent model that has been used is not incidental. The suggestion given by Azad et al. (2012) has been adopted. The roughness height has been taken (0.0002m) as per suggestion of Azad et al. (2013).

4.3 Effect of Groove at Top Surface.

To assess the effects of grooves at the top surface we have performed two different types of studies namely one groove at the end of the top surface and a pair of grooves at the end of the top surface. In both the study we have varied the diameter of the grooves.

4.3.1 A Single Groove.

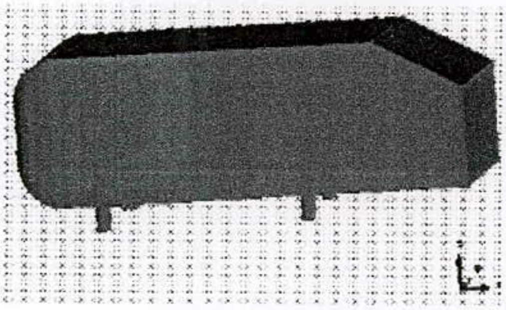

Figure 4.3.1: Ahmed body without any groove (case 0).

In these studies flow is transformed by introducing a transverse groove that is placed at the end of the top surface. Three different grooves of different radii 1mm, 2mm and 3mm are used in the simulations.

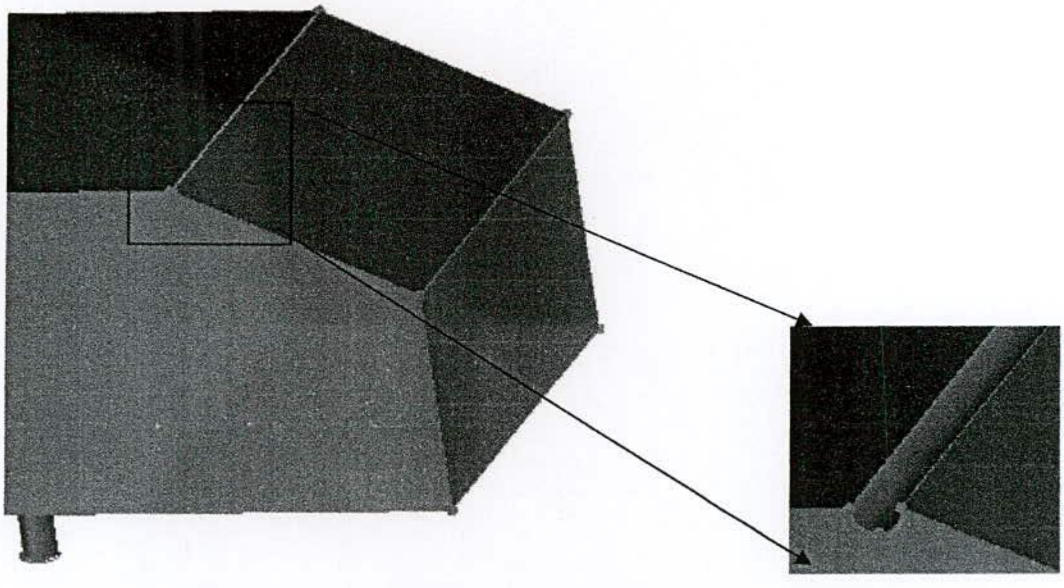

Figure 4.3.2: Ahmed body with a single groove at the end of the top surface.

A groove of 1mm radius placed transversely at the rear end of the top surface is considered as Case 1, that with radius 2 and 3mm are considered as Case 2 and Case 3 respectively. It may be mentioned that the uncontrolled flow is considered as Case 0.

For the sake of identification different walls of body has been identified by different numbers. Due to of special interest the nose, top, rear slop and back surface of the body has been labeled as wall-1, wall-2, wall-3 and wall-4 respectively.

The drag coefficient at the nose, back, the rear slop and the total are represented by C_k, C_B, C_S and C_D respectively.

Before experimentation the drag coefficients of the uncontrolled flow is compared with those of the benchmark results obtained by Lienhart et al. (2000). This comparison presented in table-4.3.1 validates the observed drag through simulation.

It has been found that though the drags at different parts are quite different but the total drags are comparable as presented in table-4.3.1. From the tabulated drag it is observed that the error is about 0.2656%.

Table 4.3.1: Validation of drag force and drag force components

(for uncontrolled flow).

	C_k	C_B	C_S	C_D	Error %
Lienhart et al.(2000)	0.0135	0.1290	0.1210	0.2635	
k-ε	0.0179	0.1289	0.1159	0.2628	0.2656

Table 4.3.2: Comparison among the different cases.

Case	Radius of groove	C_D of wall-3	Pd (m)	Total C_D
Case 0		0.128925	0.004972	0.262800
Case 1	0.003472H	0.121933	0.005197	0.258570
Case 2	0.006944H	0.121141	0.008659	0.267430
Case 3	0.010417H	0.122304	0.005194	0.272677

Pd = Perpendicular distance of vortex center from the slant surface.

Table 4.3.3: The coefficient of drag (C_D) at wall-1, wall -3, wall -4 and total.

Case	Radius of groove	C_D of wall-1	C_D of wall-3	C_D of wall-4	Total C_D
Case 0		0.017954	0.128925	0.115898	0.262800
Case 1	0.003472H	0.018009	0.121933	0.118628	0.258570
Case 2	0.006944H	0.0180256	0.121141	0.128263	0.267430
Case 3	0.010417H	0.018362	0.122304	0.132011	0.272677

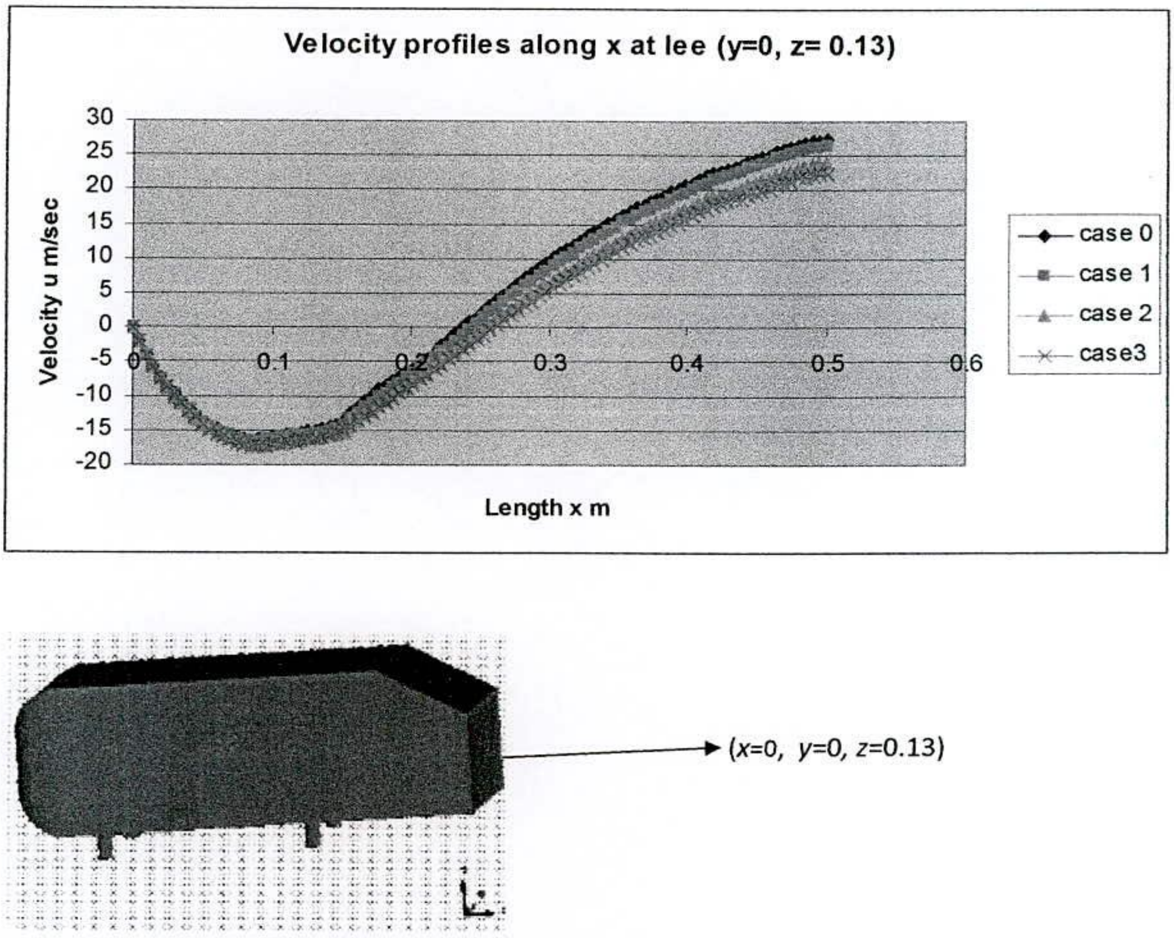

Figure 4.3.3: Velocity profiles for various value of C_D on the wall-4.

Figure 4.3.3 represents the velocity profiles of uncontrolled flow (case 0) and control flow (case 1, 2 and 3). The flow is controlled by placing transverse grooves of different radius at the end of the wall-2. It is found that with the increase in groove diameter the diameter of the vortex that are forming close rear end increases. It is observed that the drag coefficient as also being increased.

The perpendicular distances of vortex center from the slant surface, the C_D of wall-3 and the total C_D has been tabulated in table 4.3.2. From the table it revealed that Pd of control flows are of higher magnitude than that of the uncontrolled flow. It may be also mention that with the change in the radius of the groove the Pd also changes. As is known the shift of vortex from the slant surface produced less drag at the slant surface. As in our case with the insertion of the grooves the vortex has been shifted from the slant surface and thus will produce less amount of drag over the slant surface, which can be clearly observed from the table 4.3.2.

The coefficient of drag at wall-1, wall-3, wall-4 and the total C_D along with the radius of grooves are tabulated in table 4.3.3. It is seen from the table that the coefficient of drag at wall-3, has been reduced in all cases after insertion of the groove, i.e. with the introduction of the passive control the C_D at wall-3 can be reduced (though the rate of reduction is irregular). Whereas the C_D at wall-4 has been increased from the uncontrolled flow. The rate of increase of C_D at wall-4 is systematic. This is also the case in case of wall-1, where as in the case of total C_D which the insertion of the groove the total C_D has been primarily reduced, but with the increase in diameter it has increased and gone above the value of the uncontrolled scenario.

4.3.2 A pair of Grooves.

In this study flow is transformed by introducing two transverse grooves that are placed at the end of the top surface but one of the grooves was inverted. Three pairs of grooves of different radii are used in the simulations. Out of them the first one from the front is inverted groove. Here again three Cases assessed.

Case 4: Like figure 4.3.4, two grooves placed side by side at the rear end of the top surface where the first pairs of radius 1mm inverted groove and the second groove's radius was 2mm.

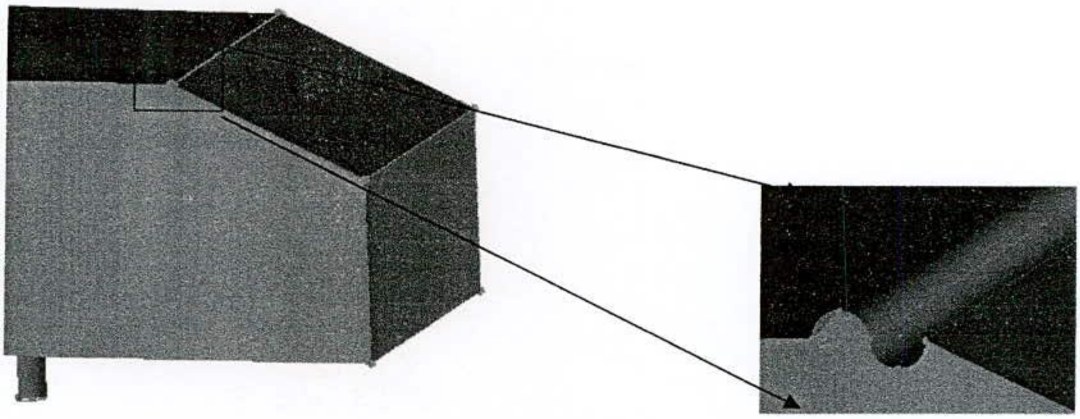

Figure.4.3.4: Ahmed body with two grooves at the end of the top surface.

Case 5: Two grooves each of radii 1 mm, placed side by side at the rear end of the top surface where the first was inverted groove.

Case 6: Two grooves placed side by side at the rear end of the top surface where the first of radius 2mm was inverted groove and the second groove's radius was 1mm.

Table 4.3.4: Comparison among the different cases.

Case	Radius of groove	C_D of wall-3	Pd (m)	Total C_D
Case 0		0.128925	0.004972	0.262800
Case 4	0.003472H & 0.006944H	0.123373	0.005197	0.274390
Case 5	0.003472H & 0.003472H	0.119297	0.007793	0.261507
Case 6	0.006944H & 0.003472H	0.1201851	0.005199	0.272401

Table 4.3.5: The coefficient of drag (C_D) at wall-1, wall -3, wall -4 and total.

Case	Radius of groove	C_D of wall-1	C_D of wall-3	C_D of wall-4	Total C_D
Case 0		0.017954	0.128925	0.115898	0.262800
Case 4	0.003472H& 0.006944H	0.018734	0.123373	0.132290	0.274390
Case 5	0.003472H& 0.003472H	0.017655	0.119297	0.124655	0.261507
Case 6	0.006944H& 0.003472H	0.017805	0.1201851	0.134411	0.272401

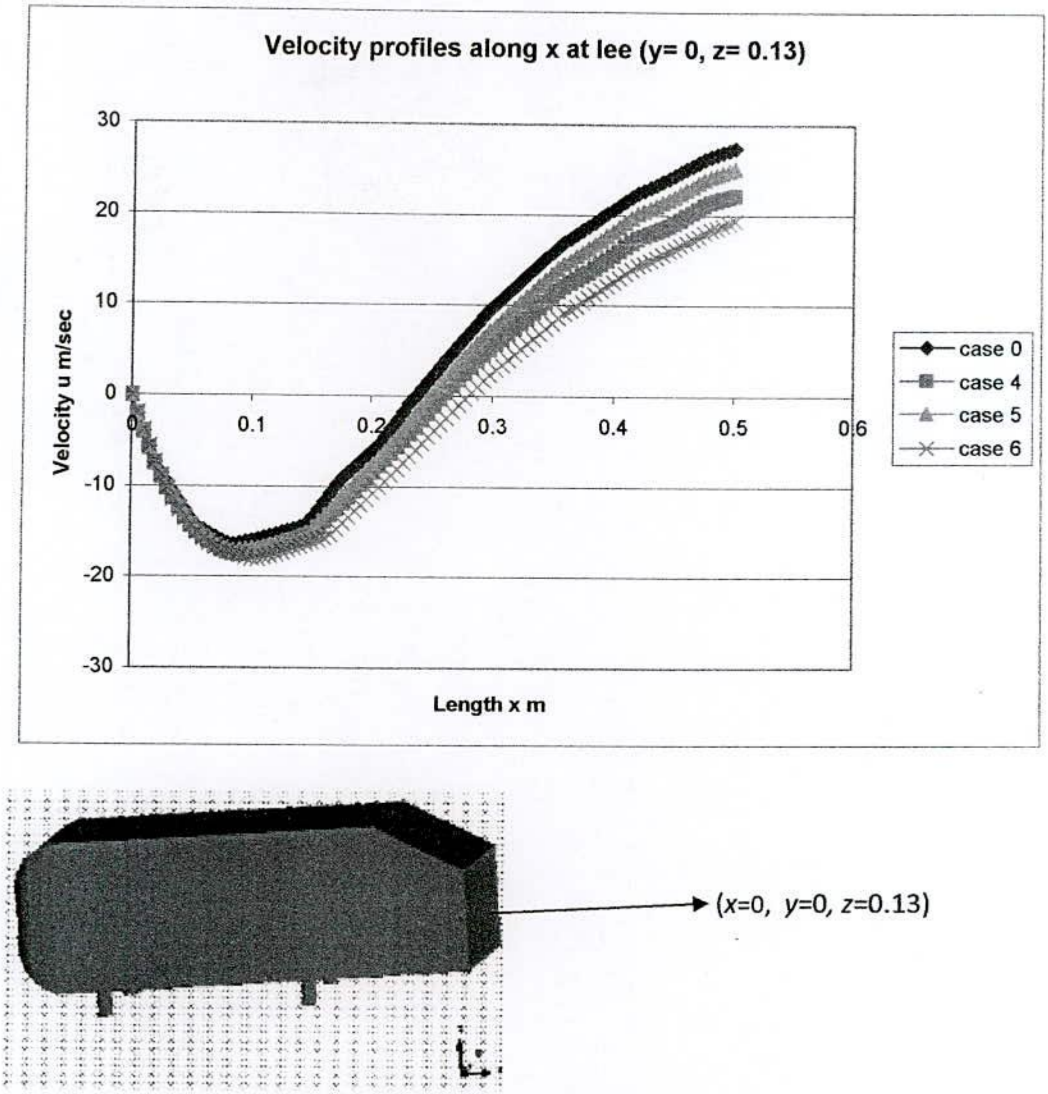

Figure 4.3.5: Velocity profiles for various value of C_D on the wall-4 .

Figure 4.3.5 represents the velocity profiles of uncontrolled flow (case 0) and control flow (case 4, 5 and 6). The flow is controlled by placing transverse grooves of different radius at the end of the wall-2. It is found that with the increase in groove diameter the diameter of the vortex that are forming at the rear end increases. And it is observed that the drag coefficient as also being increased.

The perpendicular distances of vortex center from the slant surface, the C_D of wall-3 and the total C_D has been tabulated in table 4.3.4. From the table it revealed that Pd of control flows is of higher magnitude than that of the uncontrolled flow. It may be also mention that with the change in the radius of the groove the Pd also changes. As is known the shift of vortex from the slant surface produced less drag at the slant surface. As in our case with the insertion of the grooves the vortex has been shifted from the slant surface and thus will produce less amount of drag over the slant surface, which can be clearly observed from the table 4.3.4.

The coefficient of drag at wall-1, wall-3, wall-4 and the total C_D along with the radius of grooves are tabulated in table 4.3.5. It is seen from the table that the coefficient of drag at wall-3, has been reduced in all cases after insertion of the groove, i.e. with the introduction of the passive control the C_D at wall-3 can be reduced (though the rate of reduction is irregular). Whereas the C_D at wall-4 has been increased from the uncontrolled flow. The rate of increase of C_D at wall-4 is not systematic. This is also the case in case of wall-1, where as in the case of total C_D which the insertion of the groove the total C_D has been primarily increased, but with the increase in diameter it has reduced and next it has increased and gone above the value of the uncontrolled scenario.

4.4 Effect of Groove at Slant Surface.

To view the effects of grooves at the slant surface four different studies, each with three cases is performed. One study is conducted by introducing a single groove at the end of the slant surface. The other three studies are done considering one groove at the beginning of the slant and the other groove at the end of slant surface. In the study we varied the diameter of the grooves.

4.4.1 Single Groove.

In these studies flow is transformed by introducing a transverse groove is placed at the end of the slant surface (which we shall call wall 3). Three different grooves of different radii 1mm, 2mm and 3mm are used in the simulations.

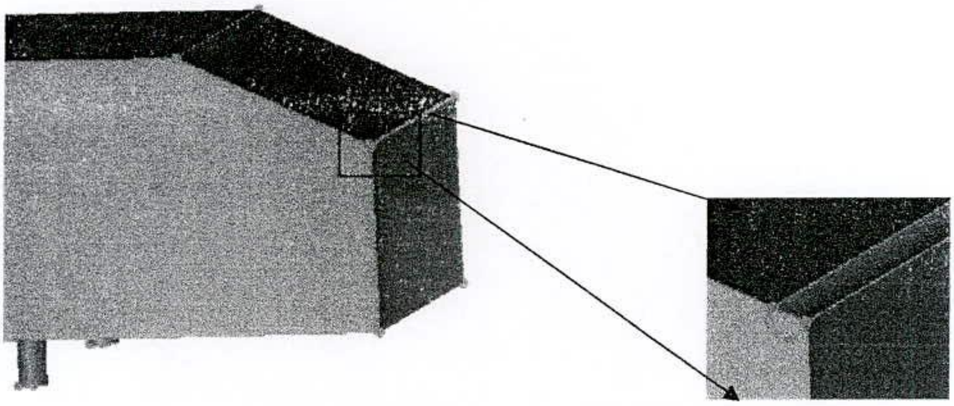

Figure 4.4.1: Ahmed body with a groove at the end of the slant surface.

Case 7: Figure 4.4.1- A groove of 1mm radius placed transversely at the rear end of the slant surface.

Case 8: A groove of 2mm radius placed transversely at the rear end of the slant surface.

Case 9: A groove of 3mm radius placed transversely at the rear end of the slant surface.

Table 4.4.1: Comparison among the different cases.

case	Radius of groove	C_D of wall-3	Pd (m)	Total C_D
Case 0		0.128925	0.004972	0.262800
Case 7	0.003472H	0.113135	0.005195	0.255172
Case 8	0.006944H	0.113603	0.005196	0.255023
Case 9	0.010417H	0.12002	0.005195	0.255927

Table 4.4.2: The coefficient of drag (C_D) at wall-1, wall -3, wall -4 and total.

Case	Radius of groove	C_D of wall-1	C_D of wall-3	C_D of wall-4	Total C_D
Case 0		0.017954	0.128925	0.115898	0.262800
Case 7	0.003472H	0.017743	0.113135	0.124293	0.255172
Case 8	0.006944H	0.018420	0.113603	0.123000	0.255023
Case 9	0.010417H	0.018155	0.12002	0.117752	0.255927

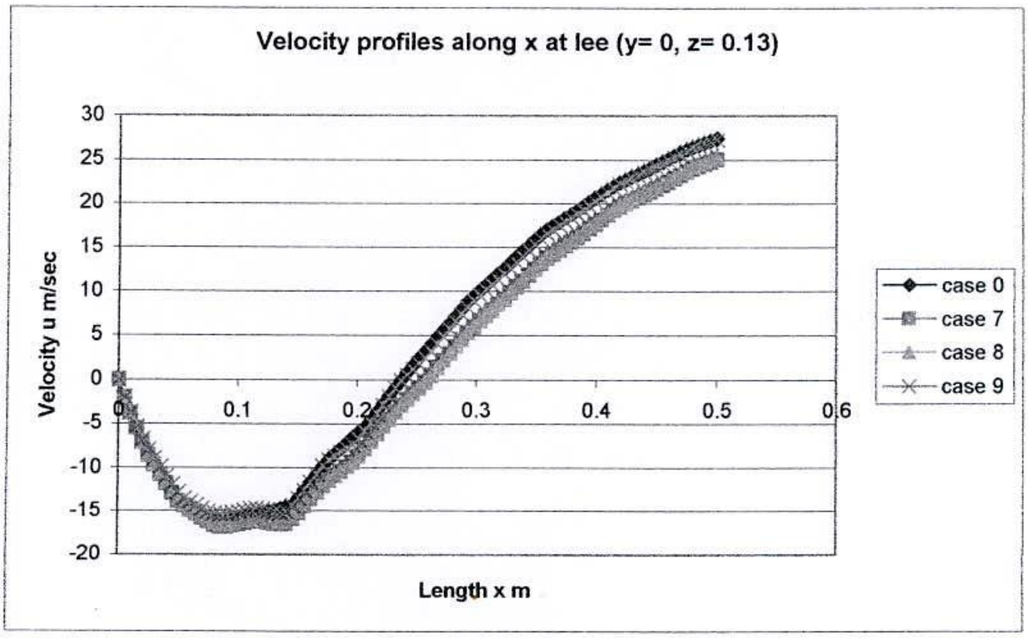

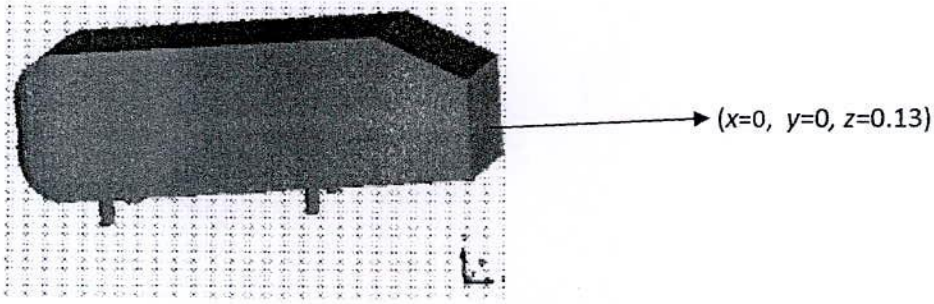

Figure 4.4.2: Velocity profiles for various value of C_D on the wall-4.

Figure 4.4.2 represents the velocity profiles of uncontrolled flow (case 0) and control flow (case 7, 8 and 9). The flow is controlled by placing transverse grooves of different radius at the end of the wall-3. It is found that with the increase in groove diameter the diameter of the vortex that are forming close the rear end increases. And it is observed that the drag coefficient as also being increased.

The perpendicular distances of vortex center from the slant surface, the C_D of wall-3 and the total C_D has been tabulated in table 4.4.1. From the table it revealed that Pd of control flows are of higher magnitude than that of the uncontrolled flow. It may be also mention that with the change in the radius of the groove the Pd also changes. As is known the shift of vortex from the slant surface produced less drag at the slant surface. As in our case with the insertion of the grooves the vortex has been shifted from the slant surface and thus will produce less amount of drag over the slant surface, which can be clearly observed from the table 4.4.1.

The coefficient of drag at wall-1, wall-3, wall-4 and the total C_D along with the radius of grooves are tabulated in table 4.4.2. It is seen from the table that the coefficient of drag at wall-3, has been reduced in all cases after insertion of the groove, i.e. with the introduction of the passive control the C_D at wall-3 can be reduced. Whereas the C_D at wall-4 has been increased from the uncontrolled flow. The rate of increase of C_D at wall-4 is systematic. This is also the case in case of wall-1, where as in the case of total C_D which the insertion of the groove the total C_D has been reduced.

4.4.2: A pair of Grooves.

(a) In these experiments two transverse grooves that are placed at the beginning and at the end of the slant surface. Three different cases of different radii are used in the simulations.

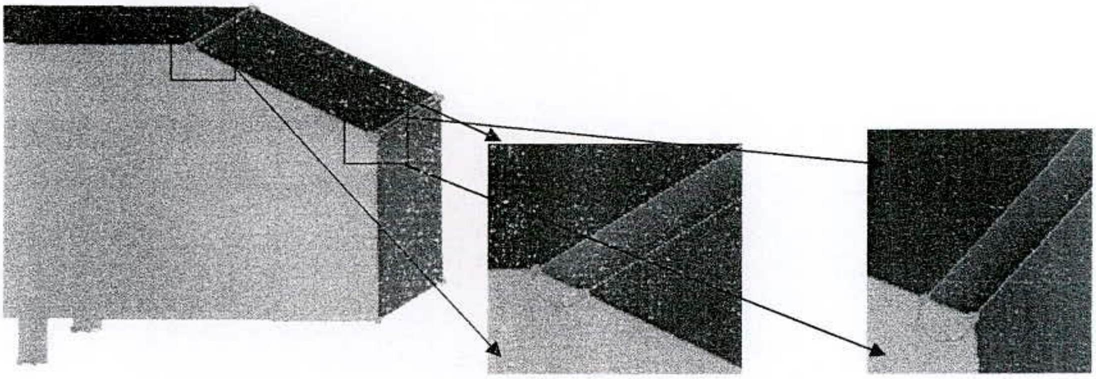

Figure 4.4.3: Ahmed body with two grooves at the beginning and at the end of the slant surface.

Case 10: Figure 4.4.3- Two grooves each of radii 3mm placed at the beginning and at the end of the slant surface.

Case 11: Like figure 4.4.3, 1st groove of radius 2mm placed at the beginning of the slant surface and the 2nd on of radius 3mm placed at the end of the slant surface.

Case 12: Like figure 4.4.3, 1st groove of radius 1mm placed at the beginning of the slant surface and the 2nd on of radius 3mm placed at the end of the slant surface.

Table 4.4.3: Comparison among the different cases.

Case	Radius of groove	CD of wall-3	Pd (m)	Total CD
Case 0		0.128925	0.004972	0.262800
Case 10	0.010417H& 0.010417H	0.112605	0.008661	0.261750
Case 11	0.006944H& 0.010417H	0.109372	0.006063	0.258405
Case 12	0.003472H& 0.010417H	0.120343	0.008660	0.25577

Table 4.4.4 The coefficient of drag (C_D) at wall-1, wall -3, wall -4 and total.

Case	Radius of groove	C_D of wall-1	C_D of wall-3	C_D of wall-4	Total C_D
Case 0		0.017954	0.128925	0.115898	0.262800
Case 10	0.010417H& 0.010417H	0.018776	0.112605	0.130376	0.26175
Case 11	0.006944H& 0.010417H	0.018648	0.109372	0.130368	0.258405
Case 12	0.003472H& 0.010417H	0.017681	0.120343	0.117746	0.25577

In the following figure (Figure 4.4.4) the velocity profiles of uncontrolled flow (case 0) and control flow (case 10, 11 and 12) are presented. The flow is controlled by placing transverse grooves of different radius at the beginning of the wall-3 and at the end of wall-3. It is found that with the increase in groove diameter the diameter of the vortex that are forming close the rear end increases irregularly. And it is observed that the drag coefficient as also being increased.

The perpendicular distances of vortex center from the slant surface, the C_D of wall-3 and the total C_D has been tabulated in table 4.4.3. From the table it revealed that Pd of control flows are of higher magnitude than that of the uncontrolled flow. It may be also mention that with the change in the radius of the groove the Pd also changes. As is known the shift of vortex from the slant surface produced less drag at the slant surface. As in our case with the insertion of the grooves the vortex has been shifted from the slant surface and thus will produce less amount of drag over the slant surface, which can be clearly observed from table 4.4.3.

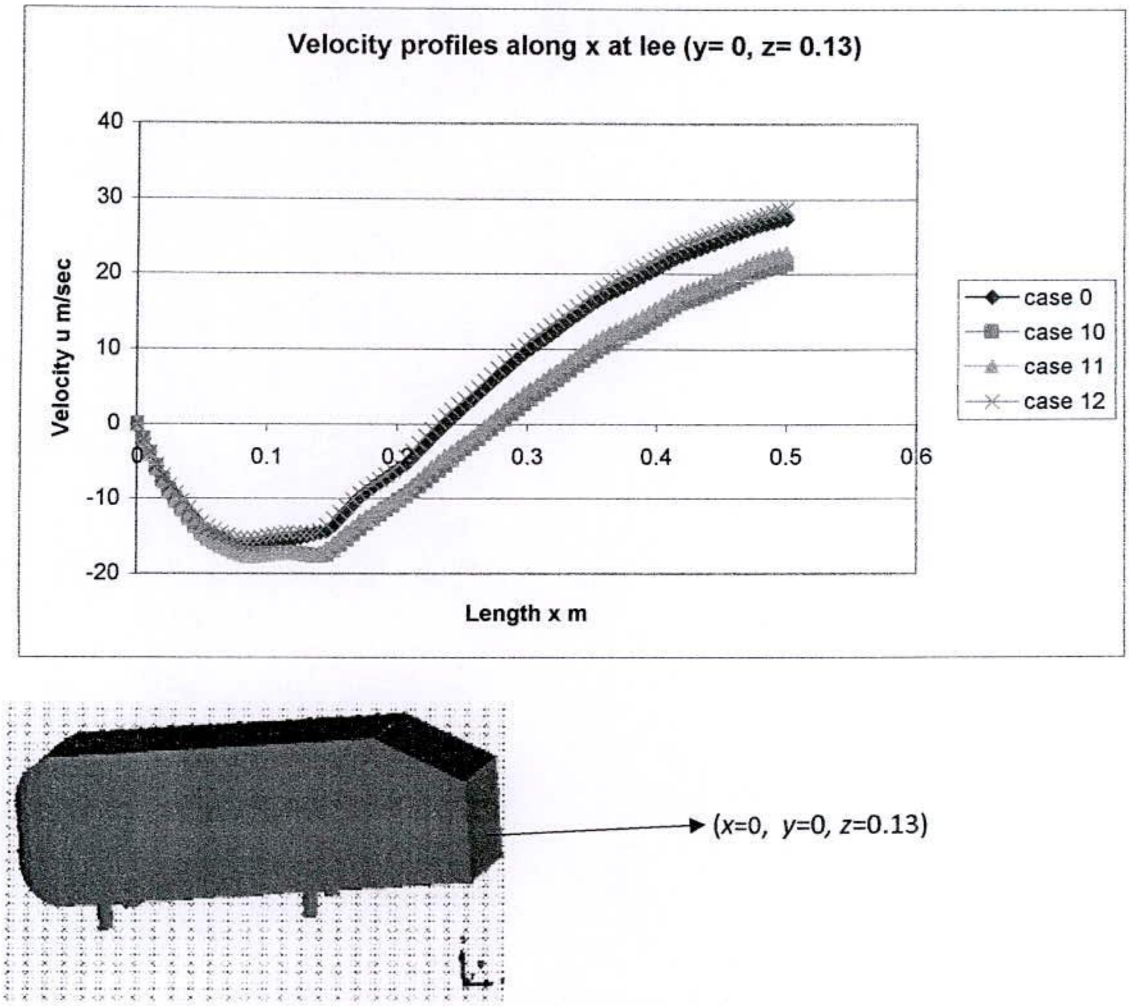

Figure 4.4.4: Velocity profiles for various value of C_D on the wall-4.

The coefficient of drag at wall-1, wall-3, wall-4 and the total C_D along with the radius of grooves are tabulated in table 4.4.3. It is seen from the table that the coefficient of drag at wall-3, has been reduced in all cases after insertion of the groove, i.e. with the introduction of the passive control the C_D at wall-3 can be reduced (though the rate of reduction is irregular). Whereas the C_D at wall-4 has been increased from the uncontrolled flow. The rate of increase of C_D at wall-4 is not systematic. This is also the case in case of wall-1, where as in the case of total C_D which the insertion of the groove the total C_D has been reduced and with the increase in diameter it has decreased gradually.

(b) In these studies two transverse grooves are placed at the beginning and at the end of the slant surface. Three different cases of different radii are used in the simulations.

Case 13: In this case two transverse grooves are placed at the beginning and at the end of the slant surface, where the groove's radii were 1mm.

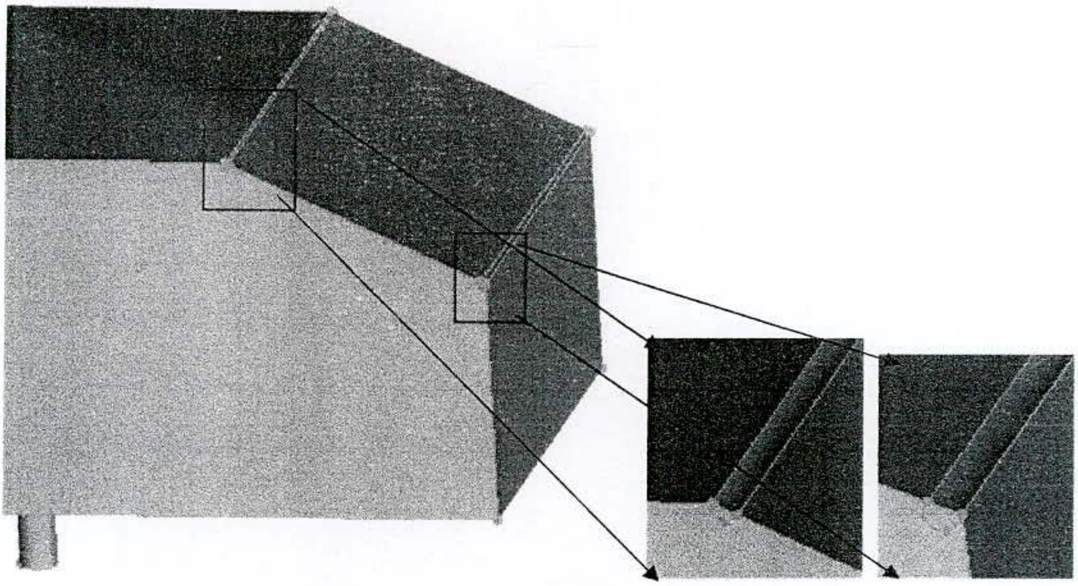

Figure 4.4.5: Ahmed body with two grooves at the beginning and at the end of the slant surface.

Case 14: Figure 4.4.5- In this case two transverse grooves are placed at the beginning and at the end of the slant surface, where the beginning groove's radius was1mm and the end groove's radius was 2 mm.

Case 15: In this case two transverse grooves are placed at beginning and at the end of the slant surface, where the beginning groove's radius was1mm and the end groove's radius was 3mm.

Table 4.4.5: Comparison among the different cases.

Case	Radius of groove	C_D of wall-3	Pd (m)	Total C_D
Case 0		0.128925	0.004972	0.262800
Case 13	0.003472H& 0.003472H	0.113964	0.005206	0.255129
Case 14	0.003472H& 0.006944H	0.107669	0.008660	0.251498
Case 15	0.003472& 0.010417H	0.120343	0.008660	0.25577

. Table 4.4.6: The coefficient of drag (C_D) at wall-1, wall -3, wall -4 and total.

Case	Radius of groove	C_D of wall-1	C_D of wall-3	C_D of wall-4	Total C_D
Case 0		0.017954	0.128925	0.115898	0.262800
Case 13	0.003472H& 0.003472H	0.018998	0.113964	0.122167	0.255129
Case 14	0.003472H& 0.006944H	0.017472	0.107669	0.126356	0.251498
Case 15	0.003472H& 0.010417H	0.017681	0.120343	0.117746	0.25577

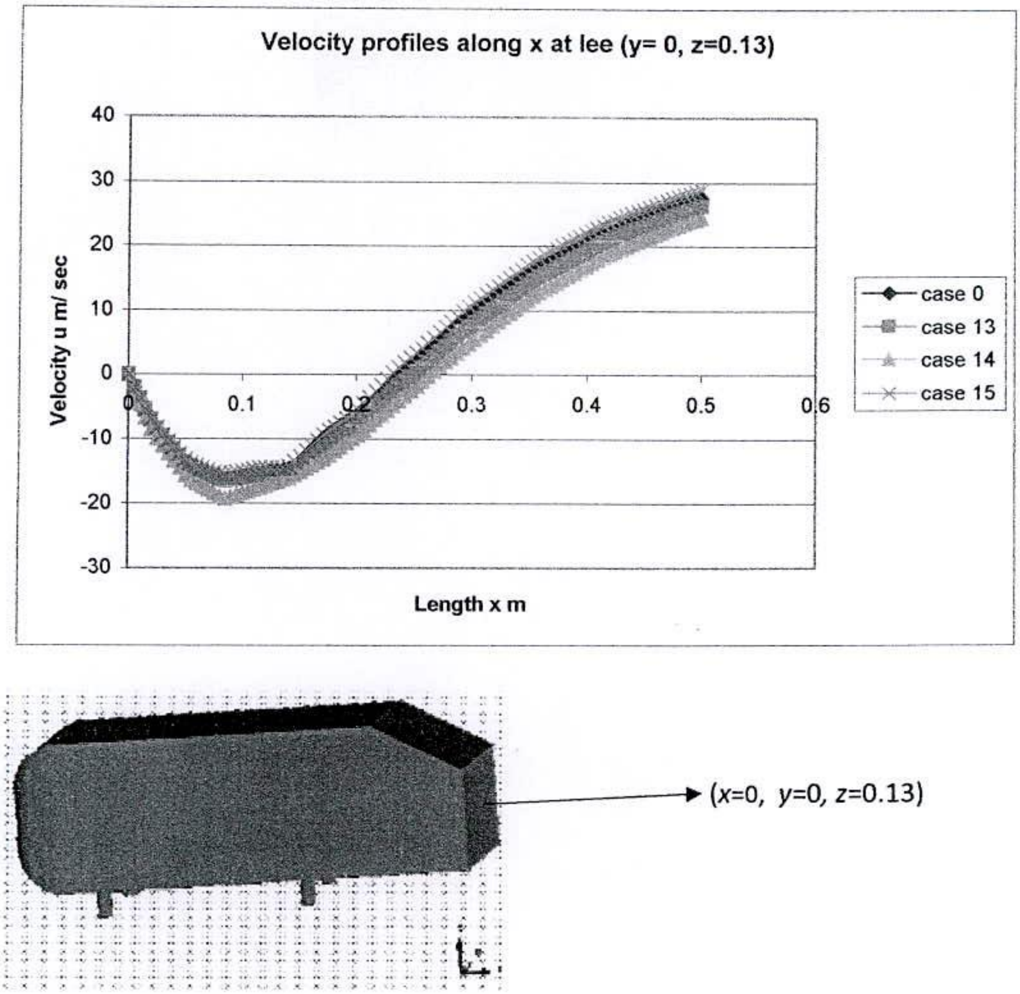

Figure 4.4.6: Velocity profiles for various value of C_D on the wall-4.

Figure 4.4.6 represents the velocity profiles of uncontrolled flow (case 0) and control flow (case 13, 14 and 15). The flow is controlled by placing transverse grooves of different radius at the front and the rear end of the wall-3. It is found that with the change in groove diameter the diameter of the vortex that are forming at the rear end also increase. It is observed that the drag coefficients as also being increased at wall- 4 but the increased in drag coefficients are irregular.

The perpendicular distances of vortex center from the slant surface, the C_D of wall-3 and the total C_D has been tabulated in table 4.4.5. From the table it revealed that Pd of control flows are of higher magnitude than that of the uncontrolled flow. It may be also mention that with the change in the radius of the groove the Pd also changes. As is known the shift of vortex from the slant surface produced less drag at the slant surface. As in our case with the insertion of the grooves the vortex has been shifted from the slant surface and thus will produce less amount of drag over the slant surface, which can be clearly observed from table 4.4.5.

The coefficient of drag at wall-1, wall-3, wall-4 and the total C_D along with the radius of grooves are tabulated in table 4.4.6. It is seen from the table that the coefficient of drag at wall-3, has been reduced in all cases after insertion of the groove, i.e. with the introduction of the passive control the C_D at wall-3 can be reduced (though the rate of reduction is irregular). Whereas the C_D at wall-4 has been increased from the uncontrolled flow. The rate of increase of C_D at wall-4 is not systematic. This is also the case in case of wall-1, whereas in the case of total C_D which the insertion of the groove the total C_D has been reduced and with the increase in diameter it has also reduced (though the rate of reduction is irregular).

(c) In these studies two transverse grooves are placed at the beginning and at the end of the slant surface. Three different cases of different radii are used in the simulations.

Case 16: 1st groove of radius 3mm placed at the beginning of the slant surface and the 2nd on of radius 1mm placed at the end of the slant surface.

Case 17: 1st groove of radius 3mm placed at the beginning of the slant surface and the 2nd on of radius 2mm placed at the end of the slant surface.

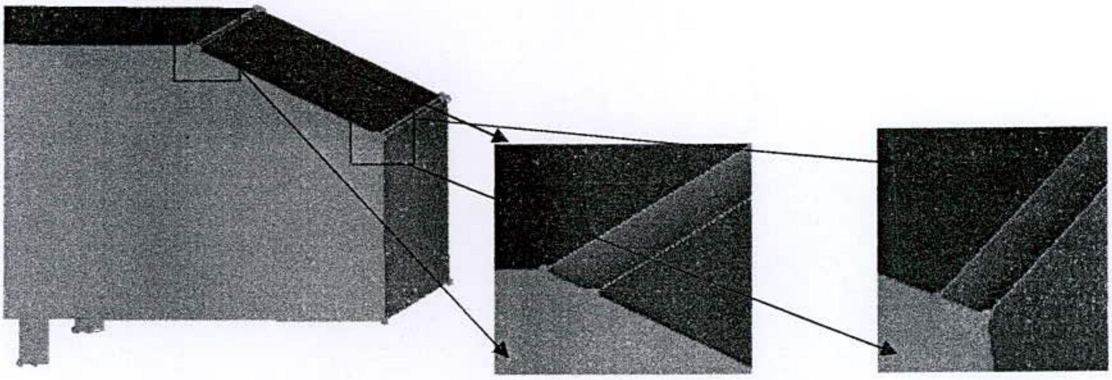

Figure 4.4.7: Ahmed body with two grooves at the beginning and at the end of the slant surface.

Case 18: Figure 4.4.7-Two grooves each of radii 3mm placed at the beginning and at the end of the slant surface.

Table 4.4.7: Comparison among the different cases.

Case	Radius of groove	C_D of wall-3	Pd (m)	Total C_D
Case 0		0.128925	0.004972	0.262800
Case 16	0.010417H& 0.003472H	0.111955	0.005195	0.26384
Case 17	0.010417H& 0.006944H	0.107474	0.005194	0.260848
Case 18	0.010417H& 0.010417H	0.112605	0.008661	0.26175

Table 4.4.8: The coefficient of drag (C_D) at wall-1, wall -3, wall -4 and total.

Case	Radius of groove	C_D of wall-1	C_D of wall-3	C_D of wall-4	Total C_D
Case 0		0.017954	0.128925	0.115898	0.262800
Case 16	0.010417H& 0.003472H	0.0189966	0.111955	0.132889	0.26384
Case 17	0.010417H& 0.006944H	0.017727	0.107474	0.1356468	0.260848
Case 18	0.010417H& 0.010417H	0.018776	0.112605	0.130376	0.26175

Figure 4.4.8, in the next page, represents the velocity profiles of uncontrolled flow (case 0) and control flow (case 16, 17 and 18). The flow is controlled by placing transverse grooves of different radius at the beginning and at the end of the wall-3. It is found that with the change in groove diameter the diameter of the vortex that are forming at the rear end also changes. It is observed that the drag coefficients as also being increased at wall-4 but the increased in drag coefficients are irregular.

The perpendicular distances of vortex center from the slant surface, the C_D of wall-3 and the total C_D has been tabulated in table 4.4.7. From the table it revealed that Pd of control flows are of higher magnitude than that of the uncontrolled flow. It may be also mention that with the change in the radius of the groove the Pd also changes. As is known the shift of vortex from the slant surface produced less drag at the slant surface. As in our case with the insertion of the grooves the vortex has been shifted from the slant surface and thus will produce less amount of drag over the slant surface, which can be clearly observed from table 4.4.7.

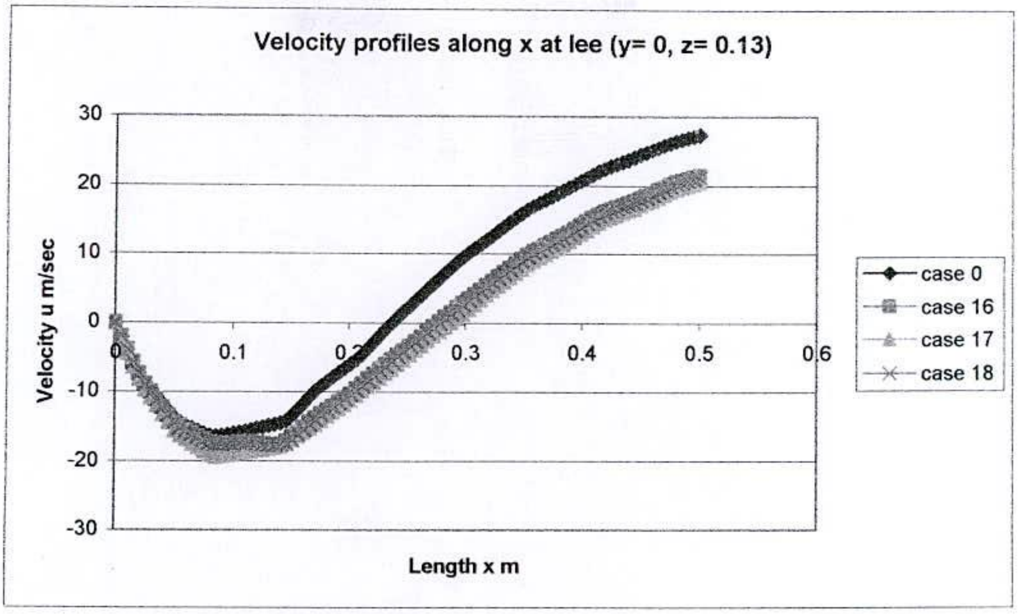

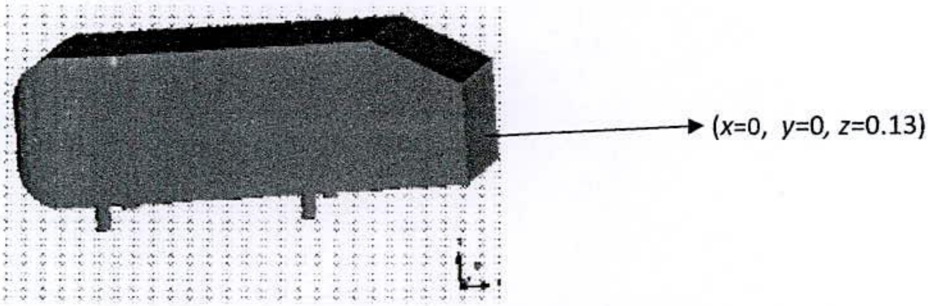

Figure 4.4.8: Velocity profiles for various value of C_D on the wall-4.

The coefficient of drag at wall-1, wall-3, wall-4 and the total C_D along with the radius of grooves are tabulated in table 4.4.8. It is seen from the table that the coefficient of drag at wall-3, has been reduced in all cases after insertion of the groove, i.e. with the introduction of the passive control the C_D at wall-3 can be reduced (though the rate of reduction is irregular). Whereas the C_D at wall-4 has been increased from the uncontrolled flow. The rate of increase of C_D at wall-4 is not systematic. This is also the case in case of wall-1, whereas in the case of total C_D which the insertion of the groove the total C_D has been primarily increased, but with the increase in diameter it has reduced and gone below the value of the uncontrolled scenario.

4.5 Effect of Groove at Top and Slant Surface.

In these studies two transverse grooves are placed at the end of the top surface and at the end of the slant surface. Three pears different grooves of different radii are used in the simulations.

Case 19: Like figure 4.5.1, two grooves of both 1mm radii placed transversely at the rear end of the top surface and at the end of the slant surface.

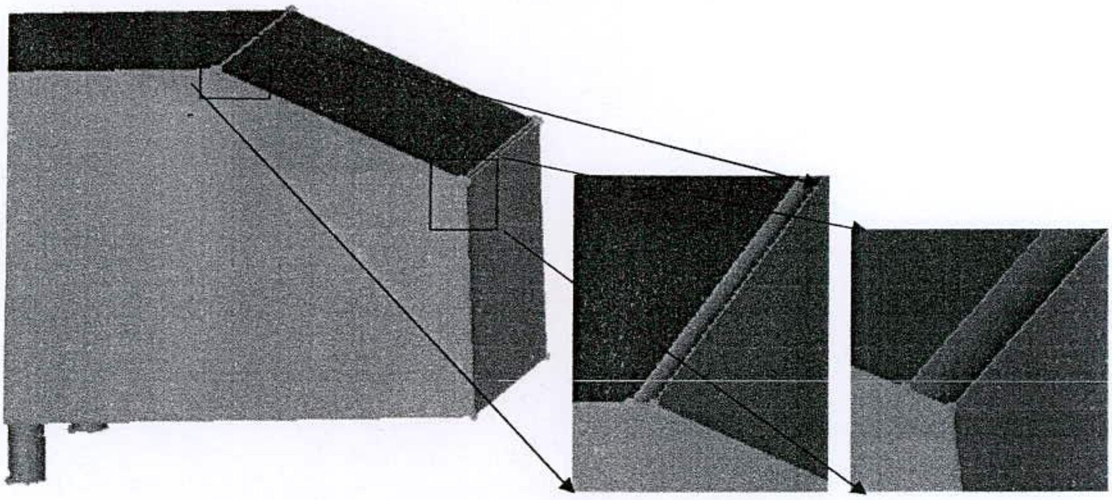

Figure 4.5.1: Ahmed body with two grooves at the beginning of the top and at the end of the slant surface.

Case 20: Figure 4.5.1- In this case two transverse grooves are placed at the end of the top surface and at the end of the slant surface, where the top groove's radius was1mm and the slant groove's radius was 2 mm.

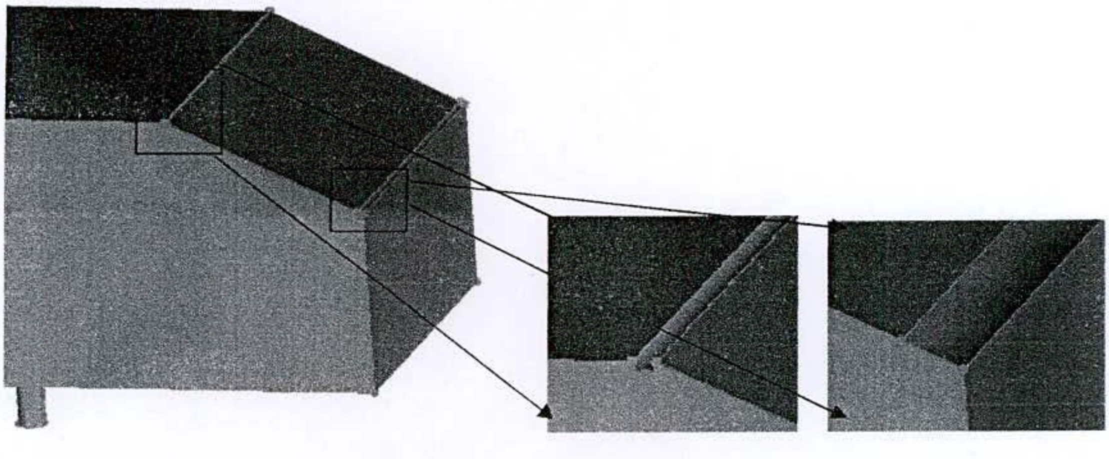

Figure 4.5.2: Ahmed body with two grooves at the beginning of the top and at the end of the slant surface.

Case 21: Figure 4.5.2-In this case two transverse grooves are placed at the end of the top surface and at the end of the slant surface, where the top groove's radius was1mm and the slant groove's radius was 3 mm.

Table 4.5.1: Data of Perpendicular distance of vortex center from the slant surface (Pd), the C_D of wall- 3 and the total C_D.

Case	Radius of groove	C_D of wall-3	Pd (m)	Total C_D
Case 0		0.128925	0.004972	0.262800
Case 19	0.003472H& 0.003472/H	0.108523	0.007793	0.252323
Case 20	0.003472H& 0.006944H	0.105448	0.008660	0.25053
Case 21	0.003472H& 0.010417H	0.123623	0.006929	0.256772

Table 4.5.2: The coefficient of drag (C_D) at wall-1, wall -3, wall -4 & total.

Case	Radius of groove	C_D of wall-1	C_D of wall-3	C_D of wall-4	Total C_D
Case 0		0.017954	0.128925	0.115898	0.262800
Case 19	0.003472H& 0.003472H	0.017418	0.108523	0.126380	0.252323
Case 20	0.003472H& 0.006944H	0.017720	0.105448	0.127363	0.25053
Case 21	0.003472H& 0.010417H	0.017919	0.123623	0.115230	0.256772

The following figure, Figure 4.5.3 represents the velocity profiles of uncontrolled flow (case 0) and controlled flow (case 19, 20 and 21). The flow is controlled by placing transverse grooves of different radius at the end of the top surface and the end of the slant surface. It is found that with the change in groove diameter the diameter of the vortex that are forming at the rear end also changes. It is observed that the changes in drag coefficients are irregular.

The perpendicular distances of vortex center from the slant surface, the C_D of wall-3 and the total C_D has been tabulated in table 4.5.1. From the table it revealed that Pds of control flows are of higher magnitude than that of the uncontrolled flow. It may be also mentioned that with the change in the radius of the groove the Pd also changes. It is known that the shift of vortex from the slant surface produce less drag at the slant surface. As in our case with the insertion of the grooves the vortex has been shifted from the slant surface and thus will produce less amount of drag over the slant surface, which can be clearly observed from table 4.5.1.

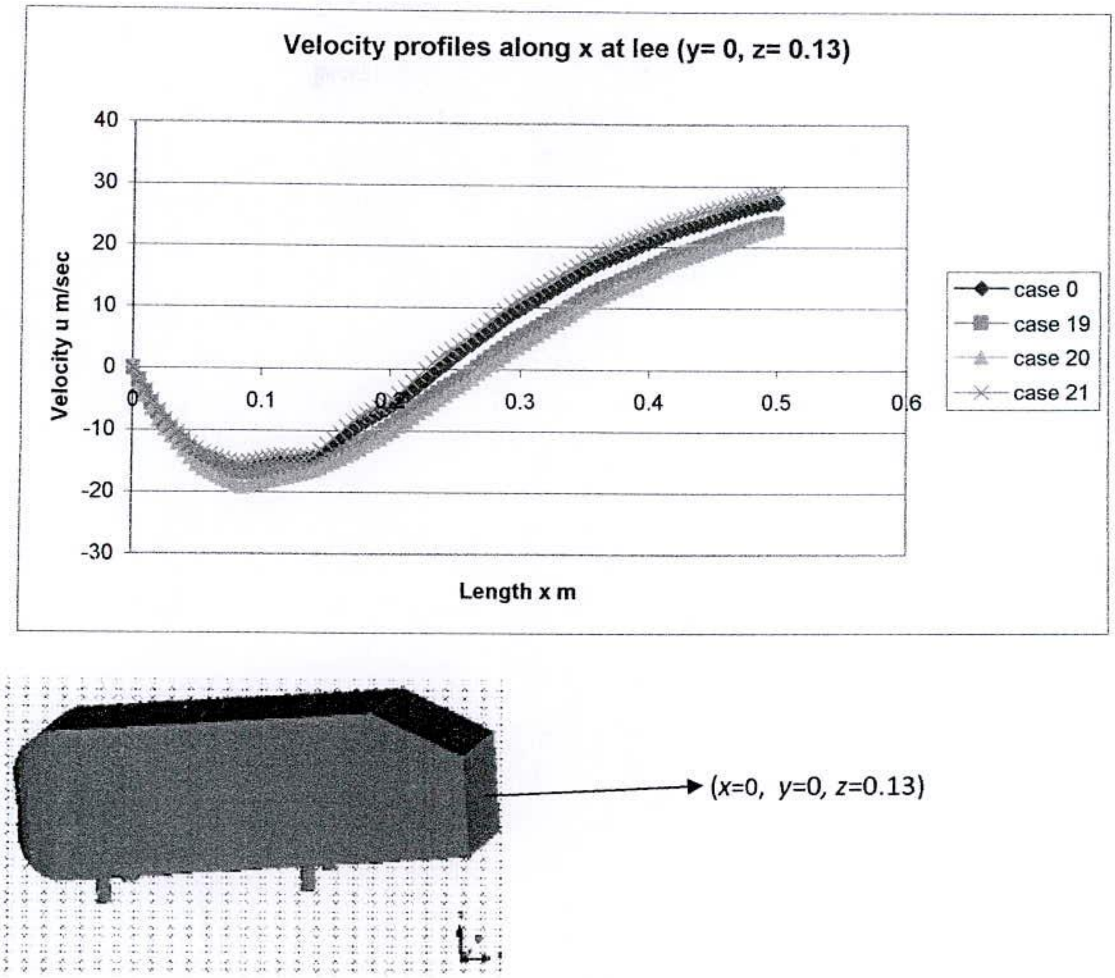

Figure 4.5.3: Velocity profiles for various value of C_D on the wall-4.

The coefficient of drag at wall-1, wall-3, wall-4 and the total C_D along with the radius of grooves are tabulated in table 4.5.2. It is seen from the table that the coefficient of drag at wall-3, has been reduced in all cases after insertion of the groove, i.e. with the introduction of the passive control the C_D at wall-3 can be reduced (though the rate of reduction is irregular). The C_D at wall-4 has been increased from the uncontrolled flow for case 19 and 20 but for the case 21 it has decreased and gone below the value of the uncontrolled scenario. This is also the case in case of wall-1, whereas in the case of total C_D which the insertion of the groove the total C_D has been reduced and with the increase in diameter it has also reduced (though the rate of reduction is irregular).

4.6 Effect of Groove at the Rear Surface.

To assess the effect of grooves at the rear surface we have performed nine (9) different types of experimentations. In the studies we have varied the radius and location of the grooves.

The studies are done by inserting groove which was:

Case 22: In this case a transverse groove of radius 2mm, placed at the beginning of the rear surface (Fig. 4.6.1).

Case 23: In this case a transverse groove of radius 2mm, placed at the end of the rear surface.

Case 24: In this case a inverted transverse groove of radius 2mm, placed at the beginning of the rear surface (Fig. 4.6.2).

Case 25: In this case a inverted transverse groove of radius 2mm, placed at the end of the rear surface.

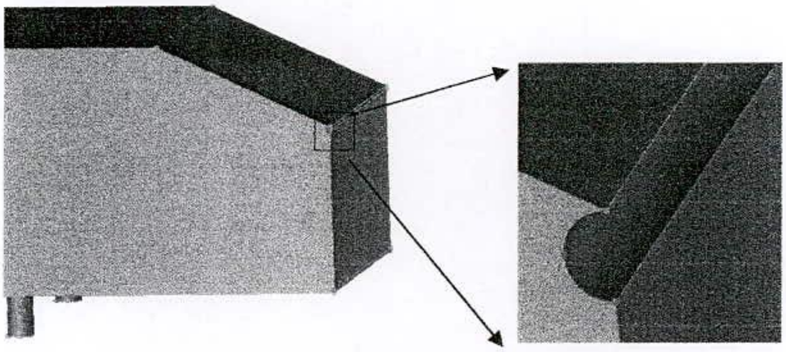

Figure 4.6.1: Ahmed body with a groove at the beginning of the rear surface.

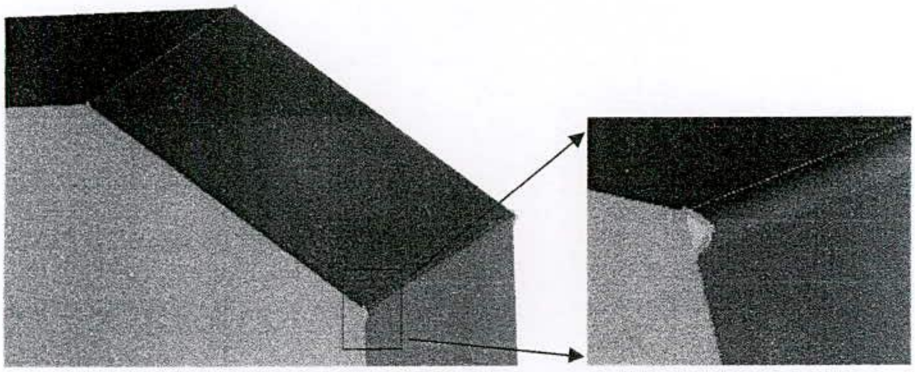

Figure 4.6.2: Ahmed body with a groove (inverted groove) at the beginning of the rear surface.

Case 26: In this case two transverse grooves of different radii, placed at the beginning and of the end of the rear surface (here different combination of radii have been considered).

Case 27: In this case two transverse grooves of equal radii, placed at the beginning and of the end of the rear surface (two cases have been considered).

Case 28: In this case a transverse groove of radius 2mm is placed at the beginning and an inverted transverse groove of radius 2mm is placed at the end of the rear surface.

Case 29: In this case a inverted transverse groove of radius 2mm is placed at the beginning and an transverse groove of radius 2mm is placed at the end of the rear surface.

Case 30: In this case two inverted transverse groove of equal radii (2mm), placed at the beginning and of the end of the rear surface.

In this study the effect of passive flow control by inserting transverse groove and inverted groove has been discussed. To observe the effect a total of 9 studies have been done with variations in number, size, type and position of grooves at the rear end of the Ahmed car body. It was expected that there will be a certain change in the drag coefficient as drag depends on the flow around the body. The location and size of the vortices that form at the wake contribute on the drag. Insertion of groove at the rear end will definitely make a change in the vortices and consequently the drag will also be changed. In this respect the experiments are done and some changes are observed. As has been expected, it is found that the drag coefficients has dependencies on number of grooves, type of grooves, size of grooves as well as on the position of the grooves. With the variation on either of the above mentioned factors change in drag coefficients are observed.

The total drags observed through the experimentations are tabulated in the following table.

Table 4.6.1: Data of number, location and type of grooves with total drag.

Case. No.	No. of groove.	Location of groove.	Radius of the gr.(mm)	Type of the groove.	Tot. Obs. drag	Change %
22	1	B	2	O	0.2775	+5.607
23	1	E	2	O	0.2782	+5.865
24	1	B	2	I	0.2748	+4.574
25	1	E	2	I	0.2791	+6.197
26	2	B	1	O	0.2765	+5.201
		E	3	O		
	2	B	1	O	0.2759	+4.971
		E	2	O		
	2	B	3	O	0.2753	+4.759
		E	2	O		
	2	B	2	O	0.2753	+4.759
		E	3	O		
27	2	B	2	O	0.2734	+4.021
		E	2	O		
	2	B	3	O	0.2775	+5.607
		E	3	O		
29	2	B	2	O	0.2751	+4.684
		E	2	I		
29	2	B	2	I	0.2766	+4.906
		E	2	O		
30	2	B	2	I	0.2766	+4.906
		E	2	I		

B = Beginning of the rear surface, E = End of the rear surface, O = Ordinary groove and I = Inverted groove.

It is seen that any sort of grooving, ordinary or inverted, placed either at the beginning or at the end has negative impact in terms of the total drag i.e. the total drag is found to increase when any grooves are placed at the rear end of the Ahmed car body. It is also observed that when any grooves are placed at the end of the rear surface the results are worse. The most worse result is found when an inverted groove of radius 2mm is placed at the end of the rear surface and it give rise about 6.197% in the total drag.

Chapter 5

5.0 CONCLUSIONS

The title of the research expresses the target of the research i.e. finally the drag should be reduced. The title itself express that Ahmed car body is to be used for CFD modeling to reduce drag. Thus an Ahmed car body is to be built through introduction of proper number of elements so that its behaviors are comparable with benchmark. Suitable turbulence model is to be chosen so that the uncontrolled flow is to be comparable to the benchmark. The related factors with the turbulence model also may require to be selected. Modifications of Ahmed car body is to be done to reduce drag. Passive control i.e. the control which cannot be changed with in the whole span of simulation is chosen. Grooves at different locations are chosen as the control parameter. With the proper selection of the above mention items drag reduction is found.

Before starting simulation to reduce drag grid independence, comparison between different turbulence models and selection of roughness height are done. On the basis of the experiments the following conclusions are made, which guided the after wards simulations:

(1) The extension of near wake separation bubble do not changes when number of elements is taken above 1.6 million (our system was capable to handle up to 2.1million elements).

(2) The velocity profiles at different locations over the made shape gave the validity of the produced Ahmed car body.

(3) Out of the k- ε, k-ω, SST and BSL turbulence model k-ε model is best in performance near the body, thus is to be used to calculate the drag.

(4) k-ε model has dependence on the selection of the roughness height. A roughness height 0.0002m is better suited for drag evaluation over Ahmed car body.

Thus drag reduction simulation are to be performed over a region consists of 1.6 to 2.1million elements with an Ahmed car body shape. Grooves are made at the end of the top surface, at the beginning of the slant surface, at the end of the slant surface and at the rear surface to modify the Ahmed car body. In the simulations k-ε turbulence model with the roughness height 0.0002m is used. The simulations by the modified Ahmed car body produced different drags, sometimes higher and sometimes lower than the uncontrolled flow. On the basis of the simulations with the different modifications by inserting grooves i.e. grooves at different locations the following conclusions can be done:

(1) Placement of any groove at the rear end of the Ahmed car body produced a total drag higher than the uncontrolled flow.

(2) The total drag increases most when any inverted groove is placed at the end of the rear surface.

(3) Total drag is reduced through insertion of grooves of different radii at the end of the slant surface and at the end of the top and at the end of the slant surface though the amounts are different.

(4) A maximum of about 4.6689% drag reduction is achieved when a groove of radius 1mm is placed at the end of the top surface and another groove of radius 2mm is placed at the end of the slant surface. Thus finally we may conclude that insertion of grooves can reduce the total drag over Ahmed car body.

References

1. Achdou, Y., Pironneau, O. and Valentin, F. "Effective boundary conditions for laminar flows over periodic rough boundaries", J. Comp. Phys., 147, 1998.

2. Ahmed, S.R. and Ramm, G.,"Some Salient Features of the Time–Averaged Ground Vehicle Wake," SAE Technical Paper, 840300,1984.

3. Ahmed, S.R., "Computational Fluid Dynamics", Chapter XV in Hucho, W. H. (Ed.), Aerodynamics of Road Vehicles, 4th Edition, SAE International, Warrendale, PA, USA, 1998.

4. Alam, F., watkins S., Song B., Steiner, T. and Humphris, C., "The Flow Around a Car A-pillar", The 13th Australasian Fluid Mechanics Conference, Melbourne, Australia, PP 461-464, 1998.

5. Alam, F., "The Effects of Car A-pillar and Windshield Geometry and Yaw Angles on Local Flow and Noise" , Ph. D. Thesis, Department of Mechanical and Manufacturing Engineering, RMIT University, Melbourne, Australia, 2000.

6. Anderson, J.D. Jr., "Computational Fluid Dynamics: The Basics with Applications", McGraw Hill, 1995.

7. Angot Ph., Bruneau Ch.-H. and Fabrie P., "A penalization method to take into account obstacles in incompressible viscous flows", Numer. Math. No. 81, 1999.

8. Arquis E. and Caltagirone J.P., "Sur les conditions hydrodynamiques au voisnage d'une interface milieu fluide- milieu poreux: application a la convection naturelle", C. R. Acad. Sci. Paris, Ser. II 299, 1984.

9. Azad, A.K., Hossain, M.A. and Islam, A.K.M.S., "Comparison of Turbulence Models for Ahmed Car Body Simulation", *5th BSME International Conference on Thermal Engineering*, IUT, Dhaka, Bangladesh, 2012.

10. Azad, A.K., Hossain, M.A. and Islam, A.K.M.S., "Effect of Roughness Height on the Turbulence Models for Ahmed Car Body Simulation", *International Conference on Mechanica , Industrial and Materials Engineering,* RUET, Rajshahi, Bangladesh, 2013.

11. Baldwin, B.S, and Lomax, H., "A Thin-layer Approximation and Algebraic Model for Separated Turbulent Flow", AIAA Paper, No 78-257,1978.

12. Baldwin, B.S. and Barth, T.J., "A One-Equation Turbulence Transport Model for High Reynolds Number Wall-Bounded flow", NASA TM – 102847, 1990.

13. Barnard, R.H., "Road Vehicle Aerodynamic Design-An Introduction", 2nd Edition, Longman ISBN 0-582-24522-2, 1996.

14. Basara, B. and Jakirlic, S., "A New Turbulence Modeling Strategy for Industrial CFD", International Journal of Numerical Methods in Fluids, Vol. 42, PP 89-116,2003.

15. Bearman, P.W., De beer D. and Harvey, J.K., "Experimental Studies of Road Vehicle Flow Fields", AIAA, Paper 89-1887, PP 1-9,1989.

16. Behnia, M., Parneix, S. and Durban, P.A., "prediction of heat transfer in an axisymmetric turbulent jet impinging on a flat plate". International journal of heat and mass transfer, V41, N12, PP 1845-1855, 1998.

17. Bourgois, S. and Tensi, J., "Controle de l'ecoulement par autour d'un cylinder par techniques fluidiques et acoustiques", 16eme Congres Francais de Mecanique, Nice, 2003.

18. Boussinesq, J., "Essai sur la Theorie des eaux Courantes", Men. Prea.Par Div. Savant a l'Acad. Sci., 23, PP 1-680, 1877.

19. Bradshaw, P., "The Response of a Constant-Pressure Turbulent Boundary Layer to the Sudden Application of an Adverse Pressure Gradient", R. & M. Number 3575, British Aeronautical Research Council, 1969.

20. Bradshaw, P., "Effects of Streamline Curvature on Turbulent Flow", AGARD-AG-169, 1973.

21. Bruneau, C.H. and Mortazavi, I., "Passive control of flow around a square cylinder using porous media, Journal Numer, Methods Fluids No. 46, 2004.

22. Bruneau, C.H., Gillieron, P. and Martazavi I., "Flow manipulation around the Ahmed body with a rear window using passive strategies", *ELSEVIER Masson SAS*, vol.335, pp 213-218, 2007.

23. Caltagirone, J.P., "Sur l'interaction fluide-milieu poreux: Appcation au calcul des efforts exerces sur un obstacle par un fluide visqueux", C.R.Acad. Sci. Paris, Ser. II 318, 1994.

24. Chen, H.C. and Patel, V.C., "Near Wall Turbulence Models for Complex Flows Including Separation", AIAA Journal, 26(6), PP 641-648, 1988.

25. Chien, K.Y., "Predictions of Chanel and Boundary Layer Flows with a Low Reynolds Number Turbulence Model", AIAA Journal, Vol. 20, No. 1, PP 33-38, 1982.

26. Chou, P.Y., "On the Velocity Correlations and Solution of the Equations of Turbulent Fluctuation", Quart. Appl. Math. , Vol. 3, PP38, 1945.

27. Clauser, F.H. " The Turbulent Boundary Layer", Advances in Applied Mechanics, Vol. IV, Academic Press, PP 1- 51, 1956.

28. Coles, D.E. and Hirst, E.A. "Computing of Turbulent Boundary – 1968", AFORST-IFP-Stanford Conference, Vol. II, Thermosciences Divison, Stanford University, California, 1969.

29. Corrsin, S. and Kistler, A.L., "The Free-Stream Boundaries of Turbulent Flows", NACA TN 3133, 1954.

30. Daly, B.J., and Harlow, F.H., "Transport Equation in Turbulent Flows", Physics of Fluids, Vol. 13, PP 2634- 2649, 1970.

31. Deardorff, J.W., "A Numerical Study of Three Dimensional Turbulent Groove Flow at Large Reynolds Number", Journal of Fluid Mechanics, Vol. 41, Pt.2, PP 453-480, 1973.

32. Donaldson, C, DuP. and Rosenbaum, H., "Calculation of the Turbulent Shear Flows Through Closure of the Reynolds Equations by Invariant Modeling", ARAP Report 127, Aeronautical Research Associates of Princetion, Princetion, New Jersey,1986.or 1968.

33. Durbin, P.A., "Near Wall turbulence closure modeling without "damping functions". Theoretical and Computational Fluid Dynamics 3, P1-13, 1991.

34. Durbin, P.A., "A Reynolds Stress Model for Near wall Turbulence", Journal of Fluid Mechanics, Vol. 249, no. 465, 1993.

35. Durbin P.A. "Separated Flow Computations with the k-ε-v^2 Model", AIAA Journal , V33, N4, PP659-664, 1995.

36. Du Pont, F., "Comparison of Numerical Methods for Modeling Ocean Circulation in Basins with Irregular Coasts", PhD Thesis McGill University, Montreal, Canada, 2001.

37. Emmons, H.W., "Shear Flow Turbulence", Proceedings of the 2nd U. S. Congress of Applied Mechanics, ASME, 1945.

38. Evanic, T. and Gillieron, P., "Reduction of the Aerodynamic Drag Due to cooling system, An Analytical and Experimental Approach", SAE paper, No. 2005-01-1017, 2004.

39. Farabee, T.M. "An Experimental Investigation of Wall Pressure Fluctuations Beneath Non-Equilibrium Turbulent Flows", Ph. D. dissertation, The Catholic University of America, 1986.

40. Fieldler, H.E. and Femholz, H.E., "On the management and control of turbulent shear flows", Prog. Aero. Sci, vol. 27, 1990.

41. Fluent Incorporated, "Fluent User's Guide", USA, 2003.

42. Fournier, G., Bourghois, S., Pellerin, S., Ta Phuoc, L., Tensi, J. and El Jabi, R., "Wall suction influence on the flow around a cylinder in laminar wake configuration by eddy simulation and experimental approaches", 39e Colloque d'Aerodynamique Applique, Centrole des ecoulements, Mars, Paris, 22-24, 2004.

43. Fricke, F.R. and Stevenson, D.C., "Pressure Fluctuations in a Separated Flow Region", journal of the Acoustic Society of America, Vol. 44 no. 5, PP 1189-1200, 1968.

44. Fricke, F.R., "Pressure Fluctuations in a Separated Flows", Journal of sound and Vibration, Vol. 17, No. 1, PP 113- 123, 1971.1971.

45. Gad-El-Hak, M., "Modern developments in flow control", Appl Mech Rev. Vol. no. 9, pp365-379, 1996.

46. George, A.R., (Ed), "Automotive Wind Noise and its Measurement", An Information Report of the SAEV Wind Noise Measurement Committee, 1997.

47. Gibson, M.M. and Launder, B.E. "Ground effects on Pressure Fluctuations in the Atmospheric Boundary Layer", Journal of Fluid Mechanics, Vol.86, Pt. 3, PP 491-511,1978.

48. Gillieron,P., "Conttrole des ecoulements appliques a l'automobile. etat de l'art", Mecanique and Industries, vol: 3 pp515-524, 2002.

49. Gillieron, P. and Spohn, A., "Flow separations generated by a simplified geometry of an automotive vehicle, in: IUTAM Symp. Unsteady Separated Flows", 2002.

50. Glezer, A, and Amitay, M, "Synthetic jets", Annual Review of Fluid Mechanics, vol. 34, pp 503-529, 2002.

51. Glushko, G., "Turbulent Boundary Layer on a Flat Plate in an Incompressible Fluid", Izvestia Akademiya Nauk SSSR, Mekh, No. 4, PP 13, 1965.

52. Hanjalic, K. and Launder, B.E., "A Reynolds stress Model of Turbulence and its Application to Thin shear Flows", Journal of Fluid Mechanics, Vol.52, PP 609-638, 1972.

53. Hanjalic, K. and Launder, B.E., "Contribution towards a Reynolds Stress Closure for Low Reynolds Number Turbulence", Journal of Fluid Mechanics, Vol. 74, Part A., PP 593-610, 1976.

54. Harinaldi, Budiarso, Rustan Tarakka and Sabar P. Simanungkalit, "Computational Analysis of Active Flow Control to Reduce Aerodynamics Drag on a Van Model", International Journal of Mechanical & Mechatronics Engineering IJMME-IJENS Vol:11 No: 03,pp24-30, 2011.

55. Hinze, J. O. "Turbulence", McGraw Hill, New York, USA 1959.

56. Hucho, W.H. (Ed.), "Aerodynamics of Road Vehicles", 4th Edition, SAE International, Warren dale, PA, USA, 1998.

57. Jones,W.P. and Launder B.E., "The Prediction of Laminarization with a Two equation Model of Turbulence", International Journal of Heat Mass Transfer, Vol. 15, pp 301-314, 1972.

58. Kalitzin, G., "Towards a robust and efficient v2f implementation with application to transonic bump flow", CTR Annual Research Briefs, PP 291-299, 2000.

59. Klebanoff, P.S., "Characteristics of Turbulence in a boundary Layer with Zero Pressure Gradient", NACA TN 3178, 1954.

60. Kolmogorov, A.N., "Equation of Turbulence Motion of an Incompressible Turbulent Fluid", Izv. Akad. SSSR Ser. Phys. VI, No 1-2, 1942, 1942.

61. Kourta, A.and Vitale, E., "Analysis and control of cavity flow", Physics of Fluids vol. 20: 077104, 2008.

62. Krajnovic, S. and Davidson,L., "Flow Around a Simplified Car, Part 1: Large Eddy Simulation", Journal of fluids Engineering, Vol. 127, PP 907-918, 2005 a.

63. Krajnovic, S. and Davidson,L., "Flow Around a Simplified Car, Part 2: Understanding the Flow", Journal of fluids Engineering, Vol. 127, PP 919-928, 2005 b.

64. Krogstad, P.A. and Kourakine, A., "Some effects of localized injection on the turbulence structure in boundary layer", Phys Fluids, vol. 12, pp 2990-2999, 2000.

65. Lam, C.K.G. and Bremhorst, K.A., "Modified Form of k-ε Model for Predicting Wall Turbulence", ASME, Journal of Fluids Engineering, Vol. 103, PP 456-460, 1981.

66 Launder, B. E. and Shima, N., "Second-Moment closure for the Near- Wall Sublayer: Development and Application", AIAA Journal, Vol. 27, No. 10, PP 1319-1326, 1989.

67. Launder, B.E. and Spalding, D.B., "Mathematical Models of Turbulence", Academic Press, 1972.

68. Launder. B.E. and Sharma, B.I., "Application of the Energy Dissipation Model of Turbulence to the Calculation of Flow Near a Spinning Disc", Letters in Heat and Mass Transfer, Volume 1, PP 131-138, 1974.

69. Launder, B.E., Reece, G.J. and Rodi, W., "Progress in the Development of Reynolds-Stress Turbulence Closure", Journal of Fluid Mechanics, Vol.68, PP 537-566, 1975.

70. Launder, B.E., Priddin, C.H. and Sharma, B.I., "The Calculation of Turbulent Boundary Layers on Spinning and Curved Surfaces", ASME, Journal of Fluid Engineering, Vol. 99, PP 231, 1977.

71. Launder, B.E. and Spalding, D.B., "The Numerical Computation of Turbulent Flows", Comput. Meth. Appl. Mech. Engg, Vol. 3, pp 269-289, 1974.

72. Leschnizer, M.A. and Rodi, W., "Calculation of Annular and Twin Parallel Jets Using Various Discretization Schemes and Turbulence Model Variations", Journal of Fluid Engineering, Vol. 103, 1981.

73. Lien, F.S. and Durban, P.A., "Non-linear k-ε-v^2 modeling with application to high lift", Proc. of the summer program, CTR NASA Ames/Stanford Univ. 5-22, 1996.

74. Lien, F.S. and Leschnizer, M.A., "Assessment of Turbulence-Transport Models Including Non-Linear RNG Eddy- Viscosity Formulation and Second-Moment Closure for Flow Over a Backward-Facing Step", Computers & Fluids, Vol. 23 PP 983- 1004, 1994.

75. Lienhart, H., Stoots, C. and Becker,S., "Flow and turbulence structure on the wake of a simplified car model (Ahmed model)", *DGLR Fach. Symp. der AG ATAB,Stuttgart University*, 2000.

76. Lilly, D.K., "On the application of Eddy Viscosity Concept in the Inertial Subrange of turbulence", NCAR Manuscript 123, 1966.

77. Liu Y. and Moser A., "Numerical modeling of air flow over the Ahmed body", In; Proceedings of the 11th Annual conference of the CHD Society of Canada, pp. 507- 512, 2003.

78. Lumley, J.L., "Computational Modeling of Turbulent Flows", Adv. Appl. Mech., Vol. 18, PP 123- 176,1978.

79. Manceau, R. and Hanjalic, K., "Elliptic Blending Model: A new Near- Wall Reynolds-Stress Turbulence Closure", Physics of Fluids", Vol. 14, No 2, PP 744-754, 2002.

80. Martinat, G., Bourguet, R., Hoarau, Y. Dehaeze, F., Jorez, B. and Braza, M., "Numerical Simulation of the Flow in the Wake of Ahmed Body Using Detached Eddy Simulation and URANS Modeling". *Peng S-H and Haase W (Eds.): Adv. in Hybrid RANS-LES Modeling,;NNFM 97*:125-31, 2008

81. Mashud, M., Bari, A.A., and Hoshen M.S., "Reduction of Fuel Consumption of a Car by Aerodynamic Drag Reduction", *International Conference on Mechanica , Industrial and Materials Engineering,* RUET, Rajshahi, Bangladesh, 2013.

82. Menter, F.R., "A Critical Evaluation of Promising Eddy- Viscosity Models" International Symposium on Turbulence, Heat and Mass Transfer, August 9-12, Lisbon, Spain, 1994.

83. Moshen, A.M., "Experimental Investigation of the Wall Pressure Fluctuations in Subsonic, Separated Flows", Boeing Company Report, No D6-17094, USA 1967.

84. Naser, J., "Flow prediction in Valve/Prot Assemblies", Ph.D. Thesis, Department of Aeronautics, Imperial College of Science, Technology and Medicine, The University of London, UK, 1990.

85. Naser, J. and Siddiqui, H., "Short Course in Computational Fluid Dynamics (CFD)", School of Engineering and Science, Swinburne University of Technology, Melbourne, Australia, 20003.

86. Nee, V.W. and Kovasznay, L.S.G., "The Calculation of Incompressible Turbulent Boundary layer By a Simple Theory" , Physics of Fluids, Vol. 12, PP 473, 1968.

87. Nienaltowska, E., "Separated Flow on the Car Body: Spectral and Spatial Characteristics Analysed from the Aeroacoustic Viewpoint", International Journal of Vehicle Design,Vol. 14, Nos 5/6, 1993.

88. Norris, H.L. and Reynolds, W.C., "Turbulent Channel Flow with a Moving Wavy Boundary", Department of Mechanical Engineering Report FM-10, Stanford University, California, USA, 1975.

89. Onorato, M., Costelli A. and Garonne A., "Measurement through wake analysis", SAE paper No. 569, 1984.

90. Pameix, S., Laurence, D. and Durbin, P.A., "A procedure for Using DNS Databases", Transactions of the ASME, 1998.

91. Park, J. and Choi, H., "Effects of uniform blowing through blowing or suction from a span wise slot on a turbulent boundary layer flow", Phys Fluids, vol. 11 pp 3095-3105, 1999.

92. Popat, B.C., "Study of Flow and Noice Generation From Car A-Pillars", Ph. D. Thesis, Department of Aeronautics, Imperial College of Science, Technology and Medicine, The university of London, UK, 1991.

93. Prandtl, L., "Berict Uder Untersuchungen zur ausgebildeten Turbulenz", Zs. Agnew. Math. Mech., 5, PP 136-139, 1925.

94. Prandtl, L., "Uber Ein Neues Formelsystem Fur Die Ausgebildete Turbulenz", Nacr. Akad. Wiss. Gottingen , math-Phys Kl., PP 6-19, 1945.

95. Reynolds, W.C. "Fundamentals of Turbulence for Turbulence Modeling Simulation", In Lecture Notes for Von Karman Institute, AGARD Lecture Series , No. 86, PP 1-66, New York NATO, 1987.

96. Roberson, J.A. and Crowe C.T., "Engineering Fluid Mechanics", 6th Edition, John Wiley & Sons, USA, 1997.

97. Rodi, W., "Influence of Buoyancy and Rotation on Equations for the Turbulent Length Scale", Proceedings of the 2nd Symposium on Turbulent Shear Flow, London, 1979.

98. Rodi, W. and Sheuerer, G., "Scrutinizing the k-ε Turbulence Model Under Adverse Pressure Gradient Conditions", ASME, Journal of Fluids Engineering, Vol. 108, PP 174-179, 1986.

99. Rotta, J., "Statistische Theorie Nichthomogener Turbulenz", Zeitsch fur Physik, Vol. 129 and 131,1951.

100. Roumeas, M., Gilleron, P. and Kourta ,A., "Reduction de trainee per controle des decollements autour d'une geometrie simplifiee: etude parametrique 2D", 17eme Congres Francais de Mecanique, 29 Aout au 02 September 2005,

101. Roumeas, M., Gilleron, P. and Kourta, A., "Drag Reduction by Flow Separation control on a Car after Body", International Journal for Numerical Method in Fluids, vol. 60, pp1222-1240, 2009.

102. Sano, M. and Hirayama, N., "Turbulent boundary layer with injection and suction through a slit", Bull JSME, vol. 28, pp 807-814, 1985.

103. Schwarz, W.R. and Bradshaw, P., "Term by Term Tests of Stress- Transport Turbulence Models in a Three-Dimensional Boundary Layer" Physic of fluids, vol. 6, PP 986, 1994.

104. Sharma, B.I., "The Behaviour of Swirling Turbulent Boundary Layer Near Walls", PhD Thesis, University of London, 1975.

105. Shih, T.H., Liou, W.W., Shabbir, A., Yang Z. and Zhu J., "A New k- ε Eddy Viscosity model for High Reynolds Number Turbulence Flows", Computers Fluids, vol. 24, No. 3. PP 227-238, 1995

106. Shir, C.C. "A Preliminary Numerical Study of Atmospheric Turbulent Flow in the Idealized Planetary Boundary Layer", J. Atmos. Sci., Vol. 30, PP 1327-1339, 1973.

107. Simpson, R.L., Ghodbane, M. and McGrath, B.E., "Surface pressure Fluctuations in a Separating Turbulent Boundary layer", Journal of Fluids Mechanics, Vol. 177, PP 167-1861, 987.

108. Simpsion, R.L., "Turbulent Boundary- Layer Separation", Annual Review of Fluid Mechanics, Vol. 21, PP 205-234, 1989.

109. Smagorinsky, J., "General Circulation Experiments with the Primitive equations I. The Basic Experiment", Mon. Weather Rev., Vol. 91, PP 99-164, 1963.

110. Smith, A.M.O. and Cebeci, T., "Numerical Solution of the Turbulent Boundary-Layer Equations", Douglas Aircraft Division Report DAC 33735, 1967.

111. Spalart, P.R. and Allmaras, S.R., "A one equation turbulence model for aerodynamics flow". AIAA Paper, No 92-0439, 1992.

112. Spalart, P.R. et al., "Comments on feasibility of LES for wings, and on a hybrid RANS/LES approach. In: Proceedings of first AFOSR international conference on DNS/LES", Greyden press, Runston Louisiana, 1997.

113. Spalart, P,R. et al., "A new version of detached eddy simulation, resistant to ambiguous grid densities", 2006.

114. Speziale, C.G., "Modeling the Pressure Gradient Velocity Correlation of Turbulence", Physic of Fluids, Vo. 28, PP 69-71, 1985.

115. Speziale, C.G., "Second Order Closure Models for Rotating Turbulent Flows", Quart. Appl. Math. Vol. 45, PP 721-733, 1987.

116. Speziale, C.G., "Analytical Methods for Development of Reynolds Stress Closure in Turbulence", Annual Review of Fluid Mechanics, Vol. 23, PP107-157, 1991.

117. Stankiewicz, W., Morzynski, M., Noack, B.R. and Thiele, F., "Stability properties of 2D flow around Ahmed Body", Proc. of 10th Int. Conf. MMA2005&CMAM2, 129-134, Trakai, 2005.

118. Travin, A. et al., "Detached eddy simulation past a circular cylinder, Flow, turbulence and combustion" P, 63, 1999.

119. Uberoi, M.S., "Effect of Wind-Tunnel Contribution on Free-Stream Turbulence" Journal of Aeronautical Sciences, Vol. 23, PP 756-764, 1956.

120. Uchida, K., Okumura, K. and Kuriyama, T., "Aerodynamic Simulations by Using Discontinuous Interface Grid and Solution Adaptive Grid Method", SEA Paper, No 970141, 1997.

121. Uruba, V. and Hladik, O., "On the Ahmad body wake", Colloquium Fluid Dynamics 2009, Prague, 1-12, October 21-23, 2009.

122. Von Kerman, T., "Some Remarks on the Statistical Theory of Turbulence", Proceedings to the 5th International Congress of Applied Mechanics, Cambridge, MA, 347, 1938.

123. Von Driest, E.R., "On Turbulent Flow Near a Wall", Journal of Aeronautical Sciences, Vol. 23, 1007, 1956.

124. Watanabe, M. and Harita, M., "The Effects of Body Shapes on Wind Noise", SAE Paper No. 780266, 1978.

125. Watkins, S and Alam, F, "Future vehicle thermal cooling and aerodynamic drag savings: where will they come from?", Proceedings of International Conference on Advanced Vehicle Technologies and Integration, China Machine Press, pp. 775-82, 17-20 January, Changchun, China, 2012.

126. Wilcox, D.C. and Chambers, T.L., "Streamline Curvature Effects on Turbulent Boundary Layers", AIAA Journal, Vol. 15, No. 4, PP 574-580, 1977.

127. Wilcox, D.C., "Multiscale Model for Turbulent Flows", AIAA Journal, Vol. 26, No. 11, PP 1311-1320, 1988.

128. Wilcox, D.C., "Turbulence Modeling for CFD", 2nd Edition, KNI Inc., California, USA, 2002.

129. Wilcox, D.C. and Rubesin, M.W., "Progress in turbulence Modeling for complex Flow Fields Including Effect of Compressibility", NASA TP 1517, 1980.

130. Wolfstein, M., "Convection Processes in Turbulent Impinging Jets", Imperical College, Heat Transfer Section Report SF/R/2, 1967.

131. Wolfstein, M., "The velocity and Temperature Distribution of One-Dimensional Flow with Turbulence Augmentation and Pressure Gradient", International Journal of Heat and Mass Transfer, Vol. 12, PP 301-318, 1969.

132. "World Energy Outlook 2007", Executive summary, China and India Insights, International Energy Agency IEA, 2007.

133. Yakhot, V. and Orszag, S.A., "Renormalization Group Analysis of Turbulence I. Basic Theory", Journal of Science Computing I, 3, 1986.

134. Zimmer, G., " The Contribution of the A-pillar Vortex to Vehicle Interior Noise" Ph.D. Thesis, School of Aerospace, Mechanical and Manufacturing Engineering, RMIT University, Melbourne, Australia, 2003.